

Doctoral theses at NTNU, 2021:397

Ehsan Allymehr

# Investigation of Hydrocarbon Two-phase Flow for Charge Reduced Heat Exchangers

ISBN 978-82-326-5890-9 (printed ver.)  
ISBN 978-82-326-6675-1 (electronic ver.)  
ISSN 1503-8181 (printed ver.)  
ISSN 2703-8084 (electronic ver.)

Doctoral theses at NTNU, 2021:397

**NTNU**  
Norwegian University of  
Science and Technology  
Thesis for the degree of  
Philosophiae Doctor  
Faculty of Engineering  
Department of Energy and Process Engineering



Ehsan Allymehr

# Investigation of Hydrocarbon Two-phase Flow for Charge Reduced Heat Exchangers

Thesis for the degree of Philosophiae Doctor

Trondheim, December 2021

Norwegian University of Science and Technology  
Faculty of Engineering  
Department of Energy and Process Engineering



Norwegian University of  
Science and Technology

**NTNU**

Norwegian University of Science and Technology

Thesis for the degree of Philosophiae Doctor

Faculty of Engineering

Department of Energy and Process Engineering

© Ehsan Allymehr

ISBN 978-82-326-5890-9 (printed ver.)

ISBN 978-82-326-6675-1 (electronic ver.)

ISSN 1503-8181 (printed ver.)

ISSN 2703-8084 (electronic ver.)

Doctoral theses at NTNU, 2021:397



Printed by Skipnes Kommunikasjon AS

# Preface

This thesis is submitted in partial fulfillment of the requirements for the degree of Doctor of Philosophy (Ph.D.) at the Norwegian University of Science and Technology (NTNU). The research described herein was carried out from July 2018 to December 2021 at the Department of Energy and Process Engineering of the Faculty of Engineering, with Professor Trygve Magne Eikevik as main supervisor and Professor Armin Hafner as co-supervisor. The present Ph.D. was funded by HighEFF—Centre for an Energy Efficient and Competitive Industry for the Future, under the FME-scheme (Centre for Environment-friendly Energy Research, 257632) with financial support from the Research Council of Norway and user partners of HighEFF.

---

# Abstract

Hydrocarbons offer an alternative to the HVAC industry as a natural working fluid with minimal environmental impact. The main challenge with hydrocarbons utilization is flammability which can be mitigated by reduction of charge in systems. Internally enhanced tubes provide a powerful tool for designing a more efficient heat exchanger leading to reductions in both volume and charge. Microfinned tubes are the most commonly utilized internally enhanced tubes that increase the heat transfer coefficient on the refrigerant fluid side in heat exchangers. Thanks to the higher heat transfer coefficients, the internal volume of the heat exchangers can be reduced.

One of the main challenges for using microfinned tubes has been the design of the heat exchangers. This is caused by a lack of reliable predictive methods. In this context, the present thesis presents experimental results for characteristics of two-phase flow of hydrocarbons. Propane (R290), isobutane (R600a), and propylene (R1270) were studied since they are commonly used in HVAC applications. Three tubes with an outer diameter of 5 mm were tested, one smooth and two microfinned. The two microfinned tubes differed in the number of fins and helix angle, causing a different increase in the available heat exchange area. One test rig was used to obtain both condensation and evaporation characteristics, which was possible due to the design of the rapidly interchangeable test sections. In evaporation tests, the effects of fluid properties, heat flux, mass flux and saturation temperature were studied in addition to the effect of internally enhanced tubes. Condensation tests were focused on fluid properties, mass flux and internal enhancement of tubes.

Additionally, the data obtained for the heat transfer coefficient and pressure drop were compared against predictive methods to find the most reliable correlations. Finally, this data were used for numerical simulation of fin-and-tube heat exchangers in different environmental conditions to compare the charge with other types of heat exchangers.

---

# Acknowledgements

I would like to express my gratitude and gratefulness to all the people who have assisted me in various ways on my path to fulfil my doctoral degree.

Above all, this work would not have been completed if not for the support and assistance from my supervisor Trygve M. Eikevik and co-supervisor Armin Hafner. With their trust and advice, any external challenge was alleviated so that the demanding journey of doctoral research could be made untroubled. Moreover, I would like to give special thanks to Ángel Álvarez Pardiñas, his experience and expert advice proved invaluable in overcoming the numerous challenges in the experimental tests and publication of scientific papers.

I would also like to thank my co-workers, and fellow Ph.D. candidates, Silje Marie Smitt, Håkon Selvnes, Knut Emil Ringstad, and Marcel Ulrich Ahrens, who created a collaborative and supportive community to share information and experiences.

Regarding my work in the laboratory, I would like to thank Håvard Rekstad and Reidar Tellebon, who with their ingenuity and creativity helped in solving the practical complications of experimental work.

On a personal note, I would like to thank my partner Gera, for all her support during these years.

Finally, none of this would have been possible if not for the endless love and support from my parents, Manoochehr and Fahimeh; thank you for everything you have done for me.

Ehsan Allymehr  
September 2021  
Trondheim

---

# Contents

<b>Preface</b>	<b>i</b>
<b>Abstract</b>	<b>iii</b>
<b>Acknowledgements</b>	<b>v</b>
<b>List of Figures</b>	<b>ix</b>
<b>List of Tables</b>	<b>xi</b>
<b>Nomenclature</b>	<b>xiii</b>
<b>1 Introduction</b>	<b>1</b>
1.1 Motivation . . . . .	1
1.2 Objectives and scope . . . . .	2
1.3 Contributions . . . . .	3
1.4 Thesis organization . . . . .	3
<b>2 Technical Background</b>	<b>7</b>
2.1 History . . . . .	7
2.2 Hydrocarbons as fourth generation working fluid . . . . .	11
2.3 State of the art on hydrocarbon two phase flow . . . . .	13
2.4 Summary . . . . .	15
<b>3 Experimental Setup</b>	<b>17</b>
3.1 Test rig . . . . .	17
3.1.1 Evaporation test section . . . . .	18
3.1.2 Condensation test section . . . . .	19
3.1.3 Test Tubes . . . . .	20
3.1.4 Instruments . . . . .	22
3.2 Validation and heat leakage tests . . . . .	23
3.2.1 Validation of evaporation tests . . . . .	23
3.2.2 Validation of condensation tests . . . . .	25
3.3 Calibration Process and Uncertainty Propagation . . . . .	26

3.4	Data Reduction . . . . .	27
<b>4</b>	<b>Summary of Research Work</b>	<b>29</b>
4.1	Organization of articles . . . . .	29
4.2	Article I: Characteristics of evaporation of propane (R290) in compact smooth and microfinned tubes . . . . .	29
4.3	Article II: Comparative analysis of evaporation of isobutane (R600a) and propylene (R1270) in compact smooth and microfinned tubes	30
4.4	Article III: Condensation of Hydrocarbons in Compact Smooth and Microfinned Tubes . . . . .	31
4.5	Article IV: Numerical study of hydrocarbon charge reduction methods in HVAC heat exchangers . . . . .	31
4.6	Summary and suggestions for future work: . . . . .	32
	<b>Bibliography</b>	<b>35</b>
	<b>A List of Publications</b>	<b>43</b>

# List of Figures

2.1	Maximum quantity of equivalent CO <sub>2</sub> quotas on refrigerants based on EU directive 517/2014. . . . .	9
2.2	A simplified visualization of adverse effects of working fluids being saturated with chlorine, fluorine and hydrogen. . . . .	10
3.1	Photograph of test rig. . . . .	17
3.2	Test rig schematic for evaporation test section. . . . .	18
3.3	Test rig schematic for condensation test section. . . . .	18
3.4	Photograph of evaporation test section. . . . .	19
3.5	Photograph of condensation test section. . . . .	19
3.6	Visualization of the internal helical cooling loop for the condensation test section. . . . .	20
3.7	Physical presentation of the geometrical parameters of the microfinned tubes. . . . .	20
3.8	Cross sectional view of the microfinned tubes. . . . .	20
3.9	Validation of the experimental data for HTC of single phase gas flow of propane in the evaporation test section against the correlation of Gnielinski, at varying Reynolds number. . . . .	23
3.10	Comparison of the experimental data for pressure drop with the equation of Darcy Weisbach for single phase gas flow of propane. . . . .	24
3.11	Validation of the experimental data for HTC of single phase gas flow of isobutane in condensation test section against the correlation of Gnielinski, at varying Reynolds number. . . . .	25



# List of Tables

2.1	Substitutes for the second generation of working fluids. . . . .	8
2.2	Alternative natural working fluid substitutes for the third generation of working fluids. . . . .	10
2.3	Chemical properties of the hydrocarbons of interest for use as working fluid in domestic applications. . . . .	12
3.1	Geometrical parameters of the test tubes and test sections. . . . .	21
3.2	List of instruments used for evaporation tests and their respective uncertainties. . . . .	22
3.3	List of instruments used for condensation tests and their respective uncertainties. . . . .	22
4.1	Content and organization of the experimental data as journal papers presented in the appendix. . . . .	29



# Nomenclature

## Greek symbols

$\alpha$	Void fraction	-
$\beta$	Spiral angle	°
$\delta_{30}$	Percentage of predicted values with less than 30% error	-
$\gamma$	Fin angle	°
$\rho$	Density	$\text{kg m}^{-3}$
$\sigma$	Surface tension	$\text{N m}^{-1}$

## Latin symbols

$c_{P\text{water}}$	Specific heat of water	$\text{kJ kg}^{-1} \text{K}^{-1}$
$d_i$	Fin tip diameter for MF tubes, internal diameter for smooth tube	mm
$d_o$	Outer diameter	mm
$E$	Enhancement Factor	-
$G$	Mass flux	$\text{kg m}^{-2} \text{s}^{-1}$
$g$	Standard gravity	$\text{m s}^{-2}$
$GWP_{100}$	Global Warming Potential over 100 years	-
$HTC$	Heat Transfer Coefficient	$\text{W m}^{-2} \text{K}^{-1}$
$HVAC$	Heating, Ventilation and Air conditioning	-
$I$	Efficiency index	-
$i$	Enthalpy of vaporization	$\text{kJ kg}^{-1}$
$k$	Thermal conductivity	$\text{W m}^{-1} \text{K}^{-1}$

## Nomenclature

---

$l_f$	Fin height	mm
$LFL$	Lower flammability limit	%Vol
$m$	Mass flow	$\text{kg s}^{-1}$
$MARD$	Mean Absolute Relative Deviation	-
$MRD$	Mean Relative Deviation	-
$N$	Dataset size	-
$n$	Number of fins	-
$NBP$	Normal boiling point	$^{\circ}\text{C}$
$ODP$	Ozone Depletion Potential	-
$P$	Penalization Factor	-
$p$	Pressure	Pa
$P_r$	Reduced pressure	-
$PWM$	Pulse Wave Modulation	-
$Q$	Heat input	W
$q$	Heat flux	$\text{W m}^{-2}$
$R_x$	Heat exchange area ratio to a smooth tube	-
$RACHP$	Refrigeration, Air conditioning and Heat pump	-
$RTD$	Resistance thermometers	-
$S$	Internal surface area of tube	$\text{mm}^2$
$T$	Temperature	$^{\circ}\text{C}$
$t_w$	Wall thickness	mm
$UFL$	Upper flammability limit	%Vol
$x$	Vapor quality	-

### Subscripts

$a$	Advectional
$amb$	Ambient condition

<i>element</i>	Heating Element
<i>f</i>	Frictional
<i>g</i>	Gas phase
<i>in</i>	Inlet conditions
<i>l</i>	Liquid phase
<i>lg</i>	Liquid to gas phase change
<i>loss</i>	Heat loss to environment
<i>pre</i>	Preheater section
<i>sat</i>	Saturated condition
<i>test</i>	Test section
<i>w</i>	Wall



# Chapter 1

## Introduction

### 1.1 Motivation

The impact of refrigeration, air conditioning and heat pump (RACHP) systems on the environment has led to efforts to limit the use of different working fluids with initiatives and regulations such as the European F-gas regulation (Schulz and Kourkoulas, 2014). The current generation of working fluids has an exceptionally high Global Warming Potential (GWP) and the progress toward a more sustainable and environmentally friendly RACHP industry requires a broad shift to working fluids with low GWP and zero Ozone Depletion Potential (ODP). Additionally, systems working with more environmentally friendly refrigerants need to be more energy-efficient to reduce the indirect impact with lower primary energy usage.

Hydrocarbons, such as propane (R290), isobutane (R600a), and propylene (R1270) have long been used as working fluids in various applications. For example, isobutane (R600a) is the most used refrigerant in domestic refrigeration and freezer units, especially in Europe (Straub, 2018). Hydrocarbons offer favorable saturation curves befitting different use cases while enjoying low GWP and zero ODP, thus they are considered to replace several groups of working fluids by 2030 (Mota-Babiloni and Makhnatch, 2021). However, the use of hydrocarbons in refrigeration systems has been long limited by flammability concerns. Studies have shown that the majority of charge is stored in heat exchangers (Li et al., 2015; Palm, 2008), thus minimizing the heat exchangers' volume seems to be the most effective method of increasing the capacity of these systems with regards to limitations on their charge. This is even more critical in the condenser's case as it could contain 50% of the total charge (Li et al., 2015). In an air sourced heat pump, the majority of the charge is stored in the condenser; nevertheless, the evaporator charge is still considerable, especially in lower temperatures where it can be more than 20% of the total charge (Li et al., 2015).

As a result special attention has been given to reducing the charge in the heat

exchangers. One of the most promising technologies seems to be the use of microfinned tubes where the internal surface of the tube has been augmented with fins to increase the available area for heat exchanger. The increase of heat exchanger area leads to an increase of heat transfer coefficient (HTC) enabling a more compact heat exchanger. Nowadays microfinned tubes are becoming increasingly common due to their potential in volume and charge reduction in hydrocarbon heat exchangers, but reliable experimental data are required to properly design and size heat exchangers in applications such as air to air heat pumps or domestic refrigerators. These data unfortunately does not currently exist.

The goal of this Ph.D. has been to study the effect of microfinned tubes for heat exchangers using hydrocarbons as working fluids. Using the experimental data obtained by the test rig, the charge in the systems utilizing heat exchangers with microfinned tubes can be compared to smooth tube heat exchangers. The results could be used to design hydrocarbon HVAC units with capacities that were not possible previously due to safety regulations.

## 1.2 Objectives and scope

The goal of this Ph.D. has been to provide a database of two phase flow characteristics of flowing hydrocarbons in compact smooth and microfinned tubes by experimentally measuring HTC and pressure drop values. The effectiveness of internally enhanced surfaces in different working conditions was studied by comparing flow characteristics of two microfinned tubes with dissimilar internal geometries to a smooth tube at similar working conditions. The overall detailed scope and objectives of this Ph.D. can be summarized as:

- Developing database for two phase flow characteristics of hydrocarbons.
- Assessment of microfinned tube effects on two phase flow characteristics.
- Comparison of prediction methods for heat transfer coefficient and pressure drop in smooth and microfinned tubes.
- Demonstrate the capabilities of microfinned tubes in charge reduction of HVAC systems' heat exchangers.

While many other hydrocarbons could be used as working fluids, the experimental studies were limited to three hydrocarbons, namely propane (R290), isobutane (R600a) and propylene (R1270). This choice was based on the widespread use of these fluids in the industry and their potential for small-scale domestic systems. A smooth tube and two microfinned tubes were selected to compare the effect of different internal surface enhancements. Development of new correlations as prediction methods and testing of hydrocarbon mixtures was not in the scope of this Ph.D.

## 1.3 Contributions

This thesis presents a series of data that aims to provide a more holistic understanding of two phase flow of hydrocarbons. The main contributions can be listed as:

- Database for characteristics of two phase flowing hydrocarbons in compact tubes.
- Further development of the effect of microfinned tubes on two phase flow characteristics.
- Providing reliable prediction methods for heat transfer coefficient and pressure drop.
- Development of a numerical simulation tool for designing heat exchangers focusing on charge reduction methods of hydrocarbons.

The novel aspects of each contribution are discussed in the context of the relevant scientific literature respectively. With regards to authorship, the experimental data was procured and calculated solely by the author, whereas the numerical simulation tool, HXSim, was updated and developed in collaboration with Geir Skaugen at SINTEF Energy.

## 1.4 Thesis organization

This document is structured as an introduction of four chapters and a collection of four journal publications, with conclusions and suggestions for further work. These chapters could be summarized as:

**Chapter 1** provides information on the Ph.D. research itself and highlights the structure of the thesis.

**Chapter 2** gives a background of the work, including information on the history of refrigeration, hydrocarbons' history as a working fluid, regulations and the prospect of hydrocarbons in the fourth generation of working fluids. Furthermore, state-of-the-art literature review is presented.

**Chapter 3** describes the experimental set up, the test procedure, data reduction and related practical matters such as safety precautions. Additionally, information regarding validation and heat leakage tests are detailed. Many of the experimental procedures are the same between the evaporation test rig and condensation one, Nevertheless there are important differences in system design and, thus, these points are highlighted for the reader in this chapter.

**Chapter 4** provides a summary of the work performed in this study in addition to several proposals for further research. The main conclusions from each paper are summarized. The first three papers provide an overview of the two-phase flow characteristics of the tested hydrocarbons. Each of the main parameters flow characteristics is separately reported. The fourth paper provides information on charge reduction methods for hydrocarbon in heat exchangers of direct and indirect systems.

The research carried out during this Ph.D. project was published in four peer reviewed journal publications that are presented as annex in this thesis and are subject to evaluation. These publications are:

- Allymehr, E., Pardiñas, Á. Á., Eikevik, T. M., and Hafner, A. Characteristics of evaporation of propane (R290) in compact smooth and microfinned tubes, *Applied Thermal Engineering*, 181:115880, 2020.
- Allymehr, E., Pardiñas, Á. Á., Eikevik, T. M., and Hafner, A. Comparative analysis of evaporation of isobutane (R600a) and propylene (R1270) in compact smooth and microfinned tubes. *Applied Thermal Engineering*, 188:116606, 2021.
- Allymehr, E., Pardiñas, Á. Á., Eikevik, T. M., and Hafner, A. Condensation of Hydrocarbons in Compact Smooth and Microfinned Tubes. *Energies*, 14(9):2647, 2021.
- Allymehr, E., Skaugen, G., Will, T., Pardiñas, Á., Eikevik, T., Hafner, A., Schnabel, L. Numerical study of hydrocarbon charge reduction methods in HVAC heat exchangers. *Energies*, 2021.

In addition to journal papers; the author has been involved in publication of several conference papers, these papers are mentioned here but are not compiled in thesis document and are not subject to evaluation.

- Allymehr, E., Roux, M., Pardiñas, Á.Á., Eikevik, T.M., Hafner, A. Experimental study of Isobutane (R600a) evaporation in microfinned and smooth tubes, *Refrigeration Science and Technology*, 2020.
- Allymehr, E., Eikevik, T.M., Hafner, A. Experimental investigation of evaporation of propane (R-290) in small pipes, *Refrigeration Science and Technology*, 2019.
- Allymehr, E., Eikevik, T.M., Hafner, A. Characteristics of propane evaporation in a microfinned tube with internal diameter of 4.47 mm, *Proceedings of the 37th UIT Heat Transfer Conference*, 2019.

- Allymehr, E., Will, T., Schnabel, L., Skaugen, G., Comparison of refrigerant charge requirements in an optimized fin and tube evaporator versus plate heat exchangers, *Proceedings of the 6th TPTPR conference*, 2021.



## Chapter 2

# Technical Background

### 2.1 History

The first generation of vapor-compression refrigeration systems, all used natural substances. Any available chemical substance that could provide sufficiently good results was used. Most notably were diethyl ether (R610), carbon dioxide (R744), ammonia (R717), sulphur dioxide (R764), methyl chloride (R40). Later, some hydrocarbons were used as refrigerants. All these substances were either flammable, toxic, or both, with the only exception being carbon dioxide (R744). Expansion of public spaces such as department stores that required cooling in summer made the safety issues regarding natural working fluids more apparent. In 1931 General Motors Research Corporation in the USA first synthesized R12 and other CFCs (ChloroFluoroCarbons) like R11 and R115. Later on, HCFCs (HydroChloroFluorCarbons) such as R22 were created and utilized. With the invention of these synthetic fluids, most natural working fluids were quickly decommissioned. The only major exception was ammonia, which, thanks to its thermodynamic properties, continued to be used in large food storage complexes. Meanwhile, some hydrocarbons survived as a working fluid in the petrochemical industry. The second generation of refrigerants dominated the market without any competition for sixty years until mid-1980s, when the global emergency concerning the destruction of the ozone layer in the stratosphere emerged. This was subsequently linked to the synthetic chemical compounds, mainly chlorine and, to a lesser extent, bromine and iodine. This global emergency led to a concentrated effort to gradually ban CFC and HCFC refrigerants in the Montreal protocol of 1987. The substitute for second-generation refrigerants was created by synthetic production of compounds similar to the previous generation by removal of chlorine and addition of hydrogen atoms. This was considered beneficial in two ways, first reducing the ozone depletion potential to zero with the added benefit of a shorter lifetime in the atmosphere. Initially, the goal was to find a suitable drop-in substitute for all second generation refrigerants i.e. fluids that could replace the previous

refrigerants in the same circuit. For example, R134a was found to substitute R12 without any alteration to the system. Substituting other fluids involved a more complicated route; in some cases, HFC mixtures were used, and zeotropic fluids with temperature glides of few degrees were accepted. This, with the flammable fluids utilization in small quantities, enabled a transition to the third generation of working fluids. The second generation of working fluids and their third generation substitutes are detailed in Table 2.1.

**Table 2.1:** Substitutes for the second generation of working fluids.

Second generation fluid		Third generation Fluid	Notes/[Composition]
R11	→	R245fa	Also R123 (Contains Chlorine but lower ODP)
R12	→	R134a	Drop in substitute
R22	→	R407C	Zeotropic [23% R32, 25% R125, 52% R134a]
R502	→	R404A	Zeotropic [44% R125, 4% R134a, 52% R143a] or R507A (Azeotropic)

In addition to the substitutes mentioned, R410A [50% R32 and 50% R-125] as a quasi azeotropic fluid found applications in residential air conditioners and heat pumps. In the early years of the 21st century, attention was drawn to global warming and, subsequently, the effect of third-generation working fluids on it. Thus, national and multinational legislations such as the Kigali amendment to the Montreal protocol were passed to reduce the use of fluids that significantly contribute to the greenhouse effect. This greenhouse effect is commonly measured with a parameter called  $GWP_{100}$  which represents the greenhouse effect caused by the chemical compound relative to that caused by the same mass of reference gas, Carbon dioxide,  $CO_2$  being released into the atmosphere, over a time horizon of 100 years.  $GWP_{100}$  is calculated based on two terms, atmospheric lifetime and radiative efficacy of the gas.

EU F-gas regulation (Schulz and Kourkoulas, 2014) is the legislation in Europe that directs the use of fluids with greenhouse effect and more specifically, those that have Florine. While this directive does not ban use of any single fluids, it severely limits how much fluids can be used in equivalent  $CO_{2e}$  terms. This gradual reduction of HFC use is shown in Figure 2.1. The baseline reference (100%) is 183.1 Mt  $CO_{2e}$  on the basis of the 2009-2012 period (Mota-Babiloni and Makhnatch, 2021).

With the outlook of the gradual phase-down of HFCs, a new generation of fluids was proposed, namely HFOs (HydroFluoroOlefins). HFOs have a reduced  $GWP_{100}$  because of the presence of a double C=C bound, making them unsatu-

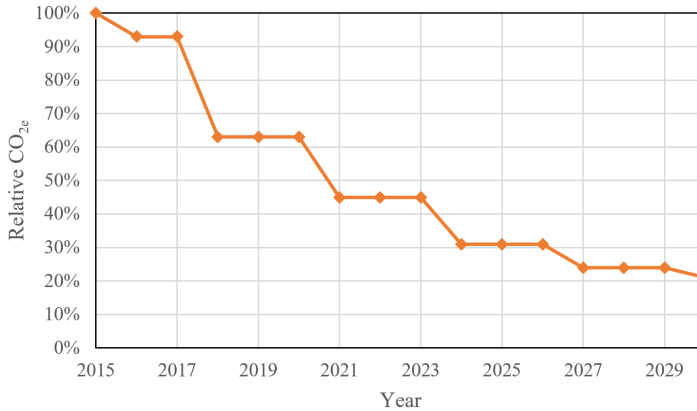


**Figure 2.1:** Maximum quantity of equivalent CO<sub>2</sub> quotas on refrigerants based on EU directive 517/2014.

rated and reducing the atmospheric lifetime. Additionally, the radiative efficacy of HFOs is significantly lower than second and third-generation working fluids (Cavallini, 2020). While the double C=C bond reduces the atmospheric lifetime of HFOs, it also leads to flammability problems. Thus, some of these fluids are classified with the safety class A2L. More importantly, the number of available HFOs does not seem to cover the full range of working fluids needed in different applications. Finally, the environmental effects of HFOs seem not to be fully understood, especially regarding the break down remains of HFOs in the atmosphere.

The move away from chlorine in the third generation (HFCs) resolved ODP problems, but the problem with GWP remains. On the other hand, if the fluid is to be saturated with hydrogen (Hydrocarbon) this increase the flammability of the fluid. Therefore, the challenge of reducing GWP<sub>100</sub> of working fluids is hindered by the physical and chemical limitations of available components. McLinden et al. (2017) concluded that there are only a few pure fluids that have the properties necessary for a refrigerant fluid and a majority of them have already been considered or used as refrigerants. Thus, it is implausible that there will ever be a fifth generation of refrigerants. A simplification of this argument is visualized in Figure 2.2. This figure shows CFCs that were fully halogenated with chlorine and fluorine, lead to long atmospheric life and ozone depletion potential. On the other hand, HFCs suffer from high GWP and fluids being saturated with hydrogen are flammable.

Meanwhile, global warming compounded with economic growth and urbanization are leading to a greater demand for refrigeration, air conditioning, and heat pump systems. This leads to a conflicting result that while we need to use more refrigeration, air conditioning and heat pump systems, we should also use less working fluids.

At present, it seems that the most sensible option is the return of the natural

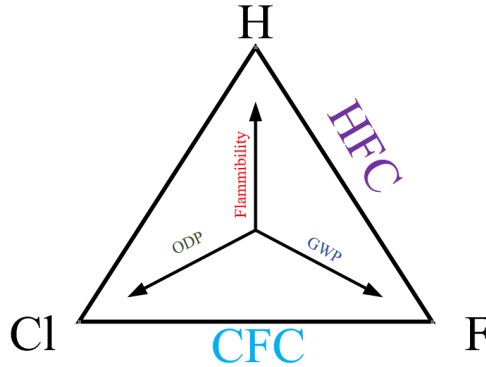


**Figure 2.2:** A simplified visualization of adverse effects of working fluids being saturated with chlorine, fluorine and hydrogen.

working fluids. While the first generation of the working fluids had many safety issues, now almost all issues could be reliably solved with the use of proper technology. Some of the most prominent natural working fluids and the third-generation fluids they can possibly replace are presented in Table 2.2.

**Table 2.2:** Alternative natural working fluid substitutes for the third generation of working fluids.

Third generation fluid ( $GWP_{100}$ )	Alternative Natural working fluid ( $GWP_{100}$ )	Name	Safety class
	R290 (3)	Propane	A3
R134a (1300)	R600a (2)	Isobutane	A3
	R1270 (2)	Propylene	A3
R407C (1624)	R1270 (2)	Propylene	A3
	R744 (1)	Carbon dioxide	A1
R404A (3943)	R717 (1)	Ammonia	B2L

It could be said that apart from  $\text{CO}_2$  (R744) that has vastly different thermophysical properties, the significant challenges with the use of natural working fluids are flammability and toxicity. The easiest mitigation method seems to be the reduction of charge in the system by various means, such as minimizing the volume of the heat exchangers. Therefore natural working fluids could provide a sustainable, environmentally friendly and efficient way for the future of refrigeration, air conditioning and heat pump systems.

## 2.2 Hydrocarbons as fourth generation working fluid

Hydrocarbons have been historically known to be suitable as working fluid. They were widely used in first generation of refrigerants. The major selling points for hydrocarbons can be summarized as:

- Cheap and readily available: crucial in emerging markets around the world, new generation of fluids can not be prohibitively expensive.
- Naturally occurring compounds: no harmful effects to the environment are expected.
- Zero ODP and very low GWP.
- Variety of fluids available: different fluids with vastly different saturation curves can cover most applications.
- Offering equivalent or superior performance compared to synthetic fluids (Harby, 2017).

Of course, the major drawback for the use of hydrocarbons is their flammability. In particular, the lower flammability limit (LFL) of hydrocarbons is very low (around 2% for propane). This means that any ignition or energy source where a low concentration of these compounds are available, will cause combustion. In order to deal with flammable working fluids, multiple national and international standards exist (Corberán et al., 2008). These standards pose different limitations on the amount of charge in the system. The most relevant standards are IEC 60335-2-40 and ISO 5149-1. Based on these standards, the charge in systems is limited by the following factors:

- Level of access: general occupancy, supervised occupancy, authorised access only.
- System type: direct, indirect.
- System use: systems for human comfort, systems not for human comfort.
- Volume of the room.
- Ventilation: availability of ventilation in machine room.
- Location of installation: mounted on window, wall, ceiling or floor.
- Lower flammability of the gas used.

The lowest allowable charge, in this case, would be for a general occupancy room that has a direct system not used for human comfort. In this condition the allowable charge is lower flammability limit [ $\text{kg m}^{-3}$ ] multiplied by the room volume [ $\text{m}^3$ ]. If one were to consider the minimum volume of a room to be  $4 \text{ m}^3$  and the LFL of propane to be  $0.038 \text{ kg m}^{-3}$ , (Corberán et al., 2008), the allowable charge would be 152 g. This value of 150 g of charge is thus known to be the maximum allowable charge where no limitation would apply to the system and the system could be used anywhere. Unfortunately, this value is too low for most applications and limits the use cases of hydrocarbon. For most domestic applications, between 0.3 to 1.0 kg of charge is required. Interestingly, one of the few applications where the charge limitations can be easily met is the domestic refrigerators/freezers that typically have less than 100 g of charge. Thus, most of the refrigerators/freezers units sold in Europe today utilize R600a (isobutane) as the working fluid (Calleja-anta and Sanchez, 2020). Nevertheless, despite efforts to reduce the charge of hydrocarbon in HVAC systems (Andersson et al., 2018; Dankwerth et al., 2019, 2020), the charge necessary for hydrocarbons in most applications is higher than the safety limits.

While risk analysis has been performed on these systems showing that with careful installation, reaching the lower flammability limit is improbable (Tang et al., 2018), concerns remain. On the other hand, it could be argued that the risk of using A2L refrigerants without the proper brazing processes and hermetic compressors is much higher than a system with A3 refrigerant and proper installation and hermetic equipment.

For domestic applications, the most relevant hydrocarbons are propane (R290), isobutane (R600a) and propylene (R1270). These three fluids offer a large range of pressures and saturation temperatures. Notable physical characteristics of these fluids are summarized in Table 2.3.

**Table 2.3:** Chemical properties of the hydrocarbons of interest for use as working fluid in domestic applications.

	Unit	Range/Value		
		R290	R600a	R1270
Chemical formula	[-]	$\text{C}_3\text{H}_8$	$\text{C}_4\text{H}_{10}$	$\text{C}_3\text{H}_6$
Molecular weight	$[\text{g mol}^{-1}]$	44.1	58.12	42.08
LFL	$[\% \text{Vol}]$	2.2	1.8	2
UFL	$[\% \text{Vol}]$	10	9.8	11.2
Auto ignition temperature	$[\text{°C}]$	470	460	485
NBP	$[\text{°C}]$	-42.1	-11.7	-47.7
Critical temperature	$[\text{°C}]$	96.7	134.7	91.8
Critical pressure	$[\text{bar}]$	42.5	36.4	46.1

An examination of the data in Table 2.3 shows that the properties related

to flammability for all three fluids to be relatively similar. On the other hand, the physical characteristics of the three fluids seem to be different, especially for R600a. The higher Normal Boiling Point (NBP) of R600a limits its application in low-temperature use cases, as in temperatures lower than  $-11.7\text{ }^{\circ}\text{C}$  the system would work partially under atmospheric pressure and there is a risk of air leaking into the system. R1270 and R290 seem to have closer properties, but the higher critical pressure of R1270 allows for working in higher pressures.

## 2.3 State of the art on hydrocarbon two phase flow

Thonon (2008) reviewed the literature on hydrocarbon heat transfer in compact heat exchangers noting that there is a need for more experimental data on in-tube flow boiling of hydrocarbons, especially in the case of microfinned tubes. In a more recent review of evaporation and condensation of hydrocarbons by Moreira et al. (2021), flow characteristics in convective and micro sized channels from multiple sources are gathered. The authors concluded that essential parameters for system design such as HTC and pressure drop have been studied by a small number of independent laboratories and data for them is scarce, thus a broader experimental database for assessment of hydrocarbon two phase behaviour is essential.

Prior research on evaporation of hydrocarbons has mainly focused on tubes of around 10 mm (Lee et al., 2005; Shin et al., 1997; Wang et al., 2014). Pamitran et al. (2010) examined the HTC of propane in stainless steel tubes of 1.5 and 3.0 mm internal diameter ( $d_i$ ) and developed a correlation based on the experimental results. Maqbool et al. (2013) investigated the evaporation of propane in a vertical circular minichannel with  $d_i$  of 1.70 mm; they reported that the HTC increases with heat flux and saturation temperature while the effect of mass flux and vapor quality is insignificant. de Oliveira et al. (2018) determined HTC and studied flow patterns of propane flowing in a tube with  $d_i$  of 1.0 mm at saturation temperature of  $25\text{ }^{\circ}\text{C}$ , and the results show a high dependency of HTC on mass flux and heat flux. More recently, Lillo et al. (2018) studied the vaporization of R290 in a tube with  $d_i$  of 6 mm at high saturation temperatures. They noted that the main heat transfer mechanism seems to be nucleate boiling, while correlations of Bertsch et al. (2009) and Friedel (1979) predicted their results for HTC and pressure drop most accurately. Longo et al. (2017a) compared the evaporation of R290 and R1270 with R404A in a small diameter tube showing that R404A and R1270 exhibit the highest HTC and lowest pressure drop, while R290 is affected by a particularly low dryout quality. There have also been several studies investigating mixtures of hydrocarbons. Wen and Ho (2005) conducted experiments with propane, butane and a mixture of them flowing in a tube with  $d_i$  of 2.46 mm, and results showed that the HTC was significantly improved compared to R134a as a working fluid. Zou et al. (2009) studied mixtures of R170 and R290 and their evaporation characteristics, proposing a correlation for prediction of

HTC. Kedzierski and Kim (1997) analyzed heat transfer of various refrigerants and their mixtures, including R290 and R134a, in a tube with  $d_i$  of 9.64 mm tube containing a twisted tape insert.

Macdonald and Garimella (2016a) studied condensation of propane in two tubes with  $d_i$  of 14.45 mm and 7.75 mm in a broad range of saturation temperature, showing that HTC is slightly dependent on diameter while the effect of saturation temperature is much more pronounced on pressure drop. The same authors utilized the obtained data to develop HTC and pressure drop correlations (Macdonald and Garimella, 2016b). Lee et al. (2006) studied the condensation of three hydrocarbons, namely, R290, R1270, and R600a comparing them to R22 in smooth tubes with  $d_i$  of 12.7 and 9.52 mm. Authors noted that HTC of hydrocarbons was higher by at least 31% compared to R22, while their pressure drop was larger by at least 50%. Del Col et al. (2012) studied the condensation of R290 in a microchannel with an internal bore of 0.96 mm, showing a satisfactory agreement with the predictive methods. Ağra and Teke (2008) reported experimental results for condensation of R600a in a smooth tube with  $d_i$  of 4 mm, observing that the flow was in annular form. Qiu et al. (2020) simulated the condensation of R290 in minichannels with diameters ranging from 0.5 to 2 mm, visualizing the different flow patterns and the effect of flow on heat transfer and pressure drop characteristics. In another numerical study by Wen et al. (2018), the authors have compared condensation performance of R1234ze(E), R134a, and R290 in a tube with  $d_i$  of 1.0 mm, reporting that R290 had a lower tendency to be stratified at lower vapor qualities. Longo et al. (2017b) studied the condensation of R404A and compared them to suitable hydrocarbon substitutes, namely, R290 and R1270, reporting that the hydrocarbons generally had a higher HTC while the pressure drop was lower compared to R404A, thus proving themselves to be promising candidates as a long term substitute. In a later publication, (Longo et al., 2018) included data for R600a, noting that, while R600a has a higher HTC, its pressure drop is significantly higher.

Several studies have dealt with the effect of enhanced geometries of different fluids. Cho and Kim (2007) compared the evaporation characteristics of CO<sub>2</sub> in smooth and microfinned tubes with outer diameter ( $d_o$ ) of 9.52 and 5 mm showing that the HTC in microfinned tubes increased by up to 210%, whilst the pressure drop increase was up to 1.9 times. Celen et al. (2018) investigated evaporation of R134a in smooth and microfinned tubes, showing that the pressure drop is increased by up to 3 times while the heat transfer coefficient is increased by 1.9 times. Colombo et al. (2012) observed the flow patterns, characteristics of evaporation and condensation of R134a in one smooth and two microfinned tubes showing that both microfinned tubes increase the HTC compared to the smooth tube and found no differences among them. Bandararra Filho et al. (2004) compared experimental results for the pressure drop of R134a in smooth and grooved tubes and developed a correlation based on the results. Bashar et al. (2020) studied condensation of R1234yf inside smooth and microfinned tubes with  $d_o$  of 2.5 mm,

showing that the HTC increase in microfinned tube can be up to 3.85 times. Diani et al. (2020) compared the condensation of R513A in a smooth tube with  $d_i$  of 3.5 mm to a microfinned tube with  $d_i$  of 3.4 mm, showing that the HTC can be up to 4.5 times higher in the microfinned tube in lower mass fluxes, while, at higher mass fluxes, this increase tends asymptotically towards the increase in the heat transfer area provided by the fins. Condensation of R134a, R22, and R410A in microfinned tubes with  $d_i$  ranging between 8.92 to 4 mm was studied by Han and Lee (2005) showing enhancement of HTC and penalization in the pressure drop having the same tendencies with increases in mass flux and vapor quality. The authors proposed a new correlation for the prediction of pressure drop and HTC.

There are few studies dealing with the effect of enhanced surfaces in evaporation and condensation of hydrocarbons. Nan and Infante Ferreira (2000) studied evaporation and condensation of propane in a smooth, microfinned, and crosshatched tube with  $d_o$  of 9.52 mm. Their results showed the increase in HTC seems to be more noticeable at higher mass fluxes and correlations for internally enhanced tubes considerably over predicted their experimental data. Furthermore, Wen et al. (2014) studied the boiling of R600a in a tube with porous inserts showing that while HTC increases compared to a smooth tube, the relative increase of pressure drop is much higher. Thus, while the state of the art for experimental results on two phase flow of refrigerants is rather extensive, there seems to be a lack of data regarding different surface enhancements and comparison with smooth tubes, specially for hydrocarbons. Furthermore, the benefits and drawbacks of the use of internally enhanced tubes in relation to charge and capacities are not fully understood and not compared to indirect systems either.

## 2.4 Summary

Hydrocarbons are an integral part of the fourth generation of working fluids in refrigeration, air conditioning and heat pump (RACHP) systems. Nevertheless, hydrocarbon utilization in many systems requires special attention to the amount of charge in the system. Smaller diameter tubes with enhanced internal surfaces can lead to more efficient and compact heat exchangers with lower charges. While there have been several studies on two-phase flow characteristics of hydrocarbons in smooth tubes, and others have analyzed the effect of internally enhanced tubes on different fluids, there have not been any studies on the effect of internal surface enhancement for hydrocarbons. Moreover, it seems that the comparison between different types of microfinned tubes is not available. It is crucial to have reliable experimental data to properly design and size heat exchangers, especially in applications where the amount of charge is limited by regulations. Since no experimental data are available to examine the correlations' accuracy, the predictive methods can be unreliable.



## Chapter 3

# Experimental Setup

### 3.1 Test rig

A test rig that was already available for a similar project at the Thermal lab of the Department of Energy and Process Engineering of Norwegian University of Science and Technology was extensively modified to perform measurements of pressure drop and heat transfer coefficient. A photograph of the test rig is shown in Figure 3.1. The test rig was the same for both condensation and evaporation with the exception of the test section. Figures 3.2 and 3.3 present the schematic of the test rig, for evaporation and condensation tests, respectively, and how the test section was changed in order to accommodate the cooling water loop. For safety reasons, the whole test section was placed inside a plastic enclosure and connected to an air suction fan. This ensures that in case of any leakage, the hydrocarbon in the enclosure does not reach lower flammability levels.



**Figure 3.1:** Photograph of test rig.

The test fluid is circulated through the system by a gear pump. Mass flow is measured downstream of the pump. By measurement of the pressure and temperature before the preheater and temperature after the preheater, the energy required to vaporize the fluid to the desired inlet quality is calculated. This energy is provided to the fluid in the preheater by means of electrical heating controlled by Pulse Wave Modulation (PWM).

Before the test section, there is an adiabatic calming section of 75 mm. The pressure drop is directly measured by a differential pressure transducer via pressures taps 547 mm away from each other at the inlet and outlet of the test section. The length of the heated section of all the tested tube is 500 mm. Two pressure sensors are connected to the test section using the same pressure taps for the differential pressure transducer. Average value of these two pressure sensors provides the saturation pressure at test section, and the fluid saturation temperature is determined from this saturation pressure.

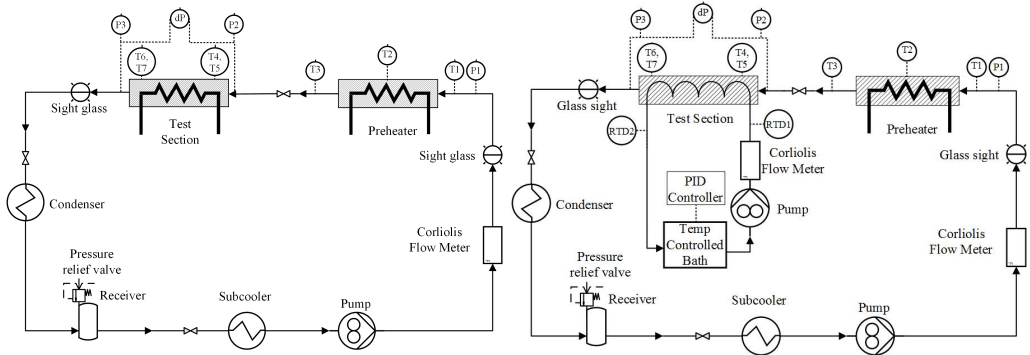


**Figure 3.2:** Test rig schematic for evaporation test section.

**Figure 3.3:** Test rig schematic for condensation test section.

### 3.1.1 Evaporation test section

An electrical heating cable is used as the heating source in the test section. For uniform distribution of heat to the test tube, a larger diameter tube is used and the space between the outer tube and the test tube is filled with molten tin. Heat input for both the preheating section and test section is controlled using PWM. The wall temperature is obtained from two pairs of thermocouples brazed to the tube wall located 100 mm from the inlet and outlet of the heated test section. These thermocouples are attached to the outer wall of the test tube by silver brazing. Contact between the thermocouples and the tube is ensured by the use of silver brazing as it has a higher melting temperature than tin. At each location, one thermocouple is in contact with the top and the other with the bottom part of the test tube. In order to minimize the heat loss, the test section was insulated using perlite and then contained by hard insulation. One of the test sections is

photographed and shown in Figure 3.4.



**Figure 3.4:** Photograph of evaporation test section.

### 3.1.2 Condensation test section

The test rig was modified to allow condensation tests. The setup for condensation has two loops, one for the refrigerant and one for the secondary cooling fluid. Heat is removed from the test section by distilled water flowing through a helical tube wound around the test section. The helical tube geometry for water loop was optimized utilizing Ansys Fluent simulation with the goal of maximizing the temperature difference between the inlet and outlet to lower the measurement uncertainty while providing a uniform heat flux. The condensation was simulated by imposing a heat transfer coefficient and a saturation temperature while the tube diameter and length were varied at different water mass flows. The internal diameter for the cooling water tube was 4.9 mm with a length of 950 mm. The space between the helical tube for secondary fluid and the test tube was filled with molten tin. Silver brazing was used for thermocouples ensuring contact between the tube and the thermocouples as silver has a higher melting temperature than tin. The water temperature is measured before and after the test section using two RTD elements. Using the temperature difference, the specific heat capacity and water mass flow, the heat removed from the test section can be calculated. Based on the results from the numerical simulation and uncertainty analysis, the water flow rate was set at roughly around 1180 mL/min. The heat flow to the test section was controlled by the temperature of water thermostatic bath through a PID controller. The set point for the PID was a heat flow of 155 W, giving a temperature difference of around 2 °C. A photograph of one of the test sections is shown in Figure 3.5, while the cooling loop is visualized in Figure 3.6.

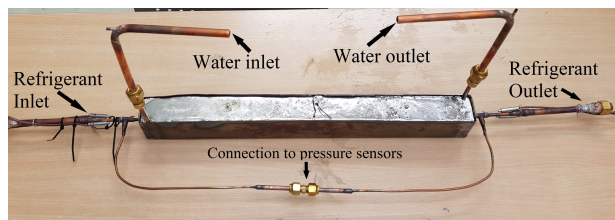


**Figure 3.5:** Photograph of condensation test section.

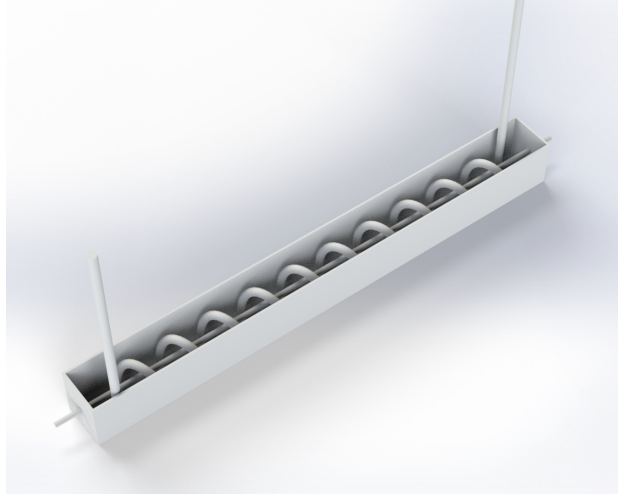


**Figure 3.6:** Visualization of the internal helical cooling loop for the condensation test section.

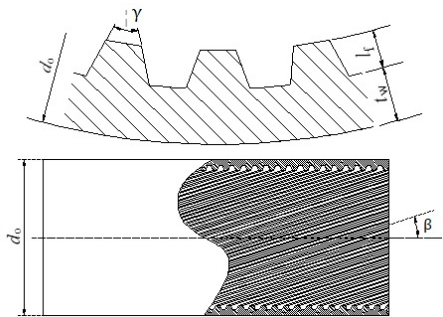


**Figure 3.7:** Physical presentation of the geometrical parameters of the microfinned tubes.

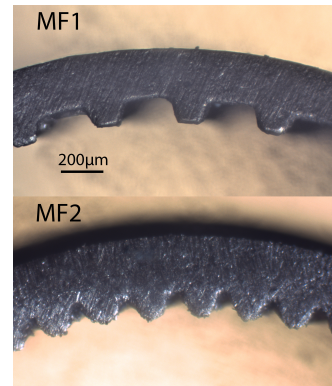


**Figure 3.8:** Cross sectional view of the microfinned tubes.

### 3.1.3 Test Tubes

One smooth tube and two internally enhanced tubes, all with an outer diameter ( $d_o$ ) of 5 mm, were studied. Table 3.1 reports geometrical parameters for the tubes. Physical representations of geometrical parameters are presented in Figure 3.7. While the fin dimensions for the two microfinned tubes are approximately the same, MF2 has a higher number of fins and spiral angle, leading to a higher available area for heat transfer. A cross-sectional view of the two tested microfinned tubes is shown in Figure 3.8.

The calculation of parameters such as heat flux and mass flux is dependent on the definition of internal diameter  $d_i$ . While for the smooth tube, this definition is

**Table 3.1:** Geometrical parameters of the test tubes and test sections.

	Unit	Smooth tube	MF1	MF2
Outer diameter ( $d_o$ )	mm	5	5	5
Internal diameter <sup>a</sup> ( $d_i$ )	mm	4.1	4.32	4.26
Wall thickness <sup>b</sup> ( $t_w$ )	mm	0.45	0.22	0.22
Actual cross sectional area	mm <sup>2</sup>	13.2	15.7	14.8
Effective diameter <sup>c</sup>	mm	-	4.47	4.34
Fin height ( $l_f$ )	mm	-	0.12	0.15
Fin number ( $n$ )	[-]	-	35	56
Fin angle ( $\gamma$ )	°	-	35	15
Spiral angle ( $\beta$ )	°	-	15	37
Heat exchange area ratio ( $R_x$ )	[-]	1	1.51	2.63
Heated test section length	mm		500	
Pressure drop measurement length	mm		547	
Test section length	mm		1005	

<sup>a</sup> Internal diameter for smooth tube, fin tip diameter for microfinned tubes.

<sup>b</sup> Length between fin root and outer diameter.

<sup>c</sup> Equivalent diameter for a smooth tube to have same actual cross section area.

unambiguous, for MF tube, different internal diameters can be defined. Namely fin root diameter, fin tip diameter, and effective diameter, where the effective diameter is the equivalent diameter for a smooth tube with the same actual cross-section area. All three internal diameters for MF tubes are reported in Table 3.1 but only fin tip diameter was considered for the data reduction process. The reason for this was the simplicity of the measurement process in the field and compatibility with predictive methods. This choice is critical and should be kept constant across tests. It should be noted that because of this definition, the values reported for mass flux and heat flux are not the actual values. Nevertheless, the simplicity of measurement and comparison with other correlations outweigh the slight deviation from the actual values. The increase in internal area for MF tubes compared to a smooth tube with the same fin tip diameter is calculated using the  $R_x$  value defined as:

$$R_x = \left\{ \frac{2 \cdot l_f \cdot n \cdot [1 - \sin(\gamma/2)]}{\pi \cdot D \cdot \cos(\gamma/2)} + 1 \right\} \cdot \frac{1}{\cos \beta} \quad (3.1)$$

This value is not directly used in the data reduction process, thus, values such as heat flux for MF tubes were calculated based on a smooth tube with the internal diameter equivalent to fin tip diameter.

### 3.1.4 Instruments

An overview of the instruments used in the evaporation and condensation test rig are given in Tables 3.2 and 3.3, respectively. Most equipment such as pumps and DAQ were reused in the condensation setup, but several components had to be changed to meet the different requirements. Most notably, for condensation of R1270 and R290, the pressure sensors were changed to accommodate higher pressures. To reduce uncertainty, the pressure sensors used for condensation of R600a were the same as those in evaporation tests. This is due to the fact that the uncertainty of measurement for pressure sensor depends on the full range of sensor and R600a has a lower condensation pressure.

**Table 3.2:** List of instruments used for evaporation tests and their respective uncertainties.

	Type	Range	Uncertainty
Flow meter	Coriolis	0-5 kg min <sup>-1</sup>	± 0.1% <sup>a</sup>
Absolute pressure sensor	Strain gauge	0-10 bar	± 0.16% <sup>b</sup>
Differential pressure sensor	Strain gauge	0-0.5 bar	± 0.15% <sup>b</sup>
Thermocouples	Type T	-	± 0.05 K
Preheater	Electrical	3450 W	±0.44% <sup>a</sup>
Test section heater	Electrical	620 W	± 0.55% <sup>a</sup>

<sup>a</sup> Of the reading <sup>b</sup> Of the set span

**Table 3.3:** List of instruments used for condensation tests and their respective uncertainties.

	Type	Range	Uncertainty
<b>Refrigerant Circuit</b>			
Flow meter	Coriolis	0-5 kg min <sup>-1</sup>	± 0.1% <sup>a</sup>
Absolute pressure sensor <sup>c</sup>	Strain gauge	0-10 bar	± 0.16% <sup>b</sup>
Absolute pressure sensor <sup>d</sup>	Strain gauge	0-20 bar	± 0.16% <sup>b</sup>
Differential pressure sensor	Strain gauge	0-0.5 bar	± 0.15% <sup>b</sup>
Thermocouples	Type T	-	± 0.05 K
Preheater	Electrical	3450 W	±0.44% <sup>a</sup>
<b>Cooling Water Circuit</b>			
Flow meter	Coriolis	0-5 kg min <sup>-1</sup>	± 0.1% <sup>a</sup>
RTD	PT 100	-	± 0.05 K

<sup>a</sup> Of the reading <sup>b</sup> Of the set span

<sup>c</sup> Used for R600a <sup>d</sup> Used for R1270 and R290

All data acquisition was performed with equipment from National Instrument (NI cDAQ 9179) and LabVIEW software. Heat input both at preheater and test section is controlled with a PWM where the input voltage (National Instruments

NI-9225) and current (National Instruments NI-9246 and National Instruments NI-9227 for preheater and test section, respectively) is measured at 50 kHz to obtain the power input. The values reported in Table 3.2 for the uncertainty of measurement of the preheater and test section heater and in Table 3.3 for the uncertainty of measurement of the preheater are based on the reported uncertainty values for voltage and current measurement units. The uncertainty of measurement for the condensation test section had to be calculated based on the coolant mass flow rate and its temperature gradient.

## 3.2 Validation and heat leakage tests

In order to ensure the results from the test rig are reliable, validation tests were performed. HTC was validated for both condensation and evaporation systems while the pressure drop was only validated for evaporation system. The reason for this was that the measurement system for pressure drop was the same in the evaporation and condensation test section.

### 3.2.1 Validation of evaporation tests

All validation tests were performed for the smooth tube. As the instruments used for the microfinned tubes are the same as the ones for smooth tube, the results from microfinned tubes are also considered to be reliable. For single-phase validation, there were three possibilities: liquid propane flow, gas propane flow, or use of another fluid. Safety limitation on the amount of charge in the system made it unfeasible to perform liquid propane flow; therefore, gas single-phase flow was implemented for validation.

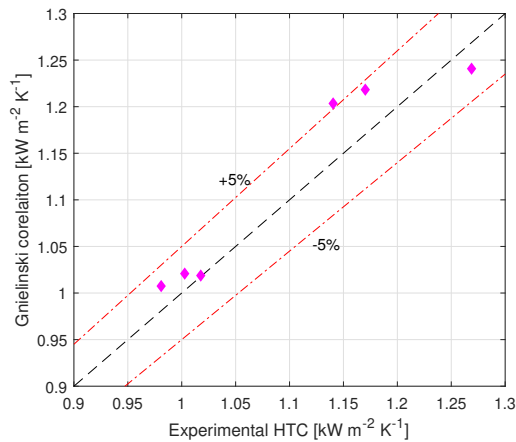


**Figure 3.9:** Validation of the experimental data for HTC of single phase gas flow of propane in the evaporation test section against the correlation of Gnielinski, at varying Reynolds number.

Because of the limitations on the test rig, more specifically, the temperature of the heater, the range of tests performed both in Reynolds number and the value of HTC are limited. Furthermore, as HTC was low, it meant that for obtaining a single data point, the system had to work over or very close to its limit for extended periods of time (in some cases more than 4 hours). Therefore, to further validate the system, it was decided to use another fluid, namely water. Still, as it would be impossible to remove water from the system once introduced, the test section was disconnected from the main test rig, connected to an auxiliary system, and tests were performed. The results were in line with the single-phase propane tests, but as separate instruments were used for measurement of liquid water HTC (for example, water mass flow meter), these data were not included in any of our reports.

Pressure drop validation was performed with gaseous propane, but as these tests were run in adiabatic condition, the limitations from HTC validation tests did not apply. Figure 3.10 presents the pressure drop validation data in single phase gas flow of propane.

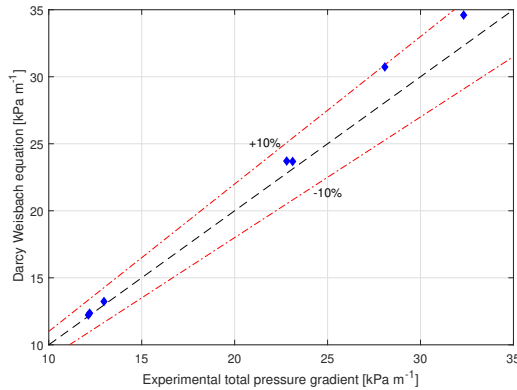


**Figure 3.10:** Comparison of the experimental data for pressure drop with the equation of Darcy Weisbach for single phase gas flow of propane.

Regarding the heat loss, the test section was insulated using perlite and then contained by hard insulation. To inspect the effectiveness of the insulation, a thermal camera was used to visualize the temperature distribution and detect any hot spots. The heat loss was accounted in the calculation steps as  $Q_{loss}$ , these values are based on the difference between the ambient temperature and a thermocouple in contact with the electrical heating tape around the test section. Several tests were performed at vacuum conditions to evaluate heat leakage at different heat fluxes. The results showed a fairly linear relationship between the temperature difference of the heating element and environment and the heat loss to the environment, taken into account by the following equation:

$$Q_{loss} = 0.2075 \cdot (T_{element} - T_{amb}) - 0.2925 \quad [W] \quad (3.2)$$

### 3.2.2 Validation of condensation tests

Similar to evaporation validation tests, condensation validation tests were performed for the smooth tube only. For single-phase validation, the safety limits on the amount of charge in the system made it unfeasible to perform tests with liquid flow; therefore, gas single-phase isobutane flow was implemented for validation.

While the limitations on the test rig, more specifically, the preheater's temperature, still applied to the condensation test section, the removal of heat from test section using water enabled validation of the test section in a broader Reynolds number range. Figure 3.11 shows the data for comparison of HTC values of gaseous isobutane with the correlation of Gnielinski at varying mass flow rates. The data in Figure 3.11 show that there is a downward trend in the value of error with increasing mass fluxes, but this should be considered with increased values of uncertainty. At lower mass fluxes for isobutane, the amount of heat exchanged was lower and thus, the water flow should also have been reduced to keep the same water temperature difference. However, this was not possible without departing from turbulent flow and creation very long thermal equilibrium lengths. Thus, the flow rate was kept high, causing the temperature change on the waterside to be lower and leading to higher uncertainty.

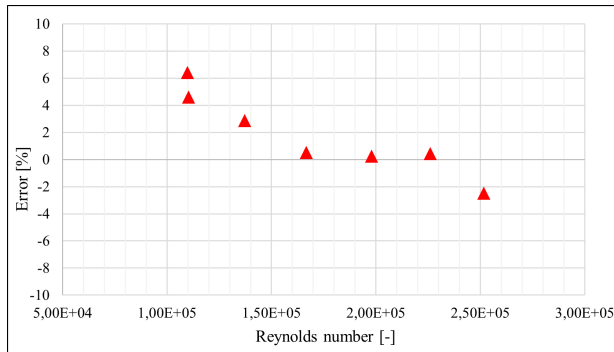


**Figure 3.11:** Validation of the experimental data for HTC of single phase gas flow of isobutane in condensation test section against the correlation of Gnielinski, at varying Reynolds number.

The value of heat loss is based on the difference between the ambient temperature and a thermocouple in contact with the test section's surface beneath the insulating material. Tests were performed at surface temperatures ranging from 29 to 49°C. The results showed a fairly linear relationship between the temperature difference of the test section's surface and the environment to the heat loss. It should be noted that because of small values of heat exchanged in these tests, the water flow regime was laminar creating uneven temperatures in the test section based on the developing thermal boundary layer. This was considered an acceptable compromise as the value of heat loss in the test rig working conditions rarely climbed above 2 W or 1% of heat input since the test section's surface

temperature was relatively close to ambient temperature. The linear relationship based on the ambient and test section's surface temperature difference, can be formulated by equation 3.3.

$$Q_{loss} = 0.602 \cdot (T_{element} - T_{amb}) + 0.145 \quad [W] \quad (3.3)$$

### 3.3 Calibration Process and Uncertainty Propagation

In order to calibrate the thermocouples, AMETEK JOFRA RTC 157 Reference Temperature Calibrator with the procedure advised by the manufacturer has been used. This unit has an accuracy of  $\pm 0.04$  °C and stability of  $\pm 0.005$  °C. The thermocouples were connected in the same manner as the testing condition (same cables, connections, DAQ) and the values were read each five degrees in the desired temperature range ( $-10$  °C to  $30$  °C). The same procedure was used to calibrate the RTD elements in a temperature range of  $-20$  to  $70$  °C. The obtained data from the calibration process were used to create a calibration file in LabVIEW.

Below, the formulation used for propagation of uncertainty is summarized. Uncertainty for wall temperature:

$$u(T_w) = \sqrt{(1/4)^2 \cdot \sum_{i=4}^7 u(T_i)} \quad (3.4)$$

Uncertainty for Saturation temperature:

$$u(T_{sat}) = \sqrt{\left(\frac{\partial T_{sat}}{\partial P_{sat}}\right)^2 \cdot u(p_{sat})^2} \quad (3.5)$$

From the Antoine equation, the relationship between saturation temperature and saturation pressure can be found; by derivation, it can be written:

$$\left(\frac{\partial T_{sat}}{\partial P_{sat}}\right) = \frac{803.99}{P_{sat} \cdot (3.9228 - \log_{10}(P_{sat}))} \quad (3.6)$$

Uncertainty for heat transfer coefficient:

$$u(h) = \sqrt{\left(\frac{u(Q_{test})}{T_w - T_{sat}}\right)^2 + \left(\frac{Q_{test} \cdot u(T_w)}{(T_w - T_{sat})^2}\right)^2 + \left(\frac{Q_{test} \cdot u(T_{sat})}{(T_w - T_{sat})^2}\right)^2} \quad (3.7)$$

where the uncertainty of the heat input is calculated as:

$$u(Q_{test}) = [u(\dot{m}_{water}) \cdot c_{P_{water}} \cdot (RTD_2 - RTD_1)]^2 + (\dot{m}_{water} \cdot c_{P_{water}})^2 \cdot (u(RTD_1)^2 + u(RTD_2)^2)]^{0.5} \quad (3.8)$$

Uncertainty for inlet vapor quality:

$$u(x_{in}) = \sqrt{\left(\frac{u(Q_{pre})}{\dot{m} \cdot i_{lg}(P_1)}\right)^2 + \left(\frac{Q_{pre} \cdot u(\dot{m})}{i_{lg}(P_1) \cdot \dot{m}^2}\right)^2} \quad (3.9)$$

Uncertainty for the change in vapor quality:

$$u(\Delta x) = \sqrt{\left(\frac{u(Q_{test})}{\dot{m} \cdot i_{lg}(P_{sat})}\right)^2 + \left(\frac{Q_{test} \cdot \ln(\dot{m}) \cdot u(\dot{m})}{i_{lg}(P_{sat})}\right)^2} \quad (3.10)$$

Uncertainty for the average vapor quality:

$$u(x) = \sqrt{u(x_{in}) + 1/4 \cdot u(\Delta x)^2} \quad (3.11)$$

### 3.4 Data Reduction

The data were recorded after the system was considered in steady state with a definition of the standard deviation of the last 15 samples being lower than 0.1°C. The data from the sensors were recorded for over 120 seconds, which were then averaged. The average vapor quality is calculated by Equation 3.12:

$$x = x_{in} \pm \frac{\Delta x}{2} = \frac{Q_{pre} - \dot{m} \cdot (i_{sat,l} - i_1)}{\dot{m} \cdot i_{lg}(p_{pre})} \pm \frac{Q_{test} - Q_{loss}}{2 \cdot \dot{m} \cdot i_{lg}(p_{sat})} \quad (3.12)$$

Where the sign for  $\Delta x/2$  is positive for evaporation test and negative for condensation tests.  $i_1$  is the enthalpy of subcooled fluid before entering the preheater,  $p_{pre}$  is the pressure at the preheater section and  $p_{sat}$  is the arithmetic average of the inlet and outlet pressure in the test section. In the evaporation test,  $Q_{test}$  is obtained directly from voltage and current of the heater while for the condensation test section the heat removed from the test section by the cooling water was calculated by Equation 3.13:

$$Q_{test} = \dot{m}_{water} \cdot c_{P_{water}} \cdot (RTD_2 - RTD_1) \quad (3.13)$$

Where  $RTD$  are thermoresistors located upstream and downstream of cooling water. The specific heat capacity of water,  $c_{P_{water}}$ , is obtained based on the average temperature of cooling water.

Heat transfer coefficient is calculated using Equation 3.14:

$$HTC = \frac{Q_{test} - Q_{loss}}{S (T_{sat} - \bar{T}_w)} \quad (3.14)$$

Where  $Q_{loss}$  is calculated based on formulation obtained from heat leakage tests and the surface temperature of test sections.  $T_{sat}$  is derived from the saturation pressure,  $p_{sat}$ . Average Wall temperature,  $\bar{T}_w$ , and Surface area,  $S$ , are defined as:

$$\bar{T}_w = \frac{1}{4} \sum_{i=1}^4 T_{w,i} \quad (3.15)$$

$$S = \pi d_i L \quad (3.16)$$

The thermal resistance of the copper wall was taken into account by considering a radial heat conduction in a cylindrical shell using the formula:

$$T_w = T_{\text{thermocouple}} - \frac{(Q_{\text{test}} - Q_{\text{loss}}) \cdot \ln \frac{d_o}{d_i}}{S \cdot k_{\text{copper}}} \quad (3.17)$$

The total pressure drop  $\Delta p$  is calculated by addition of momentum pressure drop  $\Delta p_a$  with frictional pressure drop  $\Delta p_f$ . It should be noted that in condensation settings, momentum pressure drop is negative which leads to a pressure gain.

$$\Delta p = \Delta p_f + \Delta p_a \quad (3.18)$$

The void fraction in the momentum pressure drop calculation was determined using Rouhani and Axelsson (1970) correlation and could be formulated as:

$$\alpha = \frac{x}{\rho_g} \left[ (1 + 0.12 \cdot (1 - x)) \left( \frac{x}{\rho_g} + \frac{1 - x}{\rho_l} \right) + \frac{1.18 \cdot [g \cdot \sigma (\rho_l - \rho_g)]^{0.25}}{G \cdot \rho_l^{0.5}} \right]^{-1} \quad (3.19)$$

# Chapter 4

## Summary of Research Work

### 4.1 Organization of articles

This section aims to provide a summary of the research work presented in the annex of this thesis. Table 4.1 shows the experimental data presented in each article. While the experimental data for evaporation is divided into two papers, all condensation data is reported in one journal article.

**Table 4.1:** Content and organization of the experimental data as journal papers presented in the appendix.

	R290	R600a	R1270
Evaporation	Article I	Article II	Article II
Condensation	Article III	Article III	Article III

In addition to the three first articles presenting the experimental data, Article IV uses numerical simulation methods to calculate the charge in different heat exchangers. A brief overview of the articles and main conclusions are reported here.

### 4.2 Article I: Characteristics of evaporation of propane (R290) in compact smooth and microfinned tubes

The first paper in this series of studies is focused solely on development of a test setup for evaporation of propane and reporting the results for it.

**HTC:** The saturation temperature did not seem to have a notable effect on HTC. The heat flux increases the HTC in lower vapor qualities both for smooth and MF tubes. Mass flux, on the other hand, has a marginal effect on HTC, especially in MF tubes. These findings are in accordance with a fluid that has

nucleate boiling as the dominant heat transfer mechanism.

**Pressure drop:** Lower saturation temperatures led to higher pressure drop because of higher shear stress caused by lower gas density. Heat flux did not have a notable effect. The determining factor in pressure drop was mass flux.

**Internal surface:** HTC and pressure drop of the microfinned tube were compared against the smooth tube showing that the increase of HTC was highest at the lowest tested mass flux and decreasing asymptotically toward the value for increased surface area for the tube MF1. The effectiveness of the MF2 tube in increasing HTC is lower than its increased area, pointing to a maximum beneficial increased area. Pressure drop values increased by the same value irrespective of the mass flux. Increased mass flux does not create extra turbulence to increase HTC for microfinned tubes, in the way that it happens for smooth tube, thus making the use of microfinned tubes most beneficial at lower mass fluxes.

**Correlations:** Pressure drop and HTC of the smooth tube were reliably predicted by Xu and Fang (2012) and Liu and Winterton (1991), respectively. Pressure drop and HTC for microfinned tubes were best predicted by Diani et al. (2014) and Rollmann and Spindler (2016), respectively.

### 4.3 Article II: Comparative analysis of evaporation of isobutane (R600a) and propylene (R1270) in compact smooth and microfinned tubes

The second article in this study expands the experimental evaporation data to isobutane and propylene in the same test rig with minimal changes to the test rig.

**HTC:** The saturation temperature did not seem to have a notable effect on either fluids' HTC. The heat flux increases the HTC in lower vapor quality for R1270 while it does not affect R600a. On the other hand, mass flux has a considerable effect on HTC for R600a and to a lesser extent for R1270. These behaviors point to a convective dominated heat transfer regime for R600a and a nucleate boiling dominated for R1270, albeit not as strongly as R290.

**Pressure drop:** The determining factor for pressure drop is the mass flux. R600a has a higher pressure drop compared to R1270 because of the higher liquid viscosity and lower vapor density.

**Internal surface:** The increased HTC and pressure drop for microfinned tubes for R600a and R1270 follow the same pattern as R290. That is to say the increase of HTC decreases with mass flux while pressure drop increase is the same,

leading to the same conclusion of better effect of microfinned tubes in lower mass fluxes.

**Correlations:** Pressure drop and HTC of the smooth tube were reliably predicted by Xu and Fang (2012) and Liu and Winterton (1991), respectively. Pressure drop and HTC for microfinned tubes were best predicted by Diani et al. (2014) and Rollmann and Spindler (2016), respectively.

## 4.4 Article III: Condensation of Hydrocarbons in Compact Smooth and Microfinned Tubes

In the third article of this work, condensation characteristics of all three fluids of interest have been reported. The test rig has gone through significant modifications. Most notably, the test section has been completely redesigned. The effect of heat flux and saturation temperature was not tested.

**HTC:** R290 and R1270 have a relatively similar HTC, while R600a enjoys a higher HTC because of the lower vapor density and a higher convective heat transfer from the core.

**Pressure drop:** The determining factor for pressure drop is again the mass flux. R600a has a higher pressure drop compared to R1270 and R290 because of the higher liquid viscosity and lower vapor density.

**Internal surface:** The two tested microfinned tubes differentiate themselves only at lower vapor qualities. This is caused by reaching fully annular flows at different vapor qualities based on the internal geometry of the tubes. Both microfinned tubes have a lower increase of HTC in condensation compared to evaporation. HTC is dependent on mass flux for only one of the microfinned tubes.

## 4.5 Article IV: Numerical study of hydrocarbon charge reduction methods in HVAC heat exchangers

The fourth article in this study utilizes the information obtained in the prior experimental tests for a simulation of heat exchangers in a reversible HVAC system. Additionally, data for indirect water to brine HVAC systems is presented by collaboration with an external institute.

**Direct systems:** An air to air reversible HVAC unit is studied with smooth and microfinned tubes for heat exchangers. The simulation results show that mi-

crofinned tubes can reduce the total charge by 22%, while the charge in the header increases by 11%. This reduction in charge is at the cost of up to a 9% reduction in COP.

**Indirect Systems:** A brine to water reversible HVAC unit is studied with plate heat exchangers with reduced internal volume. The simulation results show that reduction of internal volume can reduce the charge by up to 68%, which is roughly the same as the rate of internal volume reduction. This reduction in charge is at the cost of up to 11% reduction in COP.

## 4.6 Summary and suggestions for future work:

The work presented in this thesis provides a comprehensive overview of two-phase flow characteristics of evaporating and condensing hydrocarbons in smooth and microfinned tubes. Results show that hydrocarbon charge in heat exchangers can be reduced effectively using microfinned tubes without a high increase in pressure drop. Additionally, the most reliable predictive methods for pressure drop and heat transfer coefficient in all tested scenarios are reported. Simulation of the heat exchangers in reversible heat pumps/air conditioning units show promising results for utilization of microfinned tube in heat exchangers to reduce the charge without affecting the capacity.

Nevertheless, other aspects can be included in the scope of future research, these could be categorized as:

- **Flow visualisation:** fluid flow visualization with a high-speed camera could provide insight into more fundamental aspects of the two phase flow.
- **Other fluids and mixtures:** while propane, isobutane and propylene are the most likely hydrocarbon working fluid candidates, other hydrocarbons and their mixtures could yield more opportunities for the use of natural working fluids and provide alternatives for synthetic refrigerants.
- **Simulation tools:** with the availability of reliable correlations for predictions of HTC and Pressure drop in this work, they should be implemented in software simulation codes for easier access and calculations.
- **Experimental testing of heat exchangers:** amount of charge in different components, especially heat exchangers, should be more accurately studied in complete HP/AC systems using experimental tests.
- **Additively manufactured heat exchangers:** could be studied for a new generation of heat exchangers with extremely low volumes and complex internal geometries leading to lower charges.

- **Maldistribution:** any novel design for the heat exchanger should be designed with classical problems of heat exchangers in mind, such as maldistribution where the heat transfer could be seriously affected.



# Bibliography

- Andersson, K., Granryd, E., and Palm, B. Water to water heat pump minimum charge of propane. In *IIR Gustav Lorentzen Conference on Natural Refrigerants*, Valencia, Spain, 2018. International Institute of Refrigeration (IIR). doi: 10.18462/IIR.GL.2018.1264.
- Ağra, Ö. and Teke, Experimental investigation of condensation of hydrocarbon refrigerants (R600a) in a horizontal smooth tube. *International Communications in Heat and Mass Transfer*, 35(9):1165–1171, nov 2008. ISSN 07351933. doi: 10.1016/j.icheatmasstransfer.2008.07.012.
- Bandarra Filho, E. P., Saiz Jabardo, J. M., and Barbieri, P. E. L. Convective boiling pressure drop of refrigerant R-134a in horizontal smooth and microfin tubes. *International Journal of Refrigeration*, 27(8):895–903, 2004. ISSN 01407007. doi: 10.1016/j.ijrefrig.2004.04.014.
- Bashar, M. K., Nakamura, K., Kariya, K., and Miyara, A. Condensation heat transfer of R1234yf in a small diameter smooth and microfin tube and development of correlation. *International Journal of Refrigeration*, 120:331–339, 2020. ISSN 01407007. doi: 10.1016/j.ijrefrig.2020.09.002. URL <https://doi.org/10.1016/j.ijrefrig.2020.09.002>.
- Bertsch, S. S., Groll, E. A., and Garimella, S. V. A composite heat transfer correlation for saturated flow boiling in small channels. *International Journal of Heat and Mass Transfer*, 52(7-8):2110–2118, 2009. ISSN 00179310. doi: 10.1016/j.ijheatmasstransfer.2008.10.022. URL <http://dx.doi.org/10.1016/j.ijheatmasstransfer.2008.10.022>.
- Calleja-anta, D. and Sanchez, D. Experimental evaluation of natural refrigerant blends as substitutes for R-600a in a domestic fridge and freezer. 2020. doi: 10.18462/iir.gl.2020.
- Cavallini, A. The state-of-the-art on Refrigerants. In *UIT conference*, volume 1599, Padova, Italy, 2020. doi: 10.1088/1742-6596/1599/1/012001.
- Celen, A., Çebi, A., and Dalkılıç, A. S. Investigation of boiling heat transfer characteristics of R134a flowing in smooth and microfin tubes. *International*

- Communications in Heat and Mass Transfer*, 93(March):21–33, 2018. ISSN 07351933. doi: 10.1016/j.icheatmasstransfer.2018.03.006.
- Cho, J. M. and Kim, M. S. Experimental studies on the evaporative heat transfer and pressure drop of CO<sub>2</sub> in smooth and micro-fin tubes of the diameters of 5 and 9.52 mm. *International Journal of Refrigeration*, 30(6):986–994, 2007. ISSN 01407007. doi: 10.1016/j.ijrefrig.2007.01.007.
- Colombo, L. P., Lucchini, A., and Muzzio, A. Flow patterns, heat transfer and pressure drop for evaporation and condensation of R134A in microfin tubes. *International Journal of Refrigeration*, 35(8):2150–2165, dec 2012. ISSN 01407007. doi: 10.1016/j.ijrefrig.2012.08.019.
- Corberán, J. M., Segurado, J., Colbourne, D., and González, J. Review of standards for the use of hydrocarbon refrigerants in A/C, heat pump and refrigeration equipment. *International Journal of Refrigeration*, 31(4):748–756, 2008. ISSN 01407007. doi: 10.1016/j.ijrefrig.2007.12.007.
- Dankwerth, C., Methler, T., Oltersdorf, T., Schossig, Peter, Miara, Marek, and Schnabel, L. Entwicklung einer Propan-Wärmepumpe mit einer Kältemittelfüllmenge von 150 Gramm. *DKV-Tagungsband 2019*, 2019.
- Dankwerth, C., Methler, T., Oltersdorf, T., Schossig, P., and Schnabel, L. Kältemittelreduktion in Propan-Wärmepumpen - Aktuelle Arbeiten. *DKV-Tagungsband 2020*, 2020.
- de Oliveira, J. D., Passos, J. C., Copetti, J. B., and van der Geld, C. W. Flow boiling heat transfer of propane in 1.0mm tube. *Experimental Thermal and Fluid Science*, 96(September 2017):243–256, 2018. ISSN 08941777. doi: 10.1016/j.expthermflusci.2018.03.010. URL <https://doi.org/10.1016/j.expthermflusci.2018.03.010>.
- Del Col, D., Stefano, B., Matteo, B., and Luisa, R. Condensation Heat Transfer and Pressure Drop with Propane in a Minichannel. In *International Refrigeration and Air Conditioning Conference*, 2012. URL <http://docs.lib.purdue.edu/iracc%0Ahttp://docs.lib.purdue.edu/iracc>.
- Diani, A., Mancin, S., and Rossetto, L. R1234ze(E) flow boiling inside a 3.4 mm ID microfin tube. *International Journal of Refrigeration*, 47:105–119, 2014. ISSN 01407007. doi: 10.1016/j.ijrefrig.2014.07.018. URL <http://dx.doi.org/10.1016/j.ijrefrig.2014.07.018>.
- Diani, A., Brunello, P., and Rossetto, L. R513A condensation heat transfer inside tubes: Microfin tube vs. smooth tube. *International Journal of Heat and Mass Transfer*, 152:119472, 2020. ISSN 00179310. doi: 10.1016/j.ijheatmasstransfer.2020.119472. URL <https://doi.org/10.1016/j.ijheatmasstransfer.2020.119472>.

- Friedel, L. Improved friction pressure drop correlation for horizontal and vertical two-phase pipe flow. In *European Two-Phase Flow Group Meeting*, pages 485–492, Ispra, 1979.
- Han, D. and Lee, K.-J. Experimental study on condensation heat transfer enhancement and pressure drop penalty factors in four microfin tubes. *International Journal of Heat and Mass Transfer*, 48(18):3804–3816, aug 2005. ISSN 00179310. doi: 10.1016/j.ijheatmasstransfer.2005.02.041. URL <https://linkinghub.elsevier.com/retrieve/pii/S0017931005003017>.
- Harby, K. Hydrocarbons and their mixtures as alternatives to environmental unfriendly halogenated refrigerants: An updated overview. *Renewable and Sustainable Energy Reviews*, 73(February):1247–1264, 2017. ISSN 18790690. doi: 10.1016/j.rser.2017.02.039. URL <http://dx.doi.org/10.1016/j.rser.2017.02.039>.
- Kedzierski, M. and Kim, M. Convective Boiling and Condensation Heat Transfer with a Twisted-Tape Insert for R12, R22, R152a, R134a, R290, R32/R134a, R32/R152a, R290/R134a, R134a/R600a, 1997. URL <http://fire.nist.gov/bfrlpubs/build97/art030.html>.
- Lee, H., Yoon, J., Kim, J., and Bansal, P. Evaporating heat transfer and pressure drop of hydrocarbon refrigerants in 9.52 and 12.70mm smooth tube. *International Journal of Heat and Mass Transfer*, 48(12):2351–2359, jun 2005. ISSN 00179310. doi: 10.1016/j.ijheatmasstransfer.2005.01.012. URL <http://linkinghub.elsevier.com/retrieve/pii/S0017931005001158>.
- Lee, H.-S., Yoon, J.-I., Kim, J.-D., and Bansal, P. Condensing heat transfer and pressure drop characteristics of hydrocarbon refrigerants. *International Journal of Heat and Mass Transfer*, 49(11-12):1922–1927, jun 2006. ISSN 00179310. doi: 10.1016/j.ijheatmasstransfer.2005.11.008.
- Li, T., Lu, J., Chen, L., He, D., Qiu, X., Li, H., and Liu, Z. Measurement of refrigerant mass distribution within a R290 split air conditioner. *International Journal of Refrigeration*, 57(2010):163–172, 2015. ISSN 01407007. doi: 10.1016/j.ijrefrig.2015.05.012. URL <http://dx.doi.org/10.1016/j.ijrefrig.2015.05.012>.
- Lillo, G., Mastrullo, R., Mauro, A. W., and Viscito, L. Flow boiling heat transfer, dry-out vapor quality and pressure drop of propane (R290): Experiments and assessment of predictive methods. *International Journal of Heat and Mass Transfer*, 126:1236–1252, 2018. ISSN 00179310. doi: 10.1016/j.ijheatmasstransfer.2018.06.069. URL <https://doi.org/10.1016/j.ijheatmasstransfer.2018.06.069>.

- Liu, Z. and Winterton, R. H. A general correlation for saturated and sub-cooled flow boiling in tubes and annuli, based on a nucleate pool boiling equation. *International Journal of Heat and Mass Transfer*, 34(11):2759–2766, nov 1991. ISSN 00179310. doi: 10.1016/0017-9310(91)90234-6. URL <http://linkinghub.elsevier.com/retrieve/pii/0017931091902346>.
- Longo, G. A., Mancin, S., Righetti, G., and Zilio, C. Hydrocarbon refrigerants HC290 (Propane) and HC1270 (Propylene) low GWP long-term substitutes for HFC404A: A comparative analysis in vaporisation inside a small-diameter horizontal smooth tube. *Applied Thermal Engineering*, 124:707–715, 2017a. ISSN 13594311. doi: 10.1016/j.applthermaleng.2017.06.080. URL <http://dx.doi.org/10.1016/j.applthermaleng.2017.06.080>.
- Longo, G. A., Mancin, S., Righetti, G., and Zilio, C. Saturated vapour condensation of HFC404A inside a 4 mm ID horizontal smooth tube: Comparison with the long-term low GWP substitutes HC290 (Propane) and HC1270 (Propylene). *International Journal of Heat and Mass Transfer*, 108:2088–2099, 2017b. ISSN 00179310. doi: 10.1016/j.ijheatmasstransfer.2016.12.087. URL <http://dx.doi.org/10.1016/j.ijheatmasstransfer.2016.12.087>.
- Longo, G. A., Mancin, S., Righetti, G., and Zilio, C. Saturated vapor condensation of hydrocarbons inside A 4 mm ID horizontal smooth tube. *Refrigeration Science and Technology*, 2018-June(2017):620–627, 2018. ISSN 01511637. doi: 10.18462/iir.gl.2018.1229.
- Macdonald, M. and Garimella, S. Hydrocarbon condensation in horizontal smooth tubes: Part I – Measurements. *International Journal of Heat and Mass Transfer*, 93:75–85, feb 2016a. ISSN 00179310. doi: 10.1016/j.ijheatmasstransfer.2015.09.018.
- Macdonald, M. and Garimella, S. Hydrocarbon mixture condensation inside horizontal smooth tubes. *International Journal of Heat and Mass Transfer*, 100: 139–149, 2016b. ISSN 00179310. doi: 10.1016/j.ijheatmasstransfer.2016.03.114. URL <http://dx.doi.org/10.1016/j.ijheatmasstransfer.2016.03.114>.
- Maqbool, M. H., Palm, B., and Khodabandeh, R. Investigation of two phase heat transfer and pressure drop of propane in a vertical circular minichannel. *Experimental Thermal and Fluid Science*, 46:120–130, apr 2013. ISSN 08941777. doi: 10.1016/j.expthermflusci.2012.12.002.
- McLinden, M. O., Brown, J. S., Brignoli, R., Kazakov, A. F., and Domanski, P. A. Limited options for low-global-warming-potential refrigerants. *Nature Communications*, 8(1):14476, apr 2017. ISSN 2041-1723. doi: 10.1038/ncomms14476. URL <http://www.nature.com/articles/ncomms14476>.

- Moreira, T. A., Furlan, G., Oliveira, G. H. d. S. e., and Ribatski, G. Flow boiling and convective condensation of hydrocarbons: A state-of-the-art literature review. *Applied Thermal Engineering*, 182(May 2020):116129, jan 2021. ISSN 13594311. doi: 10.1016/j.applthermaleng.2020.116129. URL <https://doi.org/10.1016/j.applthermaleng.2020.116129>.
- Mota-Babiloni, A. and Makhnatch, P. Predictions of European refrigerants place on the market following F-gas regulation restrictions. *International Journal of Refrigeration*, 127(517):101–110, jul 2021. ISSN 01407007. doi: 10.1016/j.ijrefrig.2021.03.005. URL <https://doi.org/10.1016/j.ijrefrig.2021.03.005>.
- Nan, X. H. and Infante Ferreira, C. In tube evaporation and condensation of natural refrigerant R290 (Propane). *Gustav Lorentz conference*, 290:3, 2000.
- Palm, B. Hydrocarbons as refrigerants in small heat pump and refrigeration systems – A review. *International Journal of Refrigeration*, 31(4):552–563, jun 2008. ISSN 01407007. doi: 10.1016/j.ijrefrig.2007.11.016. URL <https://linkinghub.elsevier.com/retrieve/pii/S0140700707002216>.
- Pamitran, A., Choi, K.-I., Oh, J.-T., and Hrnjak, P. Characteristics of two-phase flow pattern transitions and pressure drop of five refrigerants in horizontal circular small tubes. *International Journal of Refrigeration*, 33(3):578–588, may 2010. ISSN 01407007. doi: 10.1016/j.ijrefrig.2009.12.009. URL <https://linkinghub.elsevier.com/retrieve/pii/S0140700709002862>.
- Qiu, G., Li, M., and Cai, W. The condensation heat transfer, frictional pressure drop and refrigerant charge characteristics of R290 in minichannels with different diameters. *International Journal of Heat and Mass Transfer*, 158:119966, 2020. ISSN 00179310. doi: 10.1016/j.ijheatmasstransfer.2020.119966. URL <https://doi.org/10.1016/j.ijheatmasstransfer.2020.119966>.
- Rollmann, P. and Spindler, K. New models for heat transfer and pressure drop during flow boiling of R407C and R410A in a horizontal microfin tube. *International Journal of Thermal Sciences*, 103:57–66, 2016. ISSN 12900729. doi: 10.1016/j.ijthermalsci.2015.11.010. URL <http://dx.doi.org/10.1016/j.ijthermalsci.2015.11.010>.
- Rouhani, S. Z. and Axelsson, E. Calculation of void volume fraction in the subcooled and quality boiling regions. *International Journal of Heat and Mass Transfer*, 13(2):383–393, feb 1970. ISSN 00179310. doi: 10.1016/0017-9310(70)90114-6. URL <http://linkinghub.elsevier.com/retrieve/pii/0017931070901146>.
- Schulz, M. and Kourkoulas, D. Regulation (EU) No 517/2014 of The European Parliament and of the council of 16 April 2014 on fluorinated greenhouse gases

- and repealing Regulation (EC) No 842/2006. *Off. J. Eur. Union*, 2014(517): L150, 2014.
- Shin, J. Y., Kim, M. S., and Ro, S. T. Experimental study on forced convective boiling heat transfer of pure refrigerants and refrigerant mixtures in a horizontal tube. *International Journal of Refrigeration*, 20(4):267–275, 1997. ISSN 01407007. doi: 10.1016/S0140-7007(97)00004-2.
- Straub, M. Alternative Refrigerants For Household Refrigerators Alternative Refrigerants For Household Refrigerators. In *International Refrigeration and Air Conditioning*, volume 2002, pages 1–10, 2018.
- Tang, W., He, G., Zhou, S., Sun, W., Cai, D., and Mei, K. The performance and risk assessment of R290 in a 13 kW air source heat pump. *Applied Thermal Engineering*, 144(July):392–402, 2018. ISSN 13594311. doi: 10.1016/j.applthermaleng.2018.08.070. URL <https://doi.org/10.1016/j.applthermaleng.2018.08.070>.
- Thonon, B. A review of hydrocarbon two-phase heat transfer in compact heat exchangers and enhanced geometries. *International Journal of Refrigeration*, 31(4):633–642, jun 2008. ISSN 0140-7007. URL <https://www.sciencedirect.com/science/article/pii/S014070070800039X>.
- Wang, S., Gong, M., Chen, G., Sun, Z., and Wu, J. Two-phase heat transfer and pressure drop of propane during saturated flow boiling inside a horizontal tube. *International Journal of Refrigeration*, 41:200–209, may 2014. ISSN 01407007. doi: 10.1016/j.ijrefrig.2013.03.019. URL <http://dx.doi.org/10.1016/j.ijrefrig.2013.03.019>.
- Wen, J., Gu, X., Wang, S., Li, Y., and Tu, J. The comparison of condensation heat transfer and frictional pressure drop of R1234ze(E), propane and R134a in a horizontal mini-channel. *International Journal of Refrigeration*, 92:208–224, aug 2018. ISSN 01407007. doi: 10.1016/j.ijrefrig.2018.03.006. URL <https://doi.org/10.1016/j.ijrefrig.2018.03.006>.
- Wen, M.-Y. and Ho, C.-Y. Evaporation heat transfer and pressure drop characteristics of R-290 (propane), R-600 (butane), and a mixture of R-290/R-600 in the three-lines serpentine small-tube bank. *Applied Thermal Engineering*, 25(17-18):2921–2936, dec 2005. ISSN 13594311. doi: 10.1016/j.applthermaleng.2005.02.013. URL [www.elsevier.com/locate/apthermeng](http://www.elsevier.com/locate/apthermeng)<https://linkinghub.elsevier.com/retrieve/pii/S1359431105000827>.
- Wen, M.-Y., Jang, K.-J., and Ho, C.-Y. The characteristics of boiling heat transfer and pressure drop of R-600a in a circular tube with porous inserts. *Applied Thermal Engineering*, 64:348–357, 2014. doi: 10.1016/j.applthermaleng.2013.12.074.

- Xu, Y. and Fang, X. A new correlation of two-phase frictional pressure drop for evaporating flow in pipes. *International Journal of Refrigeration*, 5(7):2039–2050, nov 2012. ISSN 0140-7007. doi: 10.1016/j.ijrefrig.2012.06.011. URL <https://www.sciencedirect.com/science/article/pii/S0140700712001570>.
- Zou, X., Gong, M. Q., Chen, G. F., Sun, Z. H., Zhang, Y., and Wu, J. F. Experimental study on saturated flow boiling heat transfer of R170/R290 mixtures in a horizontal tube. *International Journal of Refrigeration*, 33:371–380, 2009. doi: 10.1016/j.ijrefrig.2009.10.013.



# Appendix A

## List of Publications

### Publication I

Allymehr, E., Pardiñas, Á. Á., Eikevik, T. M., and Hafner, A. Characteristics of evaporation of propane (R290) in compact smooth and microfinned tubes, *Applied Thermal Engineering*, 181:115880, 2020.

### Publication II

Allymehr, E., Pardiñas, Á. Á., Eikevik, T. M., and Hafner, A. Comparative analysis of evaporation of isobutane (R600a) and propylene (R1270) in compact smooth and microfinned tubes. *Applied Thermal Engineering*, 188:116606, 2021.

### Publication III

Allymehr, E., Pardiñas, Á. Á., Eikevik, T. M., and Hafner, A. Condensation of Hydrocarbons in Compact Smooth and Microfinned Tubes. *Energies*, 14(9):2647, 2021.

### Publication IV

Allymehr, E., Skaugen, G., Will, T., Pardiñas, Á. Á., Eikevik, T. M., Hafner, A., Schnabel, L. Numerical study of hydrocarbon charge reduction methods in HVAC heat exchangers. *Energies*, 14(15):4480, 2021.



# Article I





# Characteristics of evaporation of propane (R290) in compact smooth and microfinned tubes

Ehsan Allymehr<sup>\*</sup>, Ángel Álvarez Pardiñas, Trygve Magne Eikevik, Armin Hafner

Department of Energy and Process Engineering, NTNU Norwegian University of Science and Technology, Kolbjørn Hejes vei 1D, 7491 Trondheim, Norway

## HIGHLIGHTS

- Evaporation of propane studied experimentally in smooth and microfinned tubes.
- Heat transfer coefficient and pressure drop are obtained experimentally.
- Mass flux does not increase heat transfer coefficient in microfinned tubes.
- Predictive methods have different accuracies for different microfinned tubes.

## ARTICLE INFO

### Keywords:

Hydrocarbon  
Refrigeration  
Heat transfer  
Pressure drop  
Microfinned

## ABSTRACT

Evaporation of flowing propane and the effect of enhanced geometry on heat transfer coefficient and pressure drop is experimentally investigated. One smooth tube and two microfinned tubes with an outer diameter of 5 mm were tested. Heat transfer coefficient and pressure drop were determined for saturation temperatures of 0, 5 and 10 °C for smooth tube, and the effect of using tubes with enhanced geometries was evaluated at heat fluxes ranging between 15 and 33 kW m<sup>-2</sup> and mass fluxes between 250 and 500 kW m<sup>-2</sup> s<sup>-1</sup>. The increase of heat transfer coefficient for microfinned tubes relative to smooth tube diminishes with increasing mass flux, while the increase of pressure drop remains unaffected. Comparison of the experimental results with correlations for prediction of pressure drop and heat transfer coefficient demonstrates availability of reliable correlations. Nevertheless, correlations show considerable divergence in accuracy for different microfinned tubes.

## 1. Introduction

The majority of working fluids currently used in refrigeration systems have particularly high global warming potential (GWP) [3]. New refrigeration systems should aim towards fluids of lower GWP while being more efficient in power consumption to reduce both the direct and indirect impact on the environment. Hydrocarbons and, in particular, propane (R290) have long been considered an alternative refrigerant as they have a favorable saturation curve for various applications, low GWP and zero Ozone Depletion Potential (ODP). While Hydrocarbons were used in the first generation of refrigeration systems their application was later limited as a consequence of flammability concerns, specially as the Lower Flammability Limit (LFL) for propane is very low [13]. Although the working fluid charge for a refrigeration system utilizing propane as working fluid can be theoretically half of a comparable system using R134a (the latent heat of vaporization for propane is almost double), this is not enough to satisfy safety

regulations in specific applications where higher capacities are required.

Therefore the primary research goal with hydrocarbons has been to reduce the system charge [32]. It has been shown that the majority of the charge in refrigeration systems accumulates in heat exchangers where liquid phase is available with higher density [31]. Consequently, it is essential to decrease the volume of heat exchangers. The use of microfinned tubes provides an opportunity to use hydrocarbon systems with reduced sizes, lower charges and higher capacities by increasing the heat transfer coefficient (HTC) in heat exchangers.

Prior research on evaporation of hydrocarbons has mainly focused on tubes of around 10 mm [37,19,42]. Thonon [40] reviewed the literature on hydrocarbon heat transfer in compact heat exchangers noting that there is a need for more experimental data on in-tube flow boiling of hydrocarbons, especially in the case of microfinned tubes. To the best of our knowledge, the only available reference is Nan & Infante Ferreira [28], where evaporation and condensation of propane in a

<sup>\*</sup> Corresponding author.

E-mail address: [ehsan.allymehr@ntnu.no](mailto:ehsan.allymehr@ntnu.no) (E. Allymehr).

<https://doi.org/10.1016/j.applthermaleng.2020.115880>

Received 26 February 2020; Received in revised form 3 August 2020; Accepted 10 August 2020

Available online 01 September 2020

1359-4311/ © 2020 The Author(s). Published by Elsevier Ltd. This is an open access article under the CC BY license (<http://creativecommons.org/licenses/by/4.0/>).

Nomenclature		P	Penalization Factor [-]
<b>Greek</b>		Q	Heat input [W]
$\delta_{30}$	Percentage of predicted values with less than 30% error	q	Heat flux [ $\text{kW m}^{-2}$ ]
<b>Roman</b>		S	Heat exchange area [ $\text{m}^2$ ]
$\dot{m}$	Mass flow [ $\text{kg s}^{-1}$ ]	T	Temperature [ $^{\circ}\text{C}$ ]
$d_i$	Fin tip diameter [m]	x	Vapor quality [-]
$i_{lg}$	Enthalpy of vaporization [ $\text{kJ kg}^{-1}$ ]	<b>Subscripts</b>	
E	Enhancement Factor [-]	in	Inlet conditions
G	Mass flux [ $\text{kg m}^{-2} \text{s}^{-1}$ ]	MF	Microfinned
HTC	Heat Transfer Coefficient [ $\text{kW m}^{-2} \text{K}^{-1}$ ]	out	Outlet conditions
I	Efficiency index [-]	pre	Preheater section
ID	Internal Diameter [mm]	sat	Saturated condition
MARD	Mean Absolute Relative Deviation [-]	test	Test section
MRD	Mean Relative Deviation [-]	W	Wall

smooth, microfinned, and crosshatched tube with OD of 9.52 mm were studied. Their results showed that while the HTC is higher for microfinned tubes compared to smooth tubes, the cross hatched tubes do not make a significant difference; the increase in HTC seems to be more noticeable at higher mass fluxes. Furthermore, correlations for internally enhanced tubes considerably over predicted their experimental data. Pamitran et al. [33] examined the HTC of propane in stainless steel tubes of 1.5 and 3.0 mm inner diameter and developed a correlation based on the experimental results. Maqbool et al. [25] investigated the evaporation of propane in a 1.70 mm ID vertical circular minichannel; they reported most notably that the HTC increases with heat flux and saturation temperature while the effect of mass flux and vapor quality is insignificant. de Oliveira et al. [30] determined HTC and studied flow patterns of propane flowing in a 1.0 mm ID tube at saturation temperature of 25  $^{\circ}\text{C}$ , and the results show a high dependency of HTC on mass flux and heat flux. More recently, Lillo et al. [22] studied the vaporization of R290 in a tube with ID of 6 mm at high saturation temperatures. They noted that the main heat transfer mechanism seems to be nucleate boiling, while correlations of Bertsch et al. [2] and Friedel [11] predicted their results for HTC and pressure

drop most accurately. Longo et al. [24] compared the evaporation of R290 and R1270 with R404A in a small diameter tube showing that R404A and R1270 exhibit the highest heat transfer coefficient and lowest pressure drop, while R290 is affected by a particularly low dryout quality. There have also been several studies investigating mixtures of hydrocarbons. Wen & Ho [43] conducted experiments with propane, butane and a mixture of them flowing in a 2.46 mm ID tube, and results showed that the HTC was significantly improved compared to R134a as a working fluid. Zou et al. [46] studied mixtures of R170 and R290 and their evaporation characteristics, proposing a correlation for prediction of HTC. Kedzierski & Kim [17] analyzed heat transfer of various refrigerants and their mixtures, including R290 and R134a, in a 9.64 mm ID tube containing a twisted tape insert.

Several studies have dealt with the effect of enhanced geometries in flow boiling of different fluids. Cho & Kim [6] compared the evaporation characteristics of  $\text{CO}_2$  in smooth and microfinned tubes with OD of 9.52 and 5 mm showing that the HTC in microfinned tubes increased by up to 210%, whilst the pressure drop increase was up to 1.9 times. Celen et al. [5] investigated evaporation of R134a in smooth and microfinned tubes, showing that the pressure drop is increased by up to 3

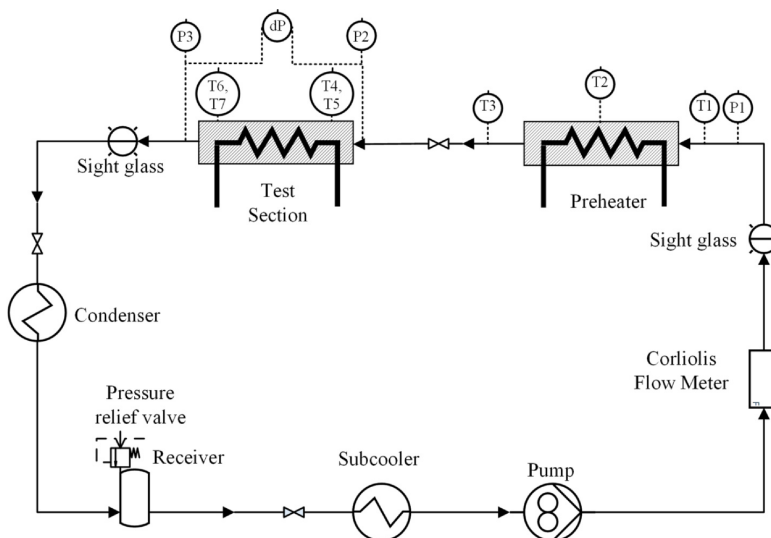


Fig. 1. Test rig schematic.

times while the heat transfer coefficient is increased by 1.9 times. Colombo et al. [9] observed the flow patterns, characteristics of evaporation and condensation of R134a in one smooth and two microfinned tubes showing that both microfinned tubes increase the HTC compared to the smooth tube and found no differences among them. Bandarra Filho et al. [11] compared experimental results for the pressure drop of R134a in smooth and grooved tubes and developed a correlation based on the results.

Thus, while the state of the art for experimental results on evaporation of refrigerants is rather extensive, there seems to be a lack of data regarding different surface enhancements and comparison with smooth tubes specially for hydrocarbons. This paper aims to increase the available information on flow boiling of R290 in compact smooth and microfinned tubes by providing a database of HTC, pressure drop and comparison with relevant correlations. The two microfinned tubes (MF1 and MF2), and the smooth tube have an outer diameter of 5 mm. They were tested at mass fluxes ranging from 250 to 500  $\text{kW m}^{-2} \text{s}^{-1}$  and the heat flux ranged from 15 to 33  $\text{kW m}^{-2}$ . Furthermore, the smooth tube was tested at three saturation temperatures of 0, 5 and 10  $^{\circ}\text{C}$ .

## 2. Experimental setup

An experimental test rig, located at Thermal lab of the Department of Energy and Process Engineering of Norwegian University of Science and Technology was designed to determine flow boiling HTC and pressure drop of different refrigerants. A schematic of the test rig is shown in Fig. 1. The liquid refrigerant is pumped through the system using an inverter controlled gear pump (Tuthill DGS.68), with a Coriolis mass flow meter (Rheonik RHM 03) that measures the circulated mass flow. Refrigerant is then heated up to the desired vapor quality in the preheater, using an electrical heating cable that is directly wound around the tube. An adiabatic section is located before the test section to ensure fully developed conditions. The adiabatic section consists of two parts: the first is 1 meter long with ID of 8 mm and later a length of 75 mm of the corresponding test tube. Heat input both at preheater and test section is controlled with a Pulse Wave Modulation (PWM) where the input voltage (National Instruments NI-9225) and current (National Instruments NI-9246 and National Instruments NI-9227 for preheater and test section, respectively) is measured at 50 kHz to obtain the power input. The heated test section length is 500 mm and goes through a 30 mm OD copper tube of the same length. An electrical heating cable is wound around the outer tube and the distance between the outer tube and the test tube is filled with tin to distribute the heat evenly along the test section. Tin was melted in by placing tin bars in between the outer tube and test tube while the whole test section was placed vertically and the outer copper tube was heated using a torch. Presence of voids in tin was checked by controlling the final weight of the test section. At the outlet of the test section, a sight glass enables visualizing the flow; as this glass sight did not have the same diameter as the test tube, it was not used for flow pattern recognition. The two valves located upstream of the test section and downstream of the sight glass allow the replacement of test sections in a short time by limiting the effort required for vacuuming the new test section. Nonetheless, the whole test rig was

vacuumed and purged with nitrogen for the start up and before any propane was charged. After the sight glass and valve, the propane flows through a condenser and a subcooler cooled by recirculating chillers to ensure a single phase liquid flow to the pump. The saturation pressure of the system is controlled by the set temperature of the chiller connected to the condenser.

To determine the HTC, the wall temperatures were measured with two pairs of Type T thermocouples brazed to the tube wall. Thermocouples were located 100 mm from the inlet and outlet of the heated test section such that in each location, one thermocouple is in contact with the top and the other with the bottom part of the test tube. The fluid saturation temperature was obtained from the saturation pressure; pressure transducers are connected to pressures taps located at the inlet and outlet of the test Section 547 mm away from each other. Pressure drop was measured in diabatic condition directly from the differential pressure transducer connected to the same ports. A photograph of one of the test sections is shown in Fig. 2.

### 2.1. Tested tubes

Three tubes with OD of 5 mm and different internal geometries were studied. The geometrical parameters of the tubes are detailed in Table 1, and the physical representations of the parameters are presented in Fig. 3. The two microfinned tubes, MF1 and MF2, have roughly the same dimensions for the fins, while the MF2 tube has a higher number of fins and spiral angle, which results in a higher available area for heat transfer compared to the other tubes. A cross sectional view of the two tested microfinned tubes is shown in Fig. 4.

### 2.2. Uncertainty analysis and validation

Uncertainty analysis was carried out by the method elaborated in ISO [15] with a confidence level exceeding 95% (coverage factor of 2). Utilized instruments are listed in Table 2 with their respective uncertainty. The total average uncertainty for pressure drop was 4.8%, 3.7% and 3.7% for smooth, MF1 and MF2 tube, respectively. For HTC, these values were 3.6%, 6.2% and 9.0% for smooth, MF1 and MF2 tube, respectively. The increase of uncertainty for HTC values in microfinned tubes is caused by the smaller temperature differences between the saturation temperature and wall temperature. Finally, the uncertainty values for average vapor quality is 3.6%, 2.4% and 2.6% for smooth, MF1 and MF2 tube, respectively.

Single phase tests were performed to validate the test facility. Pressure drop and HTC were calculated and compared against Darcy Weisbach formula and the correlation by Gnielinski V. [12], showing an average absolute deviation of 3.7% and 2.6% for pressure drop and heat transfer coefficient, respectively.

The test section was insulated using perlite and then contained by hard insulation. To inspect the effectiveness of the insulation, a thermal camera was used to visualize the temperature distribution and detect any hot spots. Furthermore, several tests were performed at vacuum conditions to evaluate heat leakage at different heat fluxes. The results showed a fairly linear relationship between the temperature difference of the heating element and environment and the heat loss to the



Fig. 2. Photograph of a test section.

**Table 1**  
Geometrical parameters of the test tubes.

	Unit	Smooth tube	MF1	MF2
Outer diameter (OD)	mm	5	5	5
Fin tip diameter ( $d_i$ )	mm	4.1	4.32	4.26
Wall thickness ( $t_w$ )	mm	0.45	0.22	0.22
Actual cross sectional area	mm <sup>2</sup>	13.2	15.7	14.8
Fin height ( $l_f$ )	mm	–	0.12	0.15
Fin number ( $n$ )	(–)	–	35	56
Fin angle ( $\gamma$ )	°	–	35	15
Spiral angle ( $\beta$ )	°	–	15	37
Heat exchange area ratio	(–)	1	1.51	2.63

**Table 2**  
List of instruments and their respective uncertainties.

	Type	Range	Uncertainty
Flow meter	Coriolis	0–5 kg min <sup>-1</sup>	± 0.1% <sup>a</sup>
Absolute pressure sensor	Strain gauge	0–10 bar	± 0.16% <sup>b</sup>
Differential pressure sensor	Strain gauge	0–0.5 bar	± 0.15% <sup>b</sup>
Thermocouples	Type T	–	± 0.05 K
Preheater	Electrical	3450 W	± 0.44% <sup>a</sup>
Test section heater	Electrical	620 W	± 0.55% <sup>a</sup>

<sup>a</sup> Of the reading.  
<sup>b</sup> Of the set span.

**2.3. Data reduction**

The system was considered to be in a steady state when the average standard deviation of the four wall temperatures in the last 15 samples was less than 0.1 °C, if this condition was not met, it was considered to be unstable and the data was discarded. The data from the sensors were recorded for over 120 s to obtain 50 samples, which were then averaged. HTC and pressure drop values are reported for an average vapor quality value which is calculated by Eq. (2):

$$x = x_{in} + \frac{\Delta x}{2} = \frac{Q_{pre} - \dot{m} \cdot (i_{sat,l} - i_l)}{\dot{m} \cdot i_{lg}(P_{pre})} + \frac{Q_{test} - Q_{loss}}{2 \cdot \dot{m} \cdot i_{lg}(P_{sat})} \quad (2)$$

wherein  $i_l$  is the enthalpy of subcooled fluid before entering the preheater,  $P_{pre}$  is the pressure at the preheater section and  $P_{sat}$  is the arithmetic average of the inlet and outlet pressure at the test section.

Heat transfer coefficients were calculated using Eq. (3):

$$h = \frac{Q_{test} - Q_{loss}}{S(T_w - \bar{T}_{sat})} \quad (3)$$

where  $T_{sat}$  is derived from the saturation pressure,  $P_{sat}$ ,  $\bar{T}_w$  and  $S$  are defined as:

$$\bar{T}_w = \frac{1}{4} \sum_{i=1}^4 T_{w,i} \quad (4)$$

$$S = \pi d_i L \quad (5)$$

For the microfinned tubes, the parameters depending on the ID, such as mass flux and heat flux, were calculated based on a smooth tube with  $d_i$  equal to the the fin tip diameter. Thermodynamic properties are evaluated using REFPROP V10 [20].

The total pressure drop  $\Delta P_t$  is calculated by addition of the momentum pressure  $\Delta P_a$  drop with frictional pressure drop  $\Delta P_f$ , given by:  $\Delta P_a = \Delta P_f + \Delta P_a$  (6)

In order to evaluate the momentum pressure drop, the void fraction was calculated using Rouhani & Axelsson [35] correlation. Although this correlation was originally developed for vertical tubes, it takes into account several parameters that are important in mini and micro channels, therefore it has been used in multiple sources for calculation of the void fraction in horizontal tubes [22,29].

**3. Results and discussion**

**3.1. HTC and pressure drop**

Table 3 summarizes the working conditions for the three tubes. In order to analyze the effect of different parameters, tests were performed in varying mass fluxes and heat fluxes for all the tubes while the effect of saturation temperature was evaluated for the smooth tube.

Fig. 5 investigates the effect of saturation temperature on HTC of the smooth tube. Since no relation between the saturation temperature and HTC was discernible, no specific tests were performed in microfinned tubes to study the direct effect of saturation temperature.

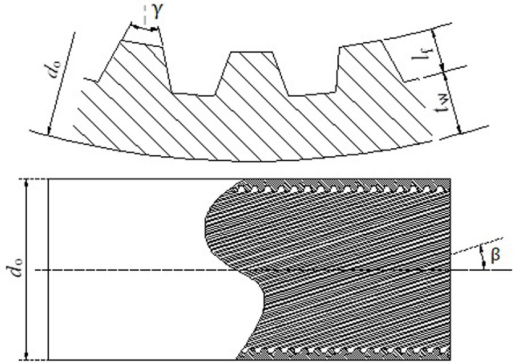


Fig. 3. Physical presentation of the geometrical parameters.

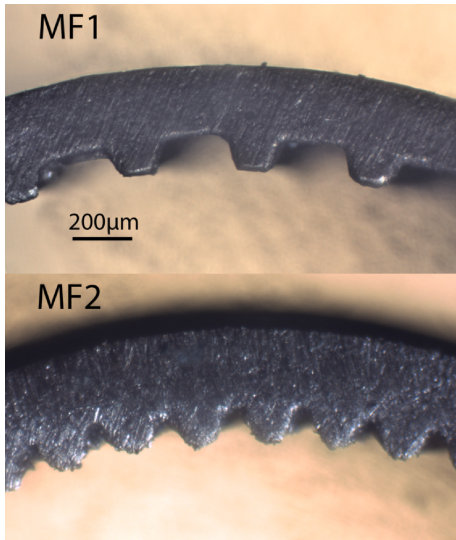


Fig. 4. Cross sectional view of the microfinned tubes.

environment, which was taken into account into calculations by Eq. (1).

$$Q_{loss} = 0.2075 \cdot (T_{element} - T_{amb}) - 0.2925 \quad [W] \quad (1)$$

Heat loss to the environment was on average 3.1% of heat input and the maximum value never exceeded 5.1% in highest heat fluxes.

**Table 3**  
Operating conditions for experimental setup.

	Unit	Range/Value
Fluid	-	Propane (R290)
Saturation Temperature [ $T_{sat}$ ]	°C	0, 5, 10
Reduced pressure [ $P_{red}$ ]	-	0.11–0.15
Heat flux [ $q$ ]	$\text{kW m}^{-2}$	15, 24, 33
Mass flux [ $G$ ]	$\text{kW m}^{-2} \text{s}^{-1}$	250–500
Tube outer diameter [OD]	mm	5
Vapor quality [ $x$ ]	-	0.14–1
Quality change [ $\Delta x$ ]	-	0.06–0.15

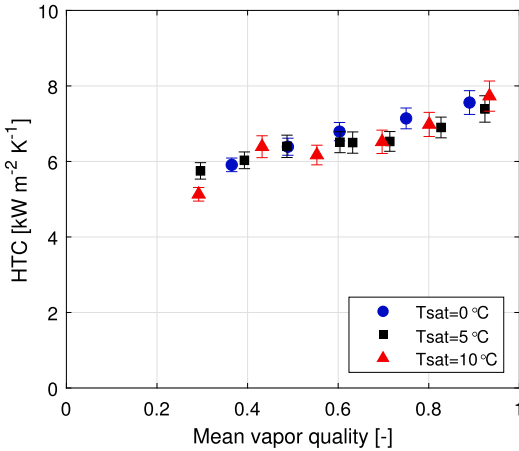


Fig. 5. Effect of saturation temperature on HTC,  $G = 250 \text{ kW m}^{-2} \text{ s}^{-1}$ ,  $q = 15 \text{ kW m}^{-2}$ .

Fig. 6 depicts the effect of heat flux on HTC for the tested tubes. The results show that by increasing the heat flux from  $15 \text{ kW m}^{-2}$  to  $24 \text{ kW m}^{-2}$  there is a considerable increase in the HTC in all vapor qualities for all the tested tubes. A further increase of heat flux to  $34 \text{ kW m}^{-2}$  diminishes the rate of increased HTC in low vapor qualities for all the tubes. In higher vapor quality regions, there is no increase of HTC for the smooth tube and HTC decreases for microfinned tubes compared to a lower heat flux. A closer look at the experimental data showed that the decrease of HTC is mainly caused by the increase in the wall temperature at the inlet section of the test tube. The reason for this remains unclear to the authors, as it would most likely require a flow visualization test to understand the underlying phenomena. Nevertheless, it can be said that this is most probably caused by the geometry of the

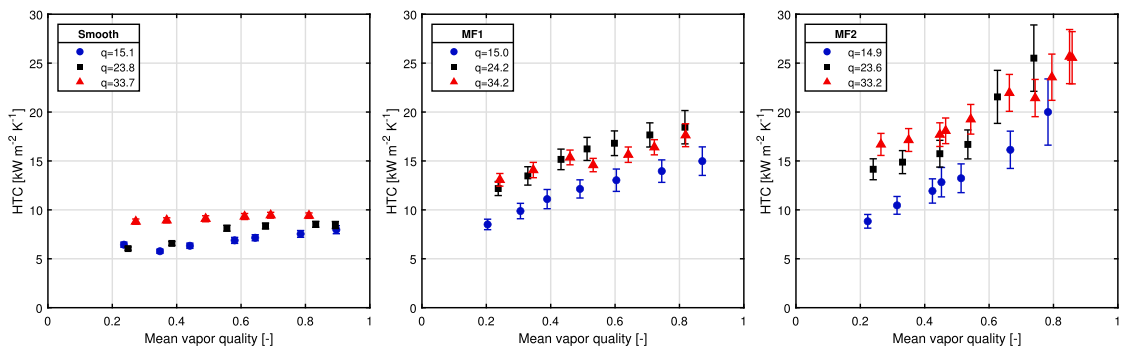


Fig. 6. Effect of heat flux on HTC with  $G = 300 \text{ kW m}^{-2} \text{ s}^{-1}$ ,  $T_{sat} = 10 \text{ °C}$  for three different tubes, heat flux ( $q$ ) in the legend reported in  $\text{kW m}^{-2}$ .

tube and the complex flow arising from it.

The effect of mass flux on HTC in different tubes can be observed in Fig. 7. HTC increases in the smooth tube with the highest mass flux at high vapor qualities, while the lowest mass fluxes exhibit a rather small increase over the whole vapor quality range, indicating an insignificant contribution from convective heat transfer mechanism. On the contrary, while both of the microfinned tubes show a substantial increase of HTC in higher vapor qualities, the HTC is largely independent of mass flux. It can be argued that the microfinned tubes' fin tips break up the liquid film and readily cause an increase in the turbulence, nullifying the effect of increased turbulence in higher mass fluxes on HTC while higher vapor qualities lead to a thinner liquid film on the wall, thus increasing the HTC.

Unlike HTC, pressure drop exhibits a dependence on saturation temperature (Fig. 8). Pressure drop for  $T_{sat} = 0 \text{ °C}$  is about 30% greater relative to the comparable case of  $T_{sat} = 10 \text{ °C}$  at intermediate vapor qualities. This can be explained by the decrease in the viscosity of the gas phase while the liquid density and liquid viscosity increase, which in turn causes an increase in the superficial velocity of the gas phase and higher shear stress in the liquid phase. The thinning of liquid film at high vapor qualities eliminates the effect of higher shear stress of the liquid phase, and the values for pressure drop seem to converge close to vapor quality of 1.

It can be seen that for all the tested tubes, the most influential factor for pressure drop is the mass flux, presented in Fig. 9. Unsurprisingly, the high HTCs for MF2 tube are coupled with large pressure drops, reaching values of up to  $100 \text{ kPa m}^{-1}$ . It can also be inferred from Fig. 9 that with the increasing mass flux, the pressure drop increases in the microfinned tubes, while in Fig. 7 it was shown that the increasing mass flux does not result in a higher HTC.

Unlike mass flux, it can be seen in Fig. 10 that the heat flux does not affect the total pressure drop in a meaningful way for any of the tubes.

Colombo et al. [9] defined three parameters to compare the effectiveness of microfinned tubes, Enhancement factor  $E$ , Penalization factor  $P$ , and efficiency index,  $I$ , which are formulated as:

$$E = \frac{h_{MF}}{h_{Smooth}} \tag{9}$$

$$P = \frac{\Delta P_{MF}}{\Delta P_{Smooth}} \tag{8}$$

$$I = \frac{E}{P} \tag{9}$$

These values were calculated at vapor quality of  $x = 0.45$  for different mass fluxes and represented in Fig. 11. The Enhancement factor gradually decreases for both MF1 and MF2, while the penalization factor remains mostly the same over the whole range, therefore diminishing efficiency index at higher mass fluxes. The downward trend

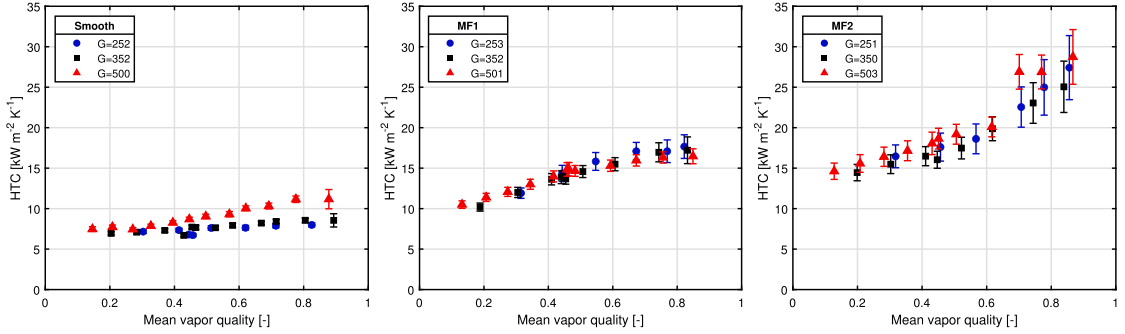


Fig. 7. Effect of mass flux on HTC with  $q = 23 \text{ kW m}^{-2}$ ,  $T_{\text{sat}} = 5 \text{ }^\circ\text{C}$  for three different tubes, mass flux (G) reported in the legend in  $\text{kW m}^{-2} \text{ s}^{-1}$ .

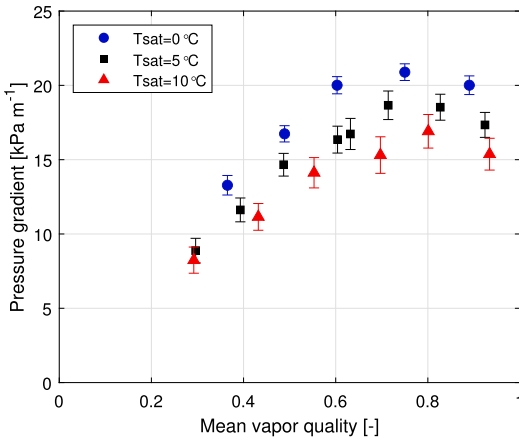


Fig. 8. Effect of saturation temperature on total pressure gradient of smooth tube at  $q = 23 \text{ kW m}^{-2}$ ,  $G = 300 \text{ kW m}^{-2} \text{ s}^{-1}$ .

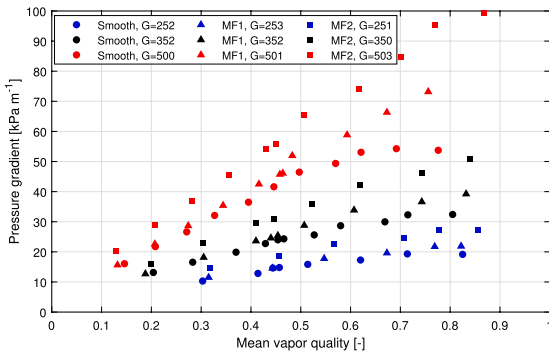


Fig. 9. Effect of mass flux on total pressure gradient at  $q = 23 \text{ kW m}^{-2}$ ,  $T_{\text{sat}} = 5 \text{ }^\circ\text{C}$  for all the tubes, mass flux (G) in  $\text{kW m}^{-2} \text{ s}^{-1}$ .

of enhancement factor can be explained by the fact that the rate of increase of HTC for the smooth tube with increasing mass flux is higher than for MF tubes. However, for mass fluxes higher than  $400 \text{ kW m}^{-2} \text{ s}^{-1}$ , HTC for smooth tube does not increase anymore. Meanwhile, there is a slight increase for MF tubes; subsequently, the enhancement factor rises. It can be argued that this happens because there is a larger area available for heat exchange in MF tubes. Furthermore, while the enhancement factor and penalization factor for the MF2 tube are higher,

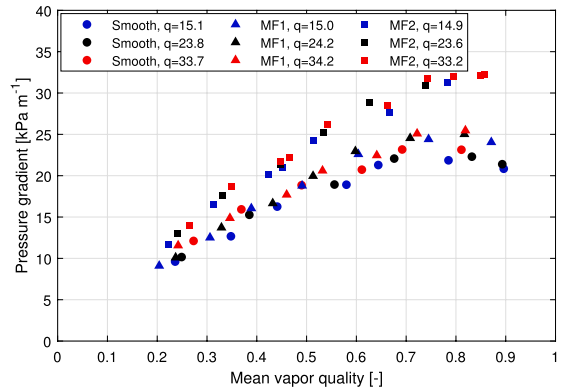


Fig. 10. Effect of heat flux on total pressure gradient at  $G = 300 \text{ kW m}^{-2} \text{ s}^{-1}$ ,  $T_{\text{sat}} = 10 \text{ }^\circ\text{C}$  for all the tubes, reported heat flux (q) in  $\text{kW m}^{-2}$ .

the efficiency index for both of the tubes is about the same.

### 3.2. Correlations

HTC and pressure drop for smooth tubes and microfinned tubes have been comprehensively compared with predictive correlations available in the literature by values of Mean Relative Deviation (MRD) and Mean Absolute Relative Deviation (MARD), defined as:

$$MRD = \frac{100}{n} \sum_{i=1}^n \frac{Predicted_i - Experimental_i}{Experimental_i} \quad (10)$$

$$MARD = \frac{100}{n} \sum_{i=1}^n \left| \frac{Predicted_i - Experimental_i}{Experimental_i} \right| \quad (11)$$

Additionally,  $\delta_{30}$  was used as a parameter to show what percentage of the predicted values have less than 30% deviation from the experimental data. Table 4 shows the values of MARD, MAD and  $\delta_{30}$  of the selected correlations for the smooth tube.

All the studied correlations for the evaluation of pressure drop in smooth tube use dimensionless quantities such as Laplace and Weber number to account for the effect of surface tension except Müller-Steinhagen & Heck [27]. Experimental pressure drop data was most accurately predicted by Xu & Fang [45], where the authors studied correlations and experimental data of 15 different fluids in tubes with hydraulic diameters between 0.81 and 19.1 mm and developed a correlation improving the accuracy especially for micro-channels. All correlations tend to slightly underestimate the experimental data in the low pressure drop range, as can be seen in Fig. 12.

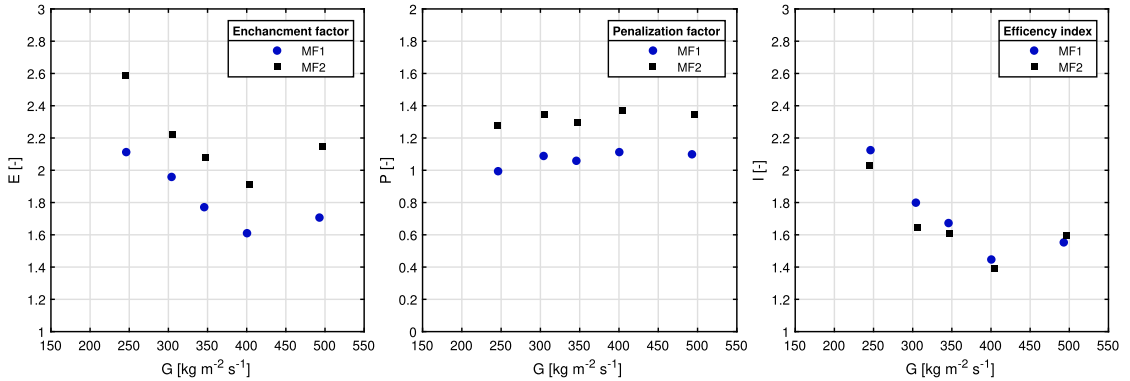


Fig. 11. Enhancement factor  $E$ , Penalization factor  $P$  and efficiency index,  $I$  as a function of mass flux,  $q = 23 \text{ kW m}^{-2}$ ,  $T_{\text{sat}} = 5 \text{ }^\circ\text{C}$ ,  $x = 0.45$ .

**Table 4**  
Comparison between experimental results and correlation for HTC and pressure drop in smooth tube.

	MRD %	MARD%	$\delta_{30}$
<b>Pressure Drop Correlations</b>			
Müller-Steinhagen & Heck [27]	-21.0	22.4	74.1
Sun & Mishima [38]	-36.9	36.9	12.3
Cavallini et al. [4]	-12.7	20.0	90.1
Xu & Fang [45]	-8.8	11.7	100
Friedel [11]	-22.6	23.0	88.9
<b>HTC Correlations</b>			
Choi et al. [8]	7.2	18.3	88.7
Liu & Winterton [23]	3.5	6.2	100
Kandlikar [16]	12.6	14.4	87.7
Tran et al. [41]	36.3	36.3	25.9
Gungor & Winterton [14]	15.7	16.7	85.2
Shah [36]	-6.2	10.9	100
Li & Wu [21]	-23.9	-26.2	59.3
Kim & Mudawar [18]	-9.2	12.1	97.5
Bertsch et al. [2]	-33.8	33.8	55.6
Lillo et al. [22]	72.5	72.5	48.1
Mohd-Yunos et al. [26]	-41.6	41.6	17.5

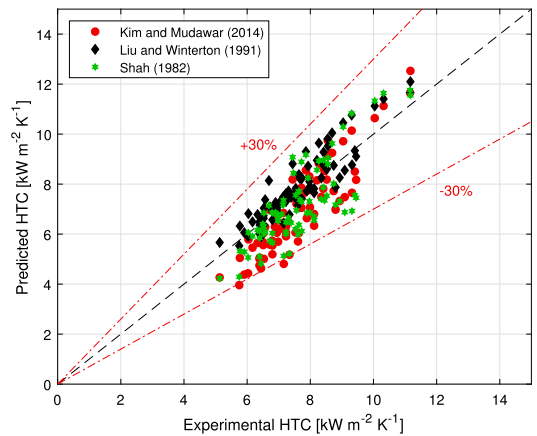


Fig. 13. Comparison between experimental data and correlations of Cavallini et al. [18], Liu & Winterton [23], Shah [36] for prediction of HTC in smooth tube.

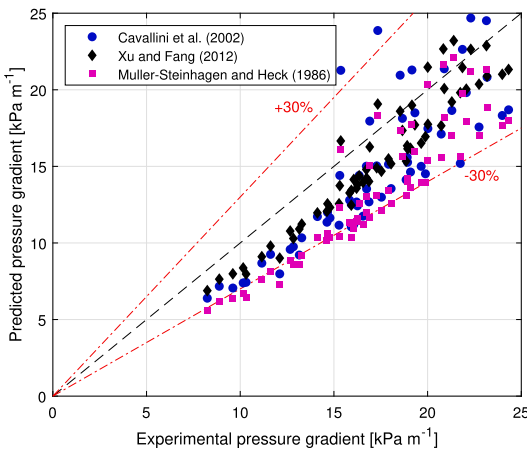


Fig. 12. Comparison between experimental data and correlations of Cavallini et al. [4], Xu & Fang [45], Müller-Steinhagen & Heck [27] for total pressure gradient in smooth tube.

Several correlations were studied for the prediction of HTC in smooth tubes. Among them, the recently developed correlation of Mohd-Yunos et al. [26], which has used genetic algorithm to improve the correlations for the prediction of HTC specifically for propane. However, this method seems to fail in accurately predicting the experimental data points in the present study. Lillo et al. [22] has developed another correlation specifically for propane evaporation HTC which is based on Wo jtan et al. [44] correlation. This correlation predicts HTC values in lower vapor qualities reasonably well while the values for higher vapor qualities are greatly over predicted. Correlations of Liu & Winterton [23] and Shah [36] perform best, being able to predict all data points with less than 30% error (Fig. 13).

For the comparison between experimental data for microfinned tubes and correlations it should be noted that for every correlation the HTC or pressure drop was calculated based on the formulation in the respective paper and compared to an equivalent value for experimental data. This is especially important in the choice of diameter and the respective value for the heat transfer area,  $S$ . The results for MF1 and MF2 are shown in Table 5. The pressure drop correlations of Diani et al. [10] and Rollmann & Spindler [34] exhibit a significant increase in MARD value for MF2 tube compared to MF1. Nevertheless, the correlation by Diani et al. [10] is capable of following the experimental pressure drop data in the whole range for both of the tubes, as depicted on Fig. 14. The gap between the two tubes grows even larger for

**Table 5**  
Comparison between experimental data and correlations for prediction of HTC and pressure drop for microfinned tubes.

	MF1			MF2		
	MAD%	MARD%	$\delta_{30}$	MAD%	MARD%	$\delta_{30}$
<b>Pressure Drop</b>						
<b>Correlations</b>						
Choi et al. [7]	-26.5	26.5	76.0	22.9	22.9	82.4
Rollmann & Spindler [34]	-6.7	8.7	100	-29.8	29.8	45.1
Diani et al. [10]	1	3	100	-12.7	12.7	100
<b>HTC Correlations</b>						
Tang & Li [39]	-23.8	24.1	72.0	39.0	40.0	33.3
Rollmann & Spindler [34]	-5.2	14.8	100	-26.3	26.3	66.7
Diani et al. [10]	-23.0	23.0	90.0	76.9	76.9	2.0

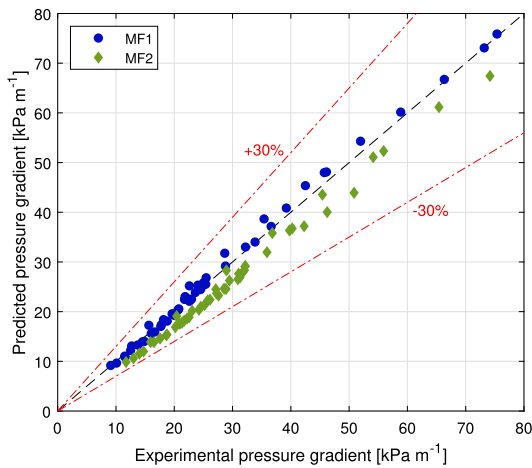


**Fig. 14.** Experimental total pressure gradient compared to the correlation of Diani et al. [10] for two tested MF tubes.

prediction of HTC for the three correlations considered (Fig. 15), particularly with the correlation of Diani et al. [10]. This can be explained by referring to databases that the prior correlations were built upon which use microfinned tubes that have a much smaller value of heat

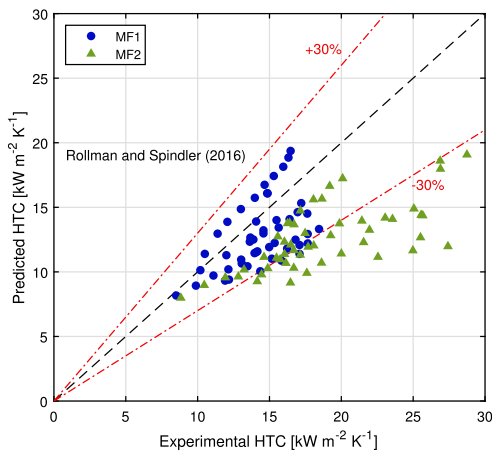
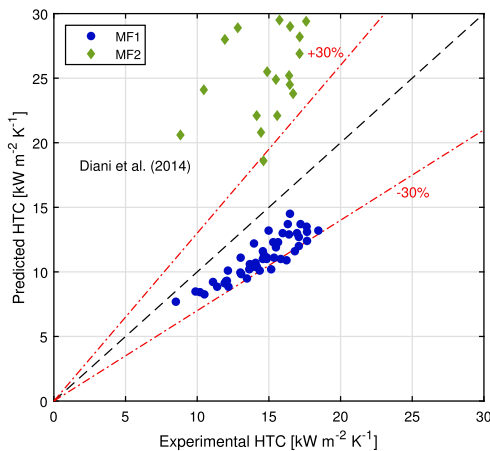


**Fig. 15.** Prediction of HTC in two microfinned tubes by correlations of Diani et al. [10] and Rollmann & Spindler [34] compared to experimental data.

exchange area ratio compared to MF2 tube.

**4. Conclusion**

The evaporation of propane in a smooth and two microfinned tubes with 5 mm OD has been studied experimentally. The heat exchange area ratios are 1.51 and 2.63 for MF1 and MF2, respectively. Heat transfer coefficient and pressure drop were determined at saturation temperatures 0, 5 and 10 °C for the smooth tube, while the three tubes were compared at heat fluxes ranging between 15 and 33 kW m<sup>-2</sup> and mass flux from 250 to 500 kW m<sup>-2</sup> s<sup>-1</sup>.

The results were critically compared, noting that saturation temperature does not affect the HTC, but the pressure drop increases with decreasing saturation temperature. With increasing heat flux, HTC increases for all three tubes (indicating a prevalence of nucleate boiling regime), but this increase is restricted to the low vapor quality range for microfinned tubes. The positive effect of mass flux on the HTC for the smooth tube is limited to the highest tested mass flux, demonstrating activation of the convective heat transfer mechanism. The HTC values with microfinned tubes remain the same with increasing mass flux, while the pressure drop increases.

The HTC enhancement comparing microfinned tubes to the smooth tube drops with increasing mass flux, while the relative increase in pressure drop remains more or less the same. Therefore, discouraging the use of MF tube in higher mass fluxes.

Finally, the experimental data has been compared with several predictive correlations available in the literature. For smooth tube correlations of Xu & Fang [45] and Liu & Winterton [23] reliably predict pressure drop and HTC, respectively. For microfinned tube accuracy of the prediction methods varied based on the tested microfinned tube. While pressure drop and HTC for MF1 are reliably predicted by Diani et al. [10] and Rollmann & Spindler [34], respectively, these correlations deviate from experimental data for MF2 tube. This can be explained by the novel design of MF2, where the number of fins and helical angle is rather high.

**Declaration of Competing Interest**

The authors declare that they have no known competing financial interests or personal relationships that could have appeared to influence the work reported in this paper.

## Acknowledgments

This publication has been funded by HighEFF – Centre for an Energy Efficient and Competitive Industry for the Future, an 8-years' Research

## Appendix A. Calibration process and uncertainty propagation

In order to calibrate the thermocouples, AMETEK JOFRA RTC 157 Reference Temperature Calibrator with the procedure advised by the manufacturer has been used. This unit has an accuracy of 0.04 °C and stability of 0.005 °C. The thermocouples were connected in the same manner as the testing condition (same cables, connections, DAQ) and the values were read each 5 °C in the desired temperature range (-10 °C to 30 °C). The obtained data from the calibration process was used to create a calibration file in LabVIEW.

Below the formulation used for propagating of uncertainty is summarized. Uncertainty for wall temperature:

$$u(T_w) = \sqrt{(1/4)^2 \cdot \sum_{i=4}^7 u(T_i)^2} \quad (\text{A.1})$$

Uncertainty for Saturation temperature:

$$u(T_{sat}) = \sqrt{\left(\frac{\partial T_{sat}}{\partial P_{sat}}\right)^2 \cdot u(P_{sat})^2} \quad (\text{A.2})$$

From Antoine equation the relationship between saturation temperature and saturation pressure can be found, by derivation it can be written:

$$\left(\frac{\partial T_{sat}}{\partial P_{sat}}\right) = \frac{803.99}{P_{sat} \cdot (3.9228 - \log_{10}(P_{sat}))} \quad (\text{A.3})$$

Uncertainty for heat transfer coefficient:

$$u(h) = \sqrt{\left(\frac{u(Q_{test})}{T_w - T_{sat}}\right)^2 + \left(\frac{Q_{test} \cdot u(T_w)}{(T_w - T_{sat})^2}\right)^2 + \left(\frac{Q_{test} \cdot u(T_{sat})}{(T_w - T_{sat})^2}\right)^2} \quad (\text{A.4})$$

Uncertainty for inlet vapor quality:

$$u(x_{in}) = \sqrt{\left(\frac{u(Q_{pre})}{\dot{m} \cdot i_g(P_1)}\right)^2 + \left(\frac{Q_{pre} \cdot u(\dot{m})}{i_g(P_1) \cdot \dot{m}^2}\right)^2} \quad (\text{A.5})$$

Uncertainty for the change in vapor quality:

$$u(\Delta x) = \sqrt{\left(\frac{u(Q_{test})}{\dot{m} \cdot i_g(P_{sat})}\right)^2 + \left(\frac{Q_{test} \cdot \ln(\dot{m}) \cdot u(\dot{m})}{i_g(P_{sat})}\right)^2} \quad (\text{A.6})$$

Uncertainty for the average vapor quality:

$$u(x) = \sqrt{u(x_{in}) + 1/4 \cdot u(\Delta x)^2} \quad (\text{A.7})$$

## References

- [1] E.P. Bandarra Filho, J.M. Saiz Jabardo, P.E.L. Barbieri, Convective boiling pressure drop of refrigerant R-134a in horizontal smooth and microfin tubes, *Int. J. Refrig.* 27 (2004) 895–903, <https://doi.org/10.1016/j.ijrefrig.2004.04.014>.
- [2] S.S. Bertsch, E.A. Groll, S.V. Gariemella, A composite heat transfer correlation for saturated flow boiling in small channels, *Int. J. Heat Mass Transf.* 52 (2009) 2110–2118, <https://doi.org/10.1016/j.ijheatmasstransfer.2008.10.022>.
- [3] B. Bolaji, Z. Huan, Ozone depletion and global warming: Case for the use of natural refrigerant – a review, *Renew. Sustain. Energy Rev.* 18 (2013) 49–54, <https://doi.org/10.1016/j.rser.2012.10.008> <https://www.sciencedirect.com/science/article/pii/S1364032112005503>.
- [4] A. Cavallini, G. Censi, D.D. Col, L. Doretto, G. Longo, L. Rossetto, Condensation of halogenated refrigerants inside smooth tubes, *HVAC&R Res.* 8 (2002) 429–451, <https://doi.org/10.1080/10789669.2002.10391299> <http://www.tandfonline.com/doi/abs/10.1080/10789669.2002.10391299>.
- [5] A. Celen, A. Çebi, A.S. Dalkılıç, Investigation of boiling heat transfer characteristics of R134a flowing in smooth and microfin tubes, *Int. Commun. Heat Mass Transf.* 93 (2018) 21–33, <https://doi.org/10.1016/j.icheatmasstransfer.2018.03.006>.
- [6] J.M. Cho, M.S. Kim, Experimental studies on the evaporative heat transfer and pressure drop of CO2 in smooth and micro-fin tubes of the diameters of 5 and 9.52 mm, *Int. J. Refrig.* 30 (2007) 986–994, <https://doi.org/10.1016/j.ijrefrig.2007.01.007>.
- [7] J.Y. Choi, M.A. Kedzierski, P.A. Domanski, Generalized pressure drop correlation for evaporation and condensation in smooth and micro-fin tubes, IIF-IIR-Commission B1 (2001) <http://fire.nist.gov/bfrlpubs/build01/PDF/b01078.pdf>.
- [8] K.-I. Choi, A. Pamitran, C.-Y. Oh, J.-T. Oh, Boiling heat transfer of R-22, R-134a, and CO2 in horizontal smooth minichannels, *Int. J. Refrig.* 30 (2007) 1336–1346, <https://doi.org/10.1016/j.ijrefrig.2007.04.007> <https://www.sciencedirect.com/science/article/pii/S014070070700076X?via%3Dihub> <https://linkinghub.elsevier.com/retrieve/pii/S014070070700076X>.
- [9] L. Colombo, A. Lucchini, A. Muzzio, Flow patterns, heat transfer and pressure drop for evaporation and condensation of R134A in microfin tubes, *Int. J. Refrig.* 35 (2012) 2150–2165, <https://doi.org/10.1016/j.ijrefrig.2012.08.019> <http://www.sciencedirect.com/science/article/pii/S014070071200206X?via%3Dihub> <https://linkinghub.elsevier.com/retrieve/pii/S014070071200206X> <https://www.sciencedirect.com/science/article/pii/S014070071200206X?via%3Dihub> <https://linkinghub.elsevier.com/retrieve/pii/S014070071200206X>.
- [10] A. Diani, S. Mancin, L. Rossetto, R1234ze(E) flow boiling inside a 3.4 mm ID microfin tube, *Int. J. Refrig.* 47 (2014) 105–119, <https://doi.org/10.1016/j.ijrefrig.2014.07.018>.
- [11] L. Friedel, Improved friction pressure drop correlation for horizontal and vertical two-phase pipe flow, in: *European Two-Phase Flow Group Meeting*, Ispra, 1979, pp. 485–492.
- [12] V. Gnielinski, New equations for heat and mass transfer in the turbulent flow in pipes and channels, *Forsch. Ingenieurwes.* 41 (1975) 8–16 <http://adsabs.harvard.edu/abs/1975STIA...7522028G>.
- [13] E. Granryd, Hydrocarbons as refrigerants — an overview, *Int. J. Refrig.* 24 (2001) 15–24, [https://doi.org/10.1016/S0140-7007\(00\)00665-7](https://doi.org/10.1016/S0140-7007(00)00665-7) <https://www.sciencedirect.com/science/article/pii/S0140700700006657>.
- [14] K. Gungor, R. Winterton, A general correlation for flow boiling in tubes and annuli, *Int. J. Heat Mass Transf.* 29 (1986) 351–358, [https://doi.org/10.1016/0017-9310\(86\)90205-X](https://doi.org/10.1016/0017-9310(86)90205-X) <http://linkinghub.elsevier.com/retrieve/pii/S0140700700006657>.
- [15] ISO, Guide to Expression of Uncertainty in Measurement, 1993.
- [16] S.G. Kandlikar, A general correlation for saturated two-phase flow boiling heat transfer inside horizontal and vertical tubes, *J. Heat Transf.* 112 (1990) 219, <https://doi.org/10.1115/1.2910348> <http://heattransfer.asmedigitalcollection.org/>.

- asme.org/article.aspx?articleid=1440331.
- [17] M. Kedzierski, M. Kim, Convective Boiling and Condensation Heat Transfer with a Twisted-Tape Insert for R12, R22, R152a, R134a, R290, R32/R134a, R32/R152a, R290/R134a, R134a/R600a, 1997. <http://fire.nist.gov/bfrlpubs/build97/art030.html>.
- [18] S.-M. Kim, I. Mudawar, Review of databases and predictive methods for heat transfer in condensing and boiling mini/micro-channel flows, *Int. J. Heat Mass Transf.* 77 (2014) 627–652, <https://doi.org/10.1016/j.ijheatmasstransfer.2014.05.036> <https://linkinghub.elsevier.com/retrieve/pii/S0017931014004360>.
- [19] H. Lee, J. Yoon, J. Kim, P. Bansal, Evaporating heat transfer and pressure drop of hydrocarbon refrigerants in 9.52 and 12.70mm smooth tube, *Int. J. Heat Mass Transf.* 48 (2005) 2351–2359, <https://doi.org/10.1016/j.ijheatmasstransfer.2005.01.012> <http://linkinghub.elsevier.com/retrieve/pii/S0017931005001158>.
- [20] E.W. Lemmon, I.H. Bell, M.L. Huber, M.O. McLinden, NIST Standard Reference Database 23: Reference Fluid Thermodynamic and Transport Properties-REFPROP, Version 10.0, National Institute of Standards and Technology, 2018. doi: <https://dx.doi.org/10.18434/T4J53C>. <https://www.nist.gov/srd/refprop>.
- [21] W. Li, Z. Wu, A general criterion for evaporative heat transfer in micro/mini-channels, *Int. J. Heat Mass Transf.* 53 (2010) 1967–1976, <https://doi.org/10.1016/j.ijheatmasstransfer.2009.12.059>.
- [22] G. Lillo, R. Mastrullo, A.W. Mauro, L. Viscito, Flow boiling heat transfer, dry-out vapor quality and pressure drop of propane (R290): Experiments and assessment of predictive methods, *Int. J. Heat Mass Transf.* 126 (2018) 1236–1252, <https://doi.org/10.1016/j.ijheatmasstransfer.2018.06.069>.
- [23] Z. Liu, R.H. Winterton, A general correlation for saturated and subcooled flow boiling in tubes and annuli, based on a nucleate pool boiling equation, *Int. J. Heat Mass Transf.* 34 (1991) 2759–2766, [https://doi.org/10.1016/0017-9310\(91\)90234-6](https://doi.org/10.1016/0017-9310(91)90234-6) <http://linkinghub.elsevier.com/retrieve/pii/0017931091902346>.
- [24] G.A. Longo, S. Mancini, G. Righetti, C. Zilio, Hydrocarbon refrigerants HC290 (Propane) and HCl270 (Propylene) low GWP long-term substitutes for HFC404A: a comparative analysis in vapourisation inside a small-diameter horizontal smooth tube, *Appl. Therm. Eng.* 124 (2017) 707–715, <https://doi.org/10.1016/j.applthermaleng.2017.06.080>.
- [25] M.H. Maqbool, B. Palm, R. Khodabandeh, Investigation of two phase heat transfer and pressure drop of propane in a vertical circular minichannel, *Exp. Thermal Fluid Sci.* 46 (2013) 120–130, <https://doi.org/10.1016/j.expthermfluidsci.2012.12.002> <http://linkinghub.elsevier.com/retrieve/pii/S0894177712003366>.
- [26] Y. Mohd-Yunos, N. Mohd-Ghazali, M. Mohamad, A.S. Pamitran, J.-T. Oh, Improvement of two-phase heat transfer correlation superposition type for propane by genetic algorithm, *Heat Mass Transf.* (2019), <https://doi.org/10.1007/s00231-019-02776-x> <http://link.springer.com/10.1007/s00231-019-02776-x>.
- [27] H. Müller-Steinhagen, K. Heck, A simple friction pressure drop correlation for two-phase flow in pipes, *Chem. Eng. Process.* 20 (1986) 297–308, [https://doi.org/10.1016/0255-2701\(86\)80008-3](https://doi.org/10.1016/0255-2701(86)80008-3) <http://users.ugent.be/mvbelleg/literatuurSCHX-StijnDaelman/ORCNext/Supercritical/LiteratureStudy/Literature/PapersSHeattransfer/Pressure-drop-friction/1986-Muller-Steinhagen-Asimp> <http://linkinghub.elsevier.com/retrieve/pii/0255270186800083>.
- [28] X.H. Nan, C. Infante Ferreira, In tube evaporation and condensation of natural refrigerant R290 (Propane), *Gustav Lorentz Conf.* 290 (2000) 3.
- [29] J.D. de Oliveira, J.B. Copetti, J.C. Passos, C.W. van der Geld, On flow boiling of R-1270 in a small horizontal tube: flow patterns and heat transfer, *Appl. Therm. Eng.* 178 (2020) 115403, <https://doi.org/10.1016/j.applthermaleng.2020.115403>.
- [30] J.D. de Oliveira, J.C. Passos, J.B. Copetti, C.W. van der Geld, Flow boiling heat transfer of propane in 1.0 mm tube, *Exp. Thermal Fluid Sci.* 96 (2018) 243–256, <https://doi.org/10.1016/j.expthermfluidsci.2018.03.010>.
- [31] B. Palm, Refrigeration systems with minimum charge of refrigerant, *Appl. Therm. Eng.* 27 (2007) 1693–1701, <https://doi.org/10.1016/j.applthermaleng.2006.07.017> <https://linkinghub.elsevier.com/retrieve/pii/S1359431106002481>.
- [32] B. Palm, Hydrocarbons as refrigerants in small heat pump and refrigeration systems – a review, *Int. J. Refrig.* 31 (2008) 552–563, <https://doi.org/10.1016/j.ijrefrig.2007.11.016> <https://linkinghub.elsevier.com/retrieve/pii/S0140700707002216>.
- [33] A. Pamitran, K.-I. Choi, J.-T. Oh, P. Hrnjak, Characteristics of two-phase flow pattern transitions and pressure drop of five refrigerants in horizontal circular small tubes, *Int. J. Refrig.* 33 (2010) 578–588, <https://doi.org/10.1016/j.ijrefrig.2009.12.009> <https://linkinghub.elsevier.com/retrieve/pii/S0140700709002862>.
- [34] P. Rollmann, K. Spindler, New models for heat transfer and pressure drop during flow boiling of R407C and R410A in a horizontal microfin tube, *Int. J. Therm. Sci.* 103 (2016) 57–66, <https://doi.org/10.1016/j.ijthermalsci.2015.11.010>.
- [35] S.Z. Rouhani, E. Axelsson, Calculation of void volume fraction in the subcooled and quality boiling regions, *Int. J. Heat Mass Transf.* 13 (1970) 383–393, [https://doi.org/10.1016/0017-9310\(70\)90114-6](https://doi.org/10.1016/0017-9310(70)90114-6) <http://linkinghub.elsevier.com/retrieve/pii/0017931070901146>.
- [36] M.M. Shah, Chart correlation for saturation boiling heat transfer: equation and further study, *ASHREA Trans.* 88 (1982).
- [37] J.Y. Shin, M.S. Kim, S.T. Ro, Experimental study on forced convective boiling heat transfer of pure refrigerants and refrigerant mixtures in a horizontal tube, *Int. J. Refrig.* 20 (1997) 267–275, [https://doi.org/10.1016/S0140-7007\(97\)00004-2](https://doi.org/10.1016/S0140-7007(97)00004-2).
- [38] L. Sun, K. Mishima, Evaluation analysis of prediction methods for two-phase flow pressure drop in mini-channels, *Int. J. Multiph. Flow* 35 (2008) 47–54, <https://doi.org/10.1016/j.ijmultiphaseflow.2008.08.003> [https://catatanstudi.files.wordpress.com/2009/11/2009-evaluation-analysis-of-prediction-methods-for-2-phase-flow-pressure-drop-in-mini-channels\\_sun.pdf](https://catatanstudi.files.wordpress.com/2009/11/2009-evaluation-analysis-of-prediction-methods-for-2-phase-flow-pressure-drop-in-mini-channels_sun.pdf).
- [39] W. Tang, W. Li, A new heat transfer model for flow boiling of refrigerants in micro-fine tubes, *Int. J. Heat Mass Transf.* 126 (2018) 1067–1078, <https://doi.org/10.1016/j.ijheatmasstransfer.2018.06.066> <https://linkinghub.elsevier.com/retrieve/pii/S0017931018315539>.
- [40] B. Thonon, A review of hydrocarbon two-phase heat transfer in compact heat exchangers and enhanced geometries, *Int. J. Refrig.* 31 (2008) 633–642 <https://www.sciencedirect.com/science/article/pii/S014070070800039X> [https://ac.els-cdn.com/S014070070800039X/1-s2.0-S014070070800039X-main.pdf?tid=7736d389-b443-4b35-8ffb-50ac91ad354f&acdnat=1536823364\\_5438da16af606309302c7cda3040a78](https://ac.els-cdn.com/S014070070800039X/1-s2.0-S014070070800039X-main.pdf?tid=7736d389-b443-4b35-8ffb-50ac91ad354f&acdnat=1536823364_5438da16af606309302c7cda3040a78).
- [41] T.N. Tran, M.W. Wambsganss, D.M. France, Small circular- and rectangular-channel boiling with two refrigerants, *Int. J. Multiph. Flow* 22 (1996) 485–498, [https://doi.org/10.1016/0301-9322\(96\)00002-X](https://doi.org/10.1016/0301-9322(96)00002-X).
- [42] S. Wang, M. Gong, G. Chen, Z. Sun, J. Wu, Two-phase heat transfer and pressure drop of propane during saturated flow boiling inside a horizontal tube, *Int. J. Refrig.* 41 (2014) 200–209, <https://doi.org/10.1016/j.ijrefrig.2013.03.019> <https://linkinghub.elsevier.com/retrieve/pii/S0140700713000741>.
- [43] M.-Y. Wen, C.-Y. Ho, Evaporation heat transfer and pressure drop characteristics of R-290 (propane), R-600 (butane), and a mixture of R-290/R-600 in the three-lines serpentine small-tube bank, *Appl. Therm. Eng.* 25 (2005) 2921–2936, <https://doi.org/10.1016/j.applthermaleng.2005.02.013> [www.elsevier.com/locate/apthermeng](http://www.elsevier.com/locate/apthermeng) <https://linkinghub.elsevier.com/retrieve/pii/S1359431105000827>.
- [44] L. Wojtan, T. Ursenbacher, J.R. Thome, Investigation of flow boiling in horizontal tubes: Part II—Development of a new heat transfer model for stratified-wavy, dryout and mist flow regimes, *Int. J. Heat Mass Transf.* 48 (2005) 2970–2985, <https://doi.org/10.1016/j.ijheatmasstransfer.2004.12.013> <https://linkinghub.elsevier.com/retrieve/pii/S001793100500027X>.
- [45] Y. Xu, X. Fang, A new correlation of two-phase frictional pressure drop for evaporating flow in pipes, *Int. J. Refrig.* 5 (2012) 2039–2050, <https://doi.org/10.1016/j.ijrefrig.2012.06.011> <https://www.sciencedirect.com/science/article/pii/S0140700712001570>.
- [46] X. Zou, M.Q. Gong, G.F. Chen, Z.H. Sun, Y. Zhang, J.F. Wu, Experimental study on saturated flow boiling heat transfer of R170/R290 mixtures in a horizontal tube, *Int. J. Refrig.* 33 (2009) 371–380, <https://doi.org/10.1016/j.ijrefrig.2009.10.013> [https://ac.els-cdn.com/S0140700709002473/1-s2.0-S0140700709002473-main.pdf?tid=55f8bed8-365a-11e7-8107-00000aab0f27&acdnat=1494514907\\_bfeb6a8c8cf41265734e5c99e5f0a5](https://ac.els-cdn.com/S0140700709002473/1-s2.0-S0140700709002473-main.pdf?tid=55f8bed8-365a-11e7-8107-00000aab0f27&acdnat=1494514907_bfeb6a8c8cf41265734e5c99e5f0a5).

## Article II





Contents lists available at ScienceDirect

## Applied Thermal Engineering

journal homepage: [www.elsevier.com/locate/apthermeng](http://www.elsevier.com/locate/apthermeng)

## Comparative analysis of evaporation of isobutane (R600a) and propylene (R1270) in compact smooth and microfinned tubes

Ehsan Allymehr<sup>a,\*</sup>, Ángel Álvarez Pardiñas<sup>b</sup>, Trygve Magne Eikevik<sup>a</sup>, Armin Hafner<sup>a</sup>

<sup>a</sup> Department of Energy and Process Engineering, NTNU Norwegian University of Science and Technology, Kolbjørn Hejes vei 1D, 7491 Trondheim, Norway

<sup>b</sup> SINTEF Energy Research, Kolbjørn Hejes vei 1, 7491 Trondheim, Norway

## ARTICLE INFO

## Keywords:

Hydrocarbon  
Refrigeration  
Heat transfer  
Pressure drop  
Microfinned

## ABSTRACT

Data base for evaporation of flowing isobutane and propylene in compact internally enhanced surfaces is extended by experimental tests in two microfinned tubes and a smooth tube. The outer diameter for all of the test tubes was 5 mm. Heat transfer coefficient and pressure drop were compared for both fluids in all tubes in comparable working conditions. Test conditions were saturation temperatures of 5, 10 and 20 °C, heat fluxes ranging between 15 and 34 k W m<sup>-2</sup> and mass fluxes between 200 and 515 kg m<sup>-2</sup> s<sup>-1</sup>. Results show that propylene has a higher heat transfer coefficient and lower pressure drop compared to isobutane. Furthermore, propylene is nucleate boiling dominant while convective heat transfer is dominant for isobutane. The tested microfinned tubes tend to have a maximum heat transfer coefficient. While for smooth tube correlations were found to reliably predict both heat transfer coefficient and pressure drop, the accuracy of correlations for microfinned tubes is shown to be greatly dependent on the testing conditions and tubes.

### 1. Introduction

Currently the majority of the working fluids used in refrigeration industries have a particularly high global warming potential (GWP). Meanwhile, a progress towards a more environmentally friendly refrigeration industry requires transitioning to working fluids that not only have a low GWP and zero Ozone Depletion Potential (ODP) but are also more energy efficient. Thus, reducing both the direct and indirect impact of refrigeration industry on environment. Historically hydrocarbons have long been used as working fluids in various applications. Propane (R290), isobutane (R600a) and propylene (R1270) are the most used hydrocarbons in small capacity refrigeration units as they offer a favorable saturation curve for different use cases while they have low GWP and zero ODP. However, the use of hydrocarbons in refrigeration systems have been long limited by the concerns about their flammability. One of the most effective ways to decrease potential risk of flammability with hydrocarbons has been to reduce the charge in the system. It has been shown that in the refrigeration systems the majority of charge accumulates in heat exchangers [31] where the fluid is in liquid phase and therefore with a higher density. Therefore, minimizing the volume of a heat exchanger with methods such as the use of microfinned tubes with a high number of fins is essential to increase the

capacity of refrigeration systems using hydrocarbon as the working fluid.

Thonon [39] reviewed the literature on hydrocarbon heat transfer in compact heat exchangers noting that there is a need for more experimental data on in-tube flow boiling of hydrocarbons, especially in the case of microfinned tubes. In a more recent review of evaporation and convective condensation of hydrocarbons by Moreira et al. [25], flow characteristics in convectional and micro sized channels from multiple sources are gathered. The authors concluded that essential parameters for system design such as HTC and pressure drop have been studied by a small number of independent laboratories and data for them is scarce, thus a broader experimental database for assessment of hydrocarbon two phase behaviour becomes essential. Prior research on evaporation of hydrocarbons has mainly focused on tubes of around 10 mm [35,17,28]. Lillo et al. [20] studied the vaporization of R290 in a tube with an internal diameter ( $d_i$ ) of 6 mm at high saturation temperatures. They noted that the main heat transfer mechanism seems to be nucleate boiling, while correlations of Bertsch et al. [2] and Friedel [10] predicted their results for Heat Transfer Coefficient (HTC) and pressure drop most accurately. Longo et al. [22] studied the characteristics of evaporation of R290 and R1270 while comparing them to R404A in a smooth tube with  $d_i$  of 4.0 mm, showing that while R404A has a higher HTC, R1270 and R290 enjoy a lower frictional pressure drop. Longo

\* Corresponding author.

E-mail address: [ehsan.allymehr@ntnu.no](mailto:ehsan.allymehr@ntnu.no) (E. Allymehr).

<https://doi.org/10.1016/j.applthermaleng.2021.116606>

Received 23 September 2020; Received in revised form 12 January 2021; Accepted 16 January 2021

Available online 30 January 2021

1359-4311/© 2021 Published by Elsevier Ltd.

Nomenclature			
<i>Greek</i>		$P$	Pressure [Pa]
$\beta$	Spiral angle	$P_r$	Reduced pressure [-]
$\delta_{30}$	Percentage of predicted values with less than 30% error	$Q$	Heat input [W]
$\gamma$	Fin angle	$q$	Heat flux [ $\text{kJ kg}^{-1}$ ]
<i>Roman</i>		$R_x$	Heat exchange area ratio to a smooth tube [-]
$d_i$	Fin tip diameter for MF tubes, internal diameter for smooth tube [mm]	$S$	Heat exchange area [ $\text{m}^2$ ]
$d_o$	Outer diameter [mm]	$T$	Temperature [ $^{\circ}\text{C}$ ]
$E$	Enhancement Factor [-]	$t_w$	Wall thickness [mm]
$G$	Mass flux [ $\text{kg m}^{-2} \text{s}^{-1}$ ]	$x$	Vapor quality [-]
$HTC$	Heat Transfer Coefficient [ $\text{k W m}^{-2} \text{K}^{-1}$ ]	<i>Subscripts</i>	
$I$	Efficiency index [-]	<i>amb</i>	Ambient condition
$i_{lg}$	Enthalpy of vaporization [ $\text{k W m}^{-2} \text{K}^{-1}$ ]	<i>element</i>	Heating Element
$l_f$	Fin height [mm]	<i>in</i>	Inlet conditions
$m$	Mass flow [ $\text{kg s}^{-1}$ ]	<i>l</i>	Liquid phase
$MARD$	Mean Absolute Relative Deviation [-]	<i>lg</i>	Liquid to gas phase change
$MRD$	Mean Relative Deviation [-]	<i>loss</i>	Heat loss to environment
$n$	Number of fins [-]	<i>pre</i>	Preheater section
$P$	Penalization Factor [-]	<i>sat</i>	Saturated condition
		<i>test</i>	Test section
		<i>w</i>	Wall

et al. [23] compared their previous results with evaporation of R600a in the same tube showing that the HTC of R600a is significantly lower than R1270 and R290. Yang et al. [43] performed similar tests for R600a in conjunction with flow visualization in a smooth tube with  $d_i$  of 6.0 mm. More recently, de Oliveira et al. [29] studied evaporation of R1270 in a tube with  $d_i$  of 1.0 mm noting a dominance of churn and annular-wavy flow, while correlation of Bertsch et al. [2] best predicted the experimental data.

Multiple studies have researched the effect of internally enhanced tubes on evaporation characteristics of different working fluids. Cho & Kim [5] compared the evaporation characteristics of  $\text{CO}_2$  in smooth and microfinned tubes with outer diameters ( $d_o$ ) of 9.52 and 5 mm showing that the HTC in microfinned tubes increased by up to 210%, whilst the pressure drop increase was up to 1.9 times. Celen et al. [4] investigated evaporation of R134a in smooth and microfinned tubes, showing that the pressure drop is increased by up to 3 times while the HTC is increased by 1.9 times. Colombo et al. [8] observed the flow patterns, characteristics of evaporation and condensation of R134a in one smooth and two microfinned tubes showing that in evaporation both microfinned tubes increase the HTC compared to the smooth tube and found no differences among them. Jiang et al. [14] compared evaporation characteristics of R22, R134a, R407C and R410A in a 9.52 mm outer diameter smooth and microfinned tube showing the highest relative increase in HTC to be 1.86 for R22 while highest increase in pressure drop was 1.45 for R407C.

There are few studies dealing with the effect of enhanced surfaces in evaporation of hydrocarbons. Nan & Infante Ferreira [27] studied evaporation and condensation of propane in a smooth, microfinned, and crosshatched tube with  $d_o$  of 9.52 mm. Their results showed the increase in HTC seems to be more noticeable at higher mass fluxes and correlations for internally enhanced tubes considerably over predicted their experimental data. Furthermore, Wen et al. [41] studied the boiling of R600a in a tubes with porous inserts showing that while HTC increases compared to a smooth tube, the relative increase of pressure drop is much higher. More recently, Allymehr et al. [1] studied the evaporation of R290 in smooth and two microfinned tubes demonstrating the prevalence of the nucleate boiling heat transfer mechanism. Moreover, the results showed that with the increase of mass flux in microfinned tube, HTC increase is limited while the pressure drop continues to rise, therefore disincentivizing the use of microfinned tubes in high mass

fluxes. Correlations for smooth tube predicted HTC and pressure drop reliably, while the correlations for microfinned tubes showed a significant dependency on the type of tube.

Consequently, while there is a number of studies that published experimental data on characteristics of evaporation of refrigerants, there is limited data available for hydrocarbons. Additionally, almost none of the previous experimental works have studied the influence of internally enhanced surfaces. As microfinned tubes are becoming increasingly common due to the potential in volume and charge reduction in hydrocarbon heat exchangers, reliable experimental data are required to properly design and size heat exchangers in applications such as air to air heat pumps or domestic refrigerators. This study contributes to completing the database on characteristics of flow boiling of R600a and R1270 in both smooth and microfinned tubes by experimentally measuring HTC and pressure drop values. The effectiveness of internally enhanced surfaces in different working conditions was studied by comparing flow characteristics of two microfinned tubes with dissimilar internal geometries to a smooth tube at similar working conditions. The two microfinned tubes are supposed to represent a more conventional internally enhanced geometry and a more aggressive increase in internal surface area. All three tested tubes have an outer diameter of 5 mm, they were tested at mass fluxes ranging from 200 to 515  $\text{kg m}^{-2} \text{s}^{-1}$  and the heat flux ranged from 15 to 34  $\text{kW m}^{-2}$ . The experimental results were further compared with relevant correlations to analyze the accuracy of available prediction methods.

## 2. Experimental setup

The experimental test rig has been previously used for determination of evaporation characteristics and thus documented in Allymehr et al. [1]. A short description of the test rig is given here for the sake of clarity and ease. Fig. 1 shows the schematic of the test rig, where the test fluid is circulated through the system by a gear pump. Mass flow is measured downstream of the pump. By measurement of the pressure and temperature before the preheater and temperature after preheater, the energy required to vaporize the fluid to the desired inlet quality is calculated. This energy is provided to the fluid in the preheater by means of electrical heating controlled by pulse wave modulation. In order to minimize the heat loss, the test section was insulated using perlite and then contained by hard insulation. Before the test section there is an

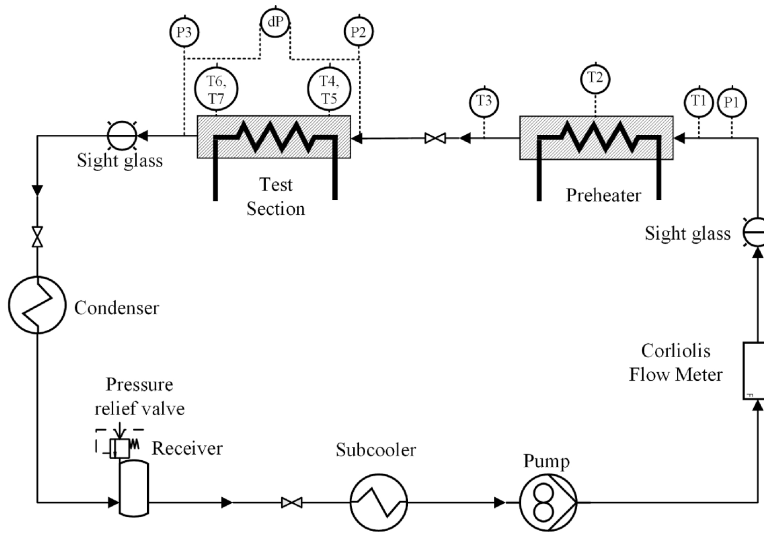


Fig. 1. Test rig schematic.

adiabatic calming section of 75 mm. An electrical heating cable is used as the heating source in the test section. For uniform distribution of heat to the test tube a larger diameter tube is used and the space between the outer tube and the test tube is filled with molten tin. Heat input for both the preheating section and test section is controlled using Pulse Wave Modulation (PWM). The pressure drop is directly measured by a differential pressure transducer via pressures taps 547 mm away from each other at the inlet and outlet of the test section. The wall temperature is obtained from the two pairs of thermocouples brazed to the tube wall located 100 mm from the inlet and outlet of the heated test section. These thermocouples are attached to the outer wall of the test tube by silver brazing. Contact between the thermocouples and the tube is ensured by use silver brazing as it has a higher melting temperature than tin. At each location, one thermocouple is in contact with the top and the other with the bottom part of the test tube. The length of the heated section of all the tested tube is 500 mm. Two pressure sensors are connected to the test section using the same pressure taps for the differential pressure transducer. Average value of these two pressure sensors provides the saturation pressure at test section, and the fluid saturation temperature is determined from this saturation pressure. A photograph of one of the test sections is shown in Fig. 2.

The sight glass located at the exit of the test section does not have the same diameter as tube and therefore is only used for visual inspection of flow. The setup is designed with valves upstream and downstream of the test section, enabling its rapid change without the need to vacuum the whole test rig. At the start-up and with changing of fluids, the test rig is purged with nitrogen and vacuumed before introducing a new fluid. The condenser and the subcooler are each plate heat exchangers. Two

separate thermal baths utilizing a secondary fluid are connected to the subcooler and the condenser to ensure a liquid flow to the pump. Moreover, the condenser is located at the lowest point and has the lowest temperature in the system, thus the saturation pressure of the system can be controlled by the temperature of thermal bath connected to the condenser.

### 2.1. Tested tubes

One smooth tube and two internally enhanced tubes were studied. All three tubes have an  $d_o$  of 5 mm. Geometrical parameters are reported in Table 1, and the physical representations of the parameters are presented in Fig. 3. The fin dimensions for the two microfinned tubes, MF1 and MF2, are roughly the same. The MF2 tube has a higher number of fins and spiral angle, which results in a higher available area for heat transfer compared to the other tested tubes. A cross sectional view of the two tested microfinned tubes is shown in Fig. 4.

### 2.2. Working conditions

Table 2 summarizes the working conditions for both of the fluids. Furthermore, the most differing fluid properties that seem to affect the evaporation characteristics are reported.

### 2.3. Uncertainty analysis and validation

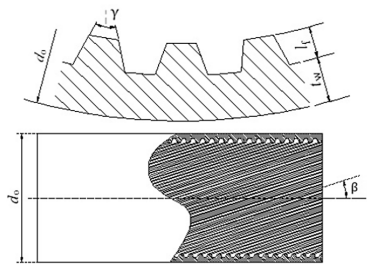
Uncertainty analysis was carried out by the method elaborated in ISO [13] with a confidence level exceeding 95% (coverage factor of 2).



Fig. 2. Photograph of a test section.

**Table 1**  
Geometrical parameters of the test tubes.

	Unit	Smooth tube	MF1	MF2
Outer diameter ( $d_o$ )	mm	5	5	5
Fin tip diameter; Internal diameter for smooth tube ( $d_i$ )	mm	4.1	4.32	4.26
Wall thickness ( $t_w$ )	mm	0.45	0.22	0.22
Actual cross sectional area	mm <sup>2</sup>	13.2	15.7	14.8
Fin height ( $l_f$ )	mm	–	0.12	0.15
Fin number ( $n$ )	(–)	–	35	56
Fin angle ( $\gamma$ )	°	–	35	15
Spiral angle ( $\beta$ )	°	–	15	37
Heat exchange area ratio ( $R_x$ )	(–)	1	1.51	2.63
Heated test section length	mm		500	
Pressure drop measurement length	mm		547	
Test section length	mm		1005	



**Fig. 3.** Physical presentation of the geometrical parameters.

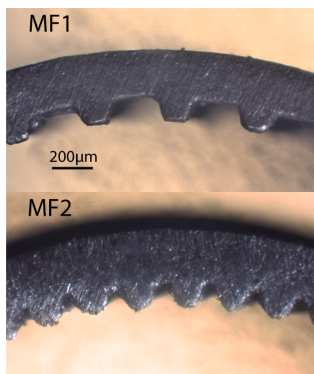


**Fig. 4.** Cross sectional view of the microfinned tubes.

Utilized instruments are listed in Table 3 with their respective uncertainty. The calibration process and formulation used for uncertainty propagation is documented in Al-lymehr et al. [1]. The average values of the uncertainty of measurement for each studied case are reported in Table 4. The increase of uncertainty for HTC values in microfinned tubes is caused by the smaller temperature differences between the saturation temperature and wall temperature. Furthermore, the higher values of average vapor quality uncertainty for R1270 is caused by the higher random error in the measurement of the mass flow in the highest mass flow. Finally, it can be said that the uncertainty of measurement of pressure drop for R600a is lower, this is because, as it will be seen later, R600a generally has a higher pressure drop and since the differential pressure sensor has a systematic uncertainty of the set span, this will be

**Table 2**  
Operating conditions for experimental setup.

	Unit	Range/Value	
		R1270	R600a
<b>Operating conditions</b>			
Saturation Temperature [ $T_{sat}$ ]	°C	5, 10	5, 10, 20
Heat flux [q]	kW m <sup>-2</sup>	15, 24, 33	15, 24, 34
Mass flux [G]	kg m <sup>-2</sup> s <sup>-1</sup>	200–515	250–500
Vapor quality [x]	–	0.13–1	0.11–1
Quality change [ $\Delta x$ ]	–	0.06–0.14	0.07–0.15
<b>Fluid properties</b>			
Reduced pressure [ $P_{red}$ ]	–	0.148–0.171	0.051–0.083
Liquid Viscosity at 10 °C	μPa s	110.4	177.5
Surface Tension at 10 °C	m N m <sup>-1</sup>	8.5	11.8
Vapor Density at 10 °C	kg m <sup>-3</sup>	16.3	5.9

**Table 3**  
List of instruments and their respective uncertainties.

	Type	Range	Uncertainty
Flow meter	Coriolis	0–5 kg min <sup>-1</sup>	±0.1% <sup>a</sup>
Absolute pressure sensor	Strain gauge	0–10 bar	±0.16% <sup>b</sup>
Differential pressure sensor	Strain gauge	0–0.5 bar	±0.15% <sup>b</sup>
Thermocouples	Type T	–	± 0.05 K
Preheater	Electrical	3450 W	±0.44% <sup>a</sup>
Test section heater	Electrical	620 W	± 0.55% <sup>a</sup>

<sup>a</sup> Of the reading.  
<sup>b</sup> Of the set span.

**Table 4**  
Average relative total uncertainty of measurement with a confidence level exceeding 95% for each tested tubes and fluid.

	R600a			R1270		
	Smooth	MF1	MF2	Smooth	MF1	MF2
HTC uncertainty [%]	3.5	6.6	9.0	4.3	8.9	8.7
Pressure drop uncertainty [%]	1.5	0.9	1.0	4.8	4.4	4.1
Average Vapor quality uncertainty [%]	1.1	1.2	1.2	4.5	4.6	5.3

percentage-wise smaller for R600a.

The test rig was validated using single phase gas flow of propane flowing through a smooth tube. Pressure drop and HTC were calculated based on Darcy Weisbach formula and the correlation by Gnielinski V. [11], showing an average absolute deviation of 3.7% and 2.6% for pressure drop and heat transfer coefficient, respectively. Vacuum heat leakage tests were performed to account for the heat loss to the environment. Heat loss was taken into account in the data reduction process by a linear relationship based on the difference of ambient and heating element temperature formulated by 1.

$$Q_{loss} = 0.2075 \cdot (T_{element} - T_{amb}) - 0.2925 \quad [W] \quad (1)$$

This heat loss was on average 2.1% of heat input and the maximum value never exceeded 4.3% in highest heat fluxes.

**2.4. Data reduction**

The four wall temperatures in the last 15 samples should have an standard deviation of less than 0.1 °C for the system to be considered in steady state. If this condition is not met, the system would be considered to be unstable and the data would not be included in the data reduction process. The data from the sensors was recorded for over 120 s to obtain 50 samples, which were then averaged. The average vapor quality value

is calculated by Eq. (2):

$$x = x_{in} + \frac{\Delta x}{2} = \frac{Q_{pre} - \dot{m} \cdot (i_{sat,l} - i_1)}{\dot{m} \cdot i_{lg}(P_{pre})} + \frac{Q_{test} - Q_{loss}}{2 \cdot \dot{m} \cdot i_{lg}(P_{sat})} \quad (2)$$

$i_1$  is the enthalpy of subcooled fluid before entering the preheater while  $P_{pre}$  is the pressure at the preheater section and  $P_{sat}$  is the arithmetic average of the inlet and outlet pressure in the test section.

Heat transfer coefficient is calculated using Eq. (3):

$$HTC = \frac{Q_{test} - Q_{loss}}{S(\bar{T}_w - \bar{T}_{sat})} \quad (3)$$

Where  $T_{sat}$  is derived from the saturation pressure,  $P_{sat}$ .  $\bar{T}_w$  and  $S$  are defined as:

$$\bar{T}_w = \frac{1}{4} \sum_{i=1}^4 T_{w,i} \quad (4)$$

$$S = \pi d_i L \quad (5)$$

The parameters depending on  $d_i$  for the microfinned tubes such as mass flux and heat flux, are calculated based on a smooth tube with internal diameter equal to the fin tip diameter. Thermodynamic properties are evaluated using REFPROP V10 [18].

The total pressure drop  $\Delta P_t$  is calculated by addition of the momentum pressure  $\Delta P_o$  drop with frictional pressure drop  $\Delta P_f$ . The void fraction in the momentum pressure drop calculation was determined using Rouhani & Axelsson [33] correlation. Although this correlation was originally developed for vertical tubes, it takes into account several parameters that are important in mini and micro channels. Therefore it has been used in multiple sources for calculation of the void fraction in horizontal tubes [20,29].

### 3. Results and discussion

#### 3.1. HTC and Pressure drop

Fig. 5 presents the effect of saturation temperature on HTC. The results for the smooth tube show no discernible change for R1270 and R600a. The results for the microfinned tube show a similar pattern, albeit the higher uncertainty levels at higher vapor quality make the comparison less clear.

Fig. 6 depicts the effect of mass flux on HTC in the smooth tube for

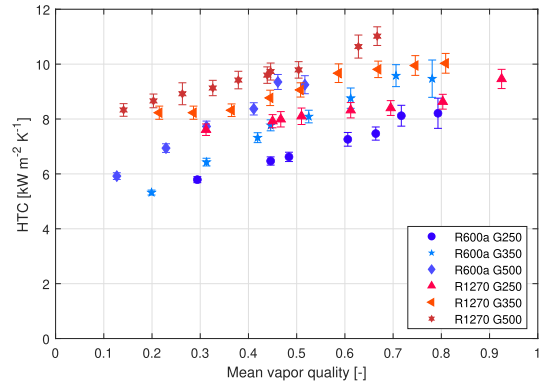


Fig. 6. Effect of mass flux on HTC in smooth tube with  $q = 24 \text{ kW m}^{-2}$ ,  $T_{sat} = 5 \text{ }^\circ\text{C}$  for R1270 and R600a, mass flux (G) in the legend reported in  $\text{kg m}^{-2} \text{ s}^{-1}$ .

both of the fluids. The results indicate that R1270 has higher HTC in all the test conditions, although the increase is more pronounced in lower vapor quality. This can be indicative of a more influential convective heat transfer mechanism in R600a, while heat transfer in R1270 is mainly carried out by nucleation boiling process, thus having a relatively milder increase in HTC with increasing vapor quality. This claim can be further supported by thermophysical properties of fluids. Table 2 shows that the surface tension of the R600a is considerably higher than R1270, this is known to suppress the nucleate boiling by increasing the smallest radius for onset of nucleate boiling [36].

Fig. 7 compares HTC of R1270 and R600a in microfinned tubes in different mass fluxes. Tube MF1 exhibits a clear distinction between fluids, as R1270 has a higher HTC compared to R600a and this increases with the vapor quality. This can be explained by arguing that the microfinned tubes enhance the convective heat transfer regime for R1270, while R600a is already benefiting from a convective energy transport, thus not enhancing the HTC in the same way. As for the MF2, it seems that the HTC is relatively higher for both of the fluids compared to MF1 in similar conditions, this increase is more noticeable at higher vapor qualities and for R600a. The effect of mass flux on HTC seems to be minute for both of the fluids. This upper limit in increase of HTC with mass flux for microfinned tubes was also observed in previous tests for R290 [1]. It can be speculated that the independence of HTC values from

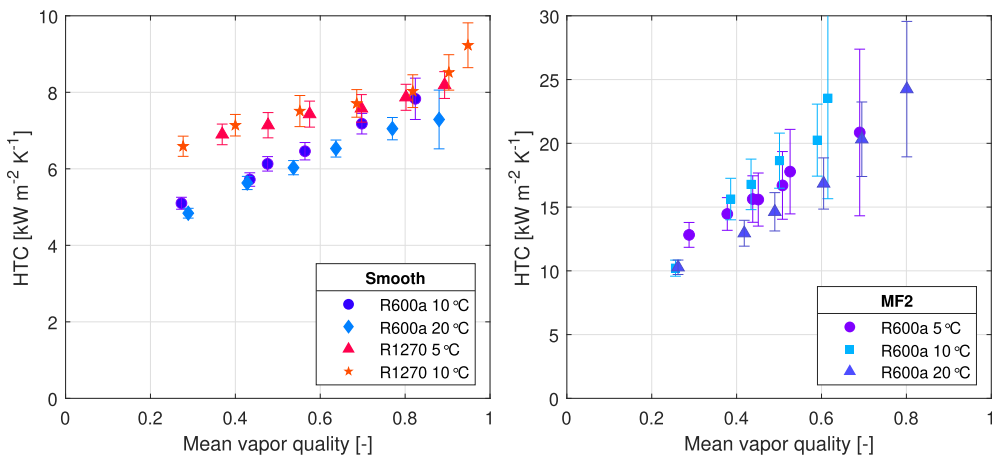


Fig. 5. Effect of saturation temperature on HTC for R1270 and R600a,  $G = 250 \text{ kg m}^{-2} \text{ s}^{-1}$ ,  $q = 15 \text{ kW m}^{-2}$ .

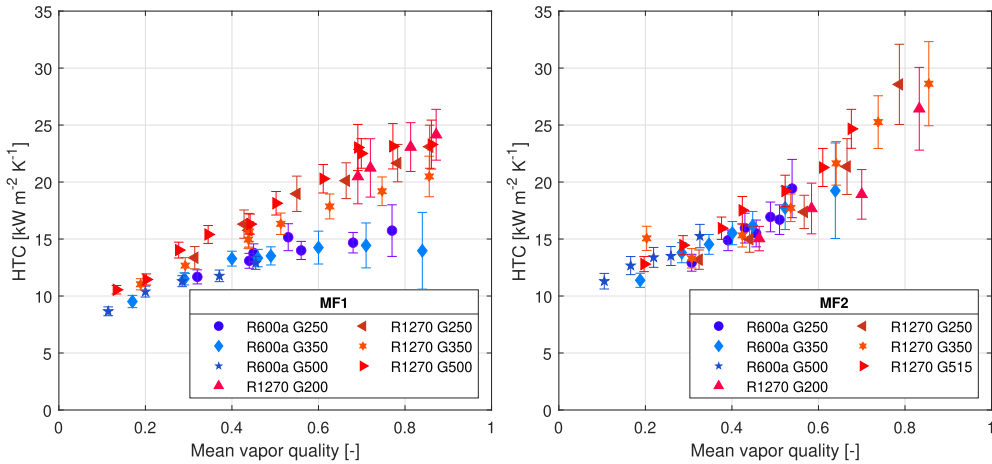


Fig. 7. Effect of mass flux on HTC on MF1 and MF2 with  $q = 24 \text{ kW m}^{-2}$ ,  $T_{sat} = 5 \text{ }^\circ\text{C}$  for R1270 and R600a, mass flux (G) reported in the legend in  $\text{kg m}^{-2} \text{ s}^{-1}$ .

mass flux is caused by the high spiral angle. With increasing mass flux the velocity of the gas core increases, but the increased longitudinal vapor flow cannot increase the swirl motion in liquid film between the fins, as the speed vectors of the phases are notably different from each other. The increased mass flux for isobutane caused the two phase instabilities to happen in lower vapor qualities. Maximum reported values of vapor quality for R600a are lower for higher mass fluxes, this is because unstable points are not reported.

The effect of heat flux on HTC of both fluids in smooth tube is presented in Fig. 8. As expected, since the nucleate boiling effect is dominant for R1270, the HTC increases dramatically with higher heat fluxes in lower vapor quality region, while R600a does not seem to benefit from an increase in the heat flux in a noticeable way.

Fig. 9 shows the effect of heat flux on the HTC of microfinned tubes. HTC values for evaporation of R600a in the MF1 tube seem to be independent of the heat flux. As for R1270 in MF1 tube, there is a considerable increase in HTC going from the lowest heat flux to the average heat flux in all vapor quality ranges. For the highest heat flux, the HTC increased in low vapor quality regions, while in higher vapor quality regions, the HTC is lower than the average heat flux. This trend is remarkable and can be seen in the MF2 tube for R1270 as well, albeit to a lesser extent. While the underlying reason for this remains unclear and

would require flow visualization tests, it is probable that the high heat fluxes at relatively low vapor qualities are able to create local dryout in the tube, while other parts of the tube are still in contact with liquid phase. This trend has also been reported for R290 [11]. Finally, the results for the MF2 tube seem to be somewhat independent of the applied heat flux or the fluid used. It could be speculated that the increase of the HTC decreases the wall temperature, suppressing nucleate boiling and eliminating the effect of heat flux in heat transfer. Seemingly the same mechanism controls the evaporation of R600a in MF1 tube. This results indicate again the limitations for increase of heat transfer by use of microfinned tubes.

The pressure drop is strongly dependent on the mass flux. This can be seen in Fig. 10, which presents the data for the pressure gradient in the smooth tube. R1270 has a lower pressure gradient for all the tested conditions compared to R600a. This is unsurprising as the liquid viscosity of R600a is considerably greater than R1270, meanwhile the vapor density for R600a is lower compared to R1270, creating a higher gas velocity that contributes to a higher shear stress. Furthermore, the results show that R600a is slightly more sensitive to the increase of the mass flux. Finally, R600a is influenced more by the higher vapor quality in higher mass fluxes. (see Fig. 11).

In order to compare the effect of MF tubes, three parameters are defined, Enhancement factor  $E$ , Penalization factor  $P$ , and efficiency index,  $I$ , which are formulated as:

$$E = \frac{h_{MF}}{h_{Smooth}} \tag{6}$$

$$P = \frac{\Delta P_{MF}}{\Delta P_{Smooth}} \tag{7}$$

$$I = \frac{E}{P} \tag{8}$$

These factors are visualized in Fig. 12 for both of the fluids. The data could not be obtained for all the mass fluxes because of difficulties in accurate control of mean vapor quality or limitations of instruments specially for R1270 flowing in MF2 tube, nevertheless the figures present a clear pattern for all the three parameters apart from R1270 in MF2. Enhancement factor,  $E$ , decreases with mass flux for all the tested cases. As mentioned earlier this happens mainly because of the increase in HTC of smooth tube in higher mass fluxes while MF tubes present a more or less constant HTC with mass flux. It is also interesting to compare the value of  $E$  with the increase in heat exchange area,  $R_x$ , it

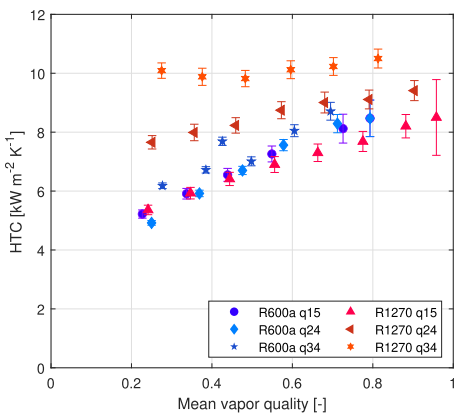


Fig. 8. Effect of heat flux on HTC on smooth tube with  $G = 300 \text{ kg m}^{-2} \text{ s}^{-1}$ ,  $T_{sat} = 10 \text{ }^\circ\text{C}$ , reported heat flux ( $q$ ) in  $\text{kW m}^{-2}$ .

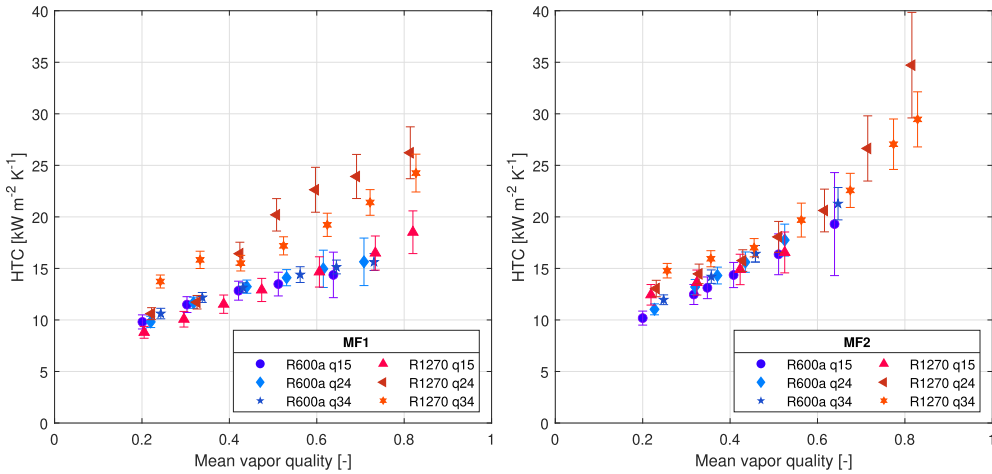


Fig. 9. Effect of heat flux on HTC in microfinned tubes with  $G = 300 \text{ kg m}^{-2} \text{ s}^{-1}$ ,  $T_{sat} = 10 \text{ }^\circ\text{C}$ , reported heat flux ( $q$ ) in  $\text{kW m}^{-2}$ .

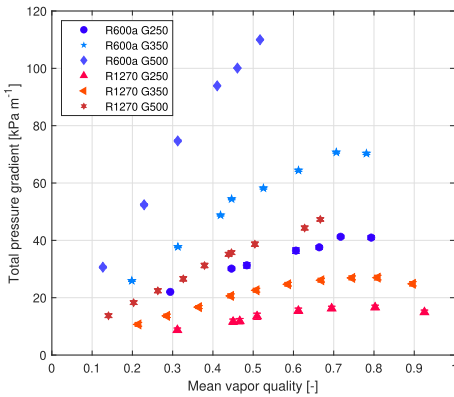


Fig. 10. Effect of mass flux on total pressure gradient of smooth tube at  $q = 24 \text{ kW m}^{-2}$  for R1270 and R600a, mass flux ( $G$ ) reported in  $\text{kg m}^{-2} \text{ s}^{-1}$ .

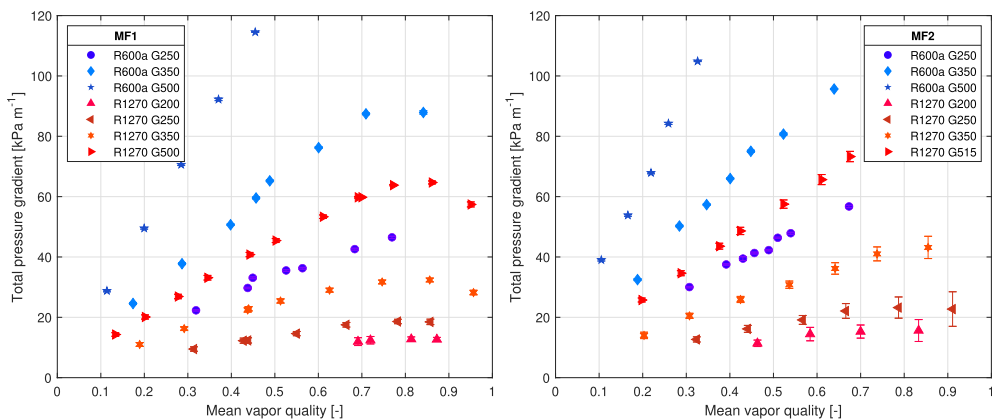


Fig. 11. Effect of mass flux on total pressure gradient of R1270 and R600a at  $q = 24 \text{ kW m}^{-2}$ ,  $T_{sat} = 5 \text{ }^\circ\text{C}$  for MF1 and MF2, mass flux ( $G$ ) in legend reported in  $\text{kg m}^{-2} \text{ s}^{-1}$ .

seems that for MF1 tube  $E$  is higher than  $R_x$  in lower mass fluxes, while in higher mass fluxes  $E$  moves asymptotically towards  $R_x$ . In MF2 tube  $E$  is lower than  $R_x$  and it further reduces in higher mass fluxes. This can be explained by arguing that in low mass fluxes the turbulence caused by the fins would affect the thermal boundary layer at the wall and increase the HTC, while in the higher mass fluxes the turbulence at smooth tube would compensate for this. Nevertheless the increase in the heat transfer area enables more heat to be transferred from the fluid in MF tubes in this condition. The results for MF2 tube also indicate that while a higher increase in the heat transfer area is beneficial for HTC, this increase is not linear and diminishing. Value of  $E$  for R1270 in MF2 seems to be an outlying point, as the increase of HTC is lower than expected. While the number of available data points is too small to make a verdict, it could be argued that although the increased turbulence would increase the HTC, the higher spiral angle,  $\beta$ , could suppress the nucleate boiling which is the dominant heat transfer mechanism for R1270. As for penalization factor,  $P$ , it is higher for MF2 tube. This was expected because of the higher fin number and spiral angle of the MF2 tube. Furthermore,  $P$  does not seem to be a function of mass flux. Finally regarding the efficiency index,  $I$ , there is a clear decrease with mass flux. If efficiency index were to be considered as how advantageous is the use of an internally

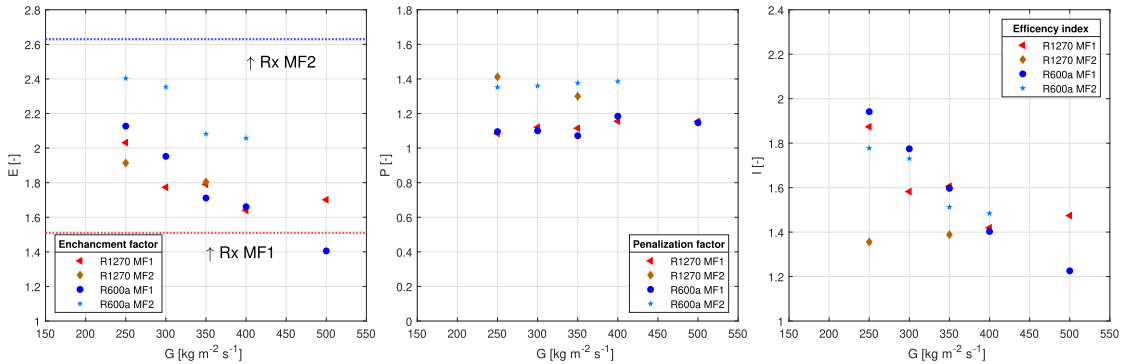


Fig. 12. Enhancement factor  $E$ , Penalization factor  $P$  and efficiency index,  $I$  as a function of mass flux,  $q = 23 \text{ kW m}^{-2}$ ,  $T_{\text{sat}} = 5 \text{ }^\circ\text{C}$ ,  $x = 0.45$ , heat exchange area increase shown with  $R_x$ .

enhanced tube, it could be concluded that the microfinned tubes are most beneficial in low mass fluxes. Interestingly with a higher  $E$  and  $P$  value, the efficiency index of MF2 tube is close to MF1 tube. Thus from this point of view, there is no difference between these internally enhanced tubes. Nevertheless, if the goal of heat exchanger design were to minimize the charge, it would still be favorable to use a tube with a higher number of fins and spiral angle, such as MF2 tube.

3.2. Correlations

The experimental data for HTC and pressure drop for all tested conditions are compared with applicable predictive correlations by values of Mean Relative Deviation (MRD) and Mean Absolute Relative Deviation (MARD), defined as:

$$MRD = \frac{100}{n} \sum_{i=1}^n \frac{Predicted_i - Experimental_i}{Experimental_i} \tag{9}$$

$$MARD = \frac{100}{n} \sum_{i=1}^n \left| \frac{Predicted_i - Experimental_i}{Experimental_i} \right| \tag{10}$$

Furthermore,  $\delta_{30}$  is defined as the percentage of the predicted values having less than 30% deviation from the experimental data. Table 5 shows the values of MRD, MARD and  $\delta_{30}$  of the selected correlations for the smooth tube.

Special care was taken to choose correlations that are most applicable to the experimental condition of this study, for example, all the studied correlations for the evaluation of pressure drop in smooth tube use dimensionless quantities such as Laplace or Weber number to account for the effect of surface tension, except Müller-Steinhagen & Heck [26]. The selection of HTC correlations was focused either on correlations developed for hydrocarbons such as Mohd-Yunos et al. [24] or those considering smaller-diameter tubes such as Bertsch et al. [2]. Furthermore, well known correlations such as Kandlikar [15] and Liu & Winterton [21] were also analyzed. Table 5 summarizes the results of comparison for both of the fluids in smooth tube.

Apart from Sun & Mishima [37], the selected correlations for pressure drop in smooth tube show a high degree of reliability in predicting experimental results, data was most accurately predicted by Xu & Fang [42] confirming the prior results for pressure drop in R290 [1]. In Xu & Fang [42] authors studied correlations and experimental data of 15 different fluids in tubes with hydraulic diameters between 0.81 and 19.1 mm and developed a correlation improving the accuracy especially for micro-channels. Notably this correlation did not have any hydrocarbons in its database. The parity plot for this correlation is shown in Fig. 13.

As for the HTC, correlation of Mohd-Yunos et al. [24] and Lillo et al.

Table 5

Comparison between experimental results and correlations for HTC and pressure drop in smooth tube.

	R600a			R1270		
	MRD %	MARD %	$\delta_{30}$	MRD %	MARD %	$\delta_{30}$
<b>Pressure Drop</b>						
<b>Correlations</b>						
Müller-Steinhagen & Heck [26]	-13.1	15.6	100	-16.7	19.4	97
Sun & Mishima [37]	-33.0	33.0	28.6	-33.4	33.4	20.9
Cavallini et al. [3]	3.0	12.7	90.0	-10.6	20.6	92.5
Xu & Fang [42]	1.8	6.6	100	-5.3	9.9	100
Friedel [10]	-20.1	20.4	94.3	-17.1	18.6	100
<b>HTC Correlations</b>						
Choi et al. [7]	1.2	15.2	88.1	0.9	24.8	80.6
Liu & Winterton [21]	15.3	15.3	90.0	6.8	8.5	100
Kandlikar [15]	19.8	19.8	90.0	-3.2	9.2	100
Tran et al. [40]	-59.0	59.0	1.4	-48.5	48.5	1.5
Gungor & Winterton [12]	9.8	12.5	94.3	4.3	9.4	97.0
Shah [34]	1.7	6.4	100	-17.5	18.5	88.1
Li & Wu [19]	-52.3	52.3	4.3	-36.1	36.1	28.4
Kim & Mudawar [16]	-29.4	29.4	51.4	-16.8	17.7	89.6
Bertsch et al. [2]	-42.3	42.3	14.3	-40.2	40.2	31.3
Mohd-Yunos et al. [24]	-52.7	52.7	5.7	-46.0	46.0	7.5
Lillo et al. [20]	30.1	30.7	71.4	92.2	92.2	55.2

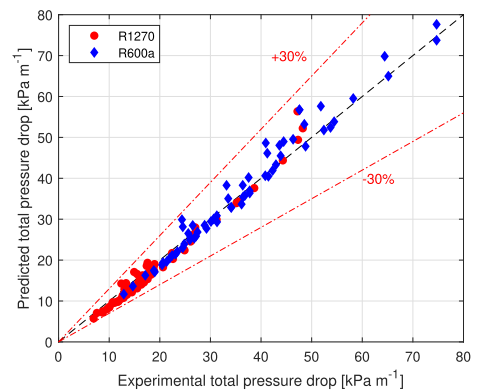


Fig. 13. Comparison between experimental data and correlations of Xu & Fang [42] for prediction of pressure drop of R600a and R1270. in smooth tube.

[20] which were explicitly developed for hydrocarbons using genetic algorithms and flow pattern observation respectively, were surprisingly the least reliable correlations. Correlation of Lillo et al. [20] is intriguing as it shows a sound agreement with experimental results in lower vapor qualities, while at higher vapor qualities over predicts the experimental data. Therefore it seems that Lillo et al. [20] emphasizes the effect of convective heat transfer, and consequently it can follow R600a experimental data more closely as the heat transfer mechanism for R600a is convection dominated.

Correlations of Liu & Winterton [21], Kandlikar [15], Gungor & Winterton [12] performed best in predicting the HTC, being able to predict more than 90% of data points with less than 30% error for both of the fluids. Almost all of these correlation are relying on the principle of dividing the boiling heat transfer in two parts, nucleate boiling and convective boiling, thus the difference between them arises from how some factors are defined based on the database used for their development. This is again similar to the results obtained for R290 in Allymehr et al. [1].

Microfinned tube correlations were calculated using the formulation provided in their respective papers. If the formulation used for microfinned correlations utilized parameter definitions other than the ones used in this study, experimental data was converted to match the correlation's definition. This point is crucial in choice of internal diameter as it affects other parameters such as mass flux,  $G$  and heat transfer area,  $S$ .

Table 6 shows the comparison data for MF1 tube for pressure drop and HTC. While Diani et al. [9] predicts R1270 data the best and Rollmann & Spindler [32] does so for R600a data, it can be said that both are capable of accurately predicting the pressure drop for both of the fluids.

As for HTC, the correlation of Padovan et al. [30] is the most accurate in both fluids, albeit the reliability is less for R1270 compared to R600a. This is even more notable for the correlation of Rollmann & Spindler [32] where  $\delta_{30}$  drops from 95.5% for R600a to 3.5% for R1270. This can be explained by arguing that the Prandtl number of R1270 in tested condition is close to the range of validity declared in Rollmann & Spindler [32] to be higher than 2.28, while R600a fits better in the range of validity.

Results for MF2 tube portrayed in Table 7 show that while Diani et al. [9] reliably predicts the pressure drop, other correlations perform significantly worse compared to MF1 tube data. Furthermore, none of the correlation seem to be able to follow the HTC of MF2 tube. While the correlation of Tang & Li [38], Rollmann & Spindler [32] show the lowest values of MRD and MARD, their predictive ability is far lower for R1270 compared to R600a. The lower availability of data for R1270 as a working fluid might be the a contributing factor for this inconsistency. The parity plot in Fig. 14 visualizes the comparison between the correlations of Rollmann & Spindler [32], Diani et al. [9] and the experimental data for MF1 and MF2.

**Table 6**

Comparison between experimental data and correlations for prediction of HTC and pressure drop for microfinned tube MF1.

	R600a MF1			R1270 MF1		
	MRD	MARD	$\delta_{30}$	MRD	MARD	$\delta_{30}$
	%	%		%	%	
<b>Pressure Drop</b>						
<b>Correlations</b>						
Choi et al. [6]	-15.9	15.9	100	28.7	28.8	41.4
Rollmann & Spindler [32]	-3.8	5.7	100	-9.6	13.2	96.6
Diani et al. [9]	13.9	13.9	100	-3.3	5.2	100
<b>HTC Correlations</b>						
Tang Li [38]	-36.9	36.9	31.8	-28.1	29.4	53.4
Rollmann & Spindler [32]	1.7	12.0	95.5	-58.8	58.8	3.5
Diani et al. [9]	-35.4	35.4	11.4	-28.6	28.9	56.9
Padovan et al. [30]	1.0	5.4	100	19.6	23.4	74.1

**Table 7**

Comparison between experimental data and correlations for prediction of HTC and pressure drop for microfinned tube MF2.

	R600a MF2			R1270 MF2		
	MRD	MARD	$\delta_{30}$	MRD	MARD	$\delta_{30}$
	%	%		%	%	
<b>Pressure Drop</b>						
<b>Correlations</b>						
Choi et al. [6]	29.5	29.5	47.2	18.9	18.9	85.4
Rollmann & Spindler [32]	-30.3	30.3	41.5	-32.6	32.6	33.3
Diani et al. [9]	-4.0	4.4	100	-14.8	14.8	100
<b>HTC Correlations</b>						
Tang & Li [38]	23.4	23.4	73.6	41.4	41.4	25.0
Rollmann & Spindler [32]	-25.6	25.6	69.8	-65.6	65.6	0
Diani et al. [9]	56.6	56.6	3.8	85.2	85.2	4.2
Padovan et al. [30]	113.2	113.2	0.0	168.1	168.1	0.0

Finally, a cross examination of Tables 6 and 7 shows that the predictive ability for HTC of Padovan et al. [30], Diani et al. [9] is significantly worse for MF2 data. A closer analysis of these correlations shows that the heat exchange area multiplier in these correlations were designed for tubes with a low increase in heat exchange area ratio, such as in MF1 tube, hence over predicting HTC data for MF2.

#### 4. Conclusion

While microfinned tubes have the potential to reduce volume and charge in heat exchangers, lack of data for key design elements makes system design challenging. This paper contributes to the available literature on flow characteristics of hydrocarbons by presenting experimental data on evaporation of isobutane (R600a) and propylene (R1270) in one smooth and two microfinned tubes with an outer diameter of 5 mm. The increased heat exchange area for microfinned tubes are 1.51 and 2.63 for MF1 and MF2, respectively. The characteristics of flow in two microfinned tubes and the smooth tube are compared in similar working conditions. Experimental data was recorded at saturation temperatures 5, 10 and 20 °C, heat fluxes ranging between 15 and 34 kW m<sup>-2</sup> and mass fluxes from 200 to 515 kg m<sup>-2</sup> s<sup>-1</sup>.

The results are critically compared, noting that saturation temperature does not strongly affect the HTC. In similar test conditions, R1270 has a higher HTC and a lower pressure drop than R600a. With increasing heat flux, HTC of R1270 increases in smooth tube and MF1 tube, specially at lower vapor qualities indicating a prevalence of nucleate boiling regime, while R600a is not affected. With increasing mass flux, HTC in smooth tube for both R600a and R1270 increases at higher vapor qualities. As for the MF2 tube, HTC values remain the same with increasing mass flux and heat flux, showing a maximum heat transfer capability. As for the pressure drop, the most decisive parameter for all fluids and tubes is the mass flux. Comparison of data between MF tubes and smooth tube showed a maximum increase of 2.4 and 2.0 for HTC of R600a and R1270, respectively. Increase of pressure drop in MF tubes were 1.15 and 1.4 for MF1 and MF2 tube, respectively. Since by increasing mass flux the relative increase in pressure drop between microfinned and smooth tubes is greater than the relative increase in HTC, the use of microfinned tubes in higher mass fluxes is discouraged.

Finally, the experimental data has been compared with several predictive correlations available in the literature. For smooth tube, correlations of Xu & Fang [42] and Liu & Winterton [21] reliably predict pressure drop and HTC, respectively. For microfinned tubes, accuracy of the prediction methods varied based on the tested tube and the fluid. Correlation of Diani et al. [9] reliably predicted all pressure drop experimental data. Correlation of Rollmann & Spindler [32] best predicted the HTC data for R600a, while there were no reliable correlation found for HTC of R1270.

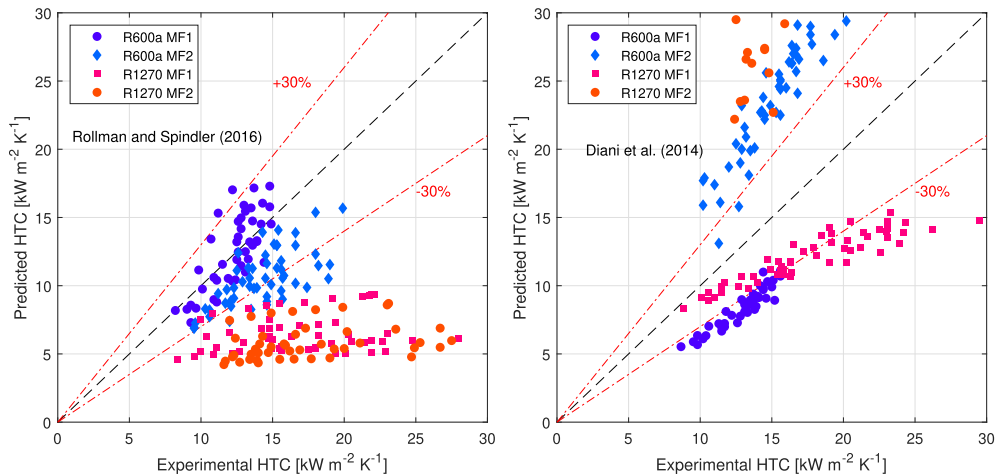


Fig. 14. Prediction of HTC in two microfinned tubes by correlations of Diani et al. [9] and Rollmann & Spindler [32] compared to experimental data.

### Declaration of Competing Interest

The authors declare that they have no known competing financial interests or personal relationships that could have appeared to influence the work reported in this paper.

### Acknowledgments

This publication has been funded by HighEFF - Centre for an Energy Efficient and Competitive Industry for the Future, an 8-years' Research Centre under the FME-scheme (Centre for Environment-friendly Energy Research, 257632). The authors gratefully acknowledge the financial support from the Research Council of Norway and user partners of HighEFF.

### References

- E. Allymehr, Á.Á. Pardiñas, T.M. Eikevik, A. Hafner, Characteristics of evaporation of propane (R290) in compact smooth and microfinned tubes, *Appl. Therm. Eng.* 181 (2020) 115880, <https://doi.org/10.1016/j.applthermaleng.2020.115880>.
- S.S. Bertsch, E.A. Groll, S.V. Garimella, A composite heat transfer correlation for saturated flow boiling in small channels, *Int. J. Heat Mass Transf.* 52 (2009) 2110–2118, <https://doi.org/10.1016/j.jheatmasstransfer.2008.10.022>.
- A. Cavallini, G. Censi, D.D. Col, L. Doretto, G. Longo, L. Rossetto, Condensation of Halogenated Refrigerants Inside Smooth Tubes, *HVAC&R Res.* 8 (2002) 429–451, <https://doi.org/10.1080/10789669.2002.10391299>, <http://www.tandfonline.com/doi/abs/10.1080/10789669.2002.10391299>.
- A. Celen, A. Çebi, A.S. Dalkılıç, Investigation of boiling heat transfer characteristics of R134a flowing in smooth and microfin tubes, *Int. Commun. Heat Mass Transfer* 93 (2018) 21–33, <https://doi.org/10.1016/j.icheatmasstransfer.2018.03.006>.
- J.M. Cho, M.S. Kim, Experimental studies on the evaporative heat transfer and pressure drop of CO<sub>2</sub> in smooth and micro-fin tubes of the diameters of 5 and 9.52 mm, *Int. J. Refrig.* 30 (2007) 986–994, <https://doi.org/10.1016/j.jrefrig.2007.01.007>.
- J.Y. Choi, M.A. Kedzierski, P.A. Domanski, Generalized Pressure Drop Correlation for Evaporation and Condensation in Smooth and Micro-Fin Tubes, IIF-IRR-Commission B1 (2001) <http://fire.nist.gov/bfrlpubs/build01/PDF/b01078.pdf>.
- K.-I. Choi, A. Pamitran, C.-Y. Oh, J.-T. Oh, Boiling heat transfer of R-22, R-134a, and CO<sub>2</sub> in horizontal smooth minichannels, *Int. J. Refrig.* 30 (2007) 1336–1346, <https://doi.org/10.1016/j.jrefrig.2007.04.007>, <https://www.sciencedirect.com/science/article/pii/S014070070700076X?via%3Dihub> <https://linkinghub.elsevier.com/retrieve/pii/S014070070700076X>. doi:10.1016/j.jrefrig.2007.04.007.
- L. Colombo, A. Lucchini, A. Muzzio, Flow patterns, heat transfer and pressure drop for evaporation and condensation of R134a in microfin tubes, *Int. J. Refrig.* 35 (2012) 2150–2165, <https://doi.org/10.1016/j.jrefrig.2012.08.019>, <https://www.sciencedirect.com/science/article/pii/S014070071200206X?via%3Dihub> <https://linkinghub.elsevier.com/retrieve/pii/S014070071200206X>.
- A. Diani, S. Mancin, L. Rossetto, R1234ze(E) flow boiling inside a 3.4 mm ID microfin tube, *Int. J. Refrig.* 47 (2014) 105–119, <https://doi.org/10.1016/j.jrefrig.2014.07.018>.
- L. Friedel, Improved friction pressure drop correlation for horizontal and vertical two-phase pipe flow, in: *European Two-Phase Flow Group Meeting, Ispra, 1979*, pp. 485–492.
- V. Gnielinski, New equations for heat and mass transfer in the turbulent flow in pipes and channels, *Forsch. Ingenieurwes.* 41 (1975) 8–16, <http://adsabs.harvard.edu/abs/1975STIA...7522028G>.
- K. Gungor, R. Winterton, A general correlation for flow boiling in tubes and annuli, *Int. J. Heat Mass Transf.* 29 (1986) 351–358, [https://doi.org/10.1016/0017-9310\(86\)90205-X](https://doi.org/10.1016/0017-9310(86)90205-X), <http://linkinghub.elsevier.com/retrieve/pii/001793108690205X>.
- ISO, 1993. Guide to Expression of Uncertainty in Measurement.
- G.B. Jiang, J.T. Tan, Q.X. Nian, S.C. Tang, W.Q. Tao, Experimental study of boiling heat transfer in smooth/micro-fin tubes of four refrigerants, *Int. J. Heat Mass Transf.* 98 (2016) 631–642, <https://doi.org/10.1016/j.jheatmasstransfer.2016.03.024>.
- S.G. Kandlikar, A General Correlation for Saturated Two-Phase Flow Boiling Heat Transfer Inside Horizontal and Vertical Tubes, *J. Heat Transf.* 112 (1990) 219, <https://doi.org/10.1115/1.2910348>.
- S.-M. Kim, I. Mudawar, Review of databases and predictive methods for heat transfer in condensing and boiling mini/micro-channel flows, *Int. J. Heat Mass Transf.* 77 (2014) 627–652, <https://doi.org/10.1016/j.jheatmasstransfer.2014.05.036>.
- H. Lee, J. Yoon, J. Kim, P. Bansal, Evaporating heat transfer and pressure drop of hydrocarbon refrigerants in 9.52 and 12.70mm smooth tube, *Int. J. Heat Mass Transf.* 48 (2005) 2351–2359, <https://doi.org/10.1016/j.jheatmasstransfer.2005.01.012>, <http://linkinghub.elsevier.com/retrieve/pii/S0017931005001158>.
- E.W. Lemmon, I.H. Bell, M.L. Huber, M.O. McLinden, NIST Standard Reference Database 23: Reference Fluid Thermodynamic and Transport Properties-REFPROP, Version 10.0, National Institute of Standards and Technology, 2018, <http://www.nist.gov/srd/refprop>. doi:https://dx.doi.org/10.18434/T4J3SC.
- W. Li, Z. Wu, A general criterion for evaporative heat transfer in micro/mini-channels, *Int. J. Heat Mass Transf.* 53 (2010) 1967–1976, <https://doi.org/10.1016/j.jheatmasstransfer.2009.12.059>.
- G. Lillo, R. Mastrullo, A.W. Mauro, L. Viscito, Flow boiling heat transfer, dry-out vapor quality and pressure drop of propane (R290): Experiments and assessment of predictive methods, *Int. J. Heat Mass Transf.* 126 (2018) 1236–1252, <https://doi.org/10.1016/j.jheatmasstransfer.2018.06.069>.
- Z. Liu, R.H. Winterton, A general correlation for saturated and subcooled flow boiling in tubes and annuli, based on a nucleate pool boiling equation, *Int. J. Heat Mass Transf.* 34 (1991) 2759–2766, [https://doi.org/10.1016/0017-9310\(91\)90234-6](https://doi.org/10.1016/0017-9310(91)90234-6), <http://linkinghub.elsevier.com/retrieve/pii/0017931091902346>.
- G.A. Longo, S. Mancin, G. Righetti, C. Zilio, Hydrocarbon refrigerants HC290 (Propane) and HCl1270 (Propylene) low GWP long-term substitutes for HFC404A: A comparative analysis in vaporisation inside a small-diameter horizontal smooth tube, *Appl. Therm. Eng.* 124 (2017) 707–715, <https://doi.org/10.1016/j.applthermaleng.2017.06.080>.
- G.A. Longo, S. Mancin, G. Righetti, C. Zilio, Hydrocarbons vaporisation inside a 4 mm ID horizontal, In: 13th IIR-Gustav Lorentzen Conference on Natural Refrigerants. Valencia, 2018. doi:10.18462/iir.gl.2018.1329.
- Y. Mohd-Yunos, N. Mohd-Phazali, M. Mohamad, A.S. Pamitran, J.-T. Oh, 2019. Improvement of two-phase heat transfer correlation superposition type for propane by genetic algorithm. *Heat and Mass Transfer*, <http://link.springer.com/10.1007/s00231-019-02776-x>. doi:10.1007/s00231-019-02776-x.
- T.A. Moreira, G. Furlan, G.H.d.s.e. Oliveira, G. Ribatski, Flow boiling and convective condensation of hydrocarbons: A state-of-the-art literature review, *Appl. Therm. Eng.* 182 (2021) 116129, <https://doi.org/10.1016/j.applthermaleng.2021.116129>.

- applthermaleng.2020.116129, <https://linkinghub.elsevier.com/retrieve/pii/S1359431120336097>.
- [26] H. Müller-Steinhagen, K. Heck, A simple friction pressure drop correlation for two-phase flow in pipes. *Chemical Engineering and Processing: Process Intensification*, 20 (1986) 297–308. [http://users.ugent.be/~mvbelleg/literatuur/SCHX - Stijn Daelman/ORCNext/Supercritical/Literature/Study/Literature/Papers/SC Heat transfer/Pressure drop-friction/1986 - Muller-Steinhagen - A simp](http://users.ugent.be/~mvbelleg/literatuur/SCHX-StijnDaelman/ORCNext/Supercritical/Literature/Study/Literature/Papers/SC%20Heat%20transfer/Pressure%20drop-friction/1986-Muller-Steinhagen-A%20simp) <http://linkinghub.elsevier.com/retrieve/pii/0255270186800083>. doi:10.1016/0255-2701(86)80008-3.
- [27] X.H. Nan, C. Infante Ferreira, In tube evaporation and condensation of natural refrigerant R290 (Propane), *Gustav Lorentz conference* 290 (2000) 3.
- [28] M. Nasr, M. Akhavan-Behabadi, M. Momenifar, P. Hanafizadeh, Heat transfer characteristic of R-600a during flow boiling inside horizontal plain tube, *Int. Commun. Heat Mass Transfer* 66 (2015) 93–99, <https://doi.org/10.1016/j.icheatmasstransfer.2015.05.024>, <https://linkinghub.elsevier.com/retrieve/pii/S0735193315001037>.
- [29] J.D. de Oliveira, J.B. Copetti, J.C. Passos, C.W. van der Geld, On flow boiling of R-1270 in a small horizontal tube: Flow patterns and heat transfer, *Appl. Therm. Eng.* 178 (2020) 115403, <https://doi.org/10.1016/j.applthermaleng.2020.115403>.
- [30] A. Padovan, D. Del Col, L. Rossetto, Experimental study on flow boiling of R134a and R410A in a horizontal microfin tube at high saturation temperatures, *Appl. Therm. Eng.* 31 (2011) 3814–3826, <https://doi.org/10.1016/j.applthermaleng.2011.07.026>.
- [31] B. Palm, Refrigeration systems with minimum charge of refrigerant, *Appl. Therm. Eng.* 27 (2007) 1693–1701, <https://doi.org/10.1016/j.applthermaleng.2006.07.017>, <https://linkinghub.elsevier.com/retrieve/pii/S1359431106002481>.
- [32] P. Rollmann, K. Spindler, New models for heat transfer and pressure drop during flow boiling of R407C and R410A in a horizontal microfin tube, *Int. J. Therm. Sci.* 103 (2016) 57–66, <https://doi.org/10.1016/j.ijthermalsci.2015.11.010>.
- [33] S.Z. Rouhani, E. Axelsson, Calculation of void volume fraction in the subcooled and quality boiling regions, *Int. J. Heat Mass Transf.* 13 (1970) 383–393, [https://doi.org/10.1016/0017-9310\(70\)90114-6](https://doi.org/10.1016/0017-9310(70)90114-6), <http://linkinghub.elsevier.com/retrieve/pii/0017931070901146>.
- [34] M.M. Shah, Chart correlation for saturation boiling heat transfer: Equation and further study, *ASHREA Trans.* 88 (1982) <https://www.osti.gov/scitech/biblio/6051573>.
- [35] J.Y. Shin, M.S. Kim, S.T. Ro, Experimental study on forced convective boiling heat transfer of pure refrigerants and refrigerant mixtures in a horizontal tube, *Int. J. Refrig.* 20 (1997) 267–275, [https://doi.org/10.1016/S0140-7007\(97\)00004-2](https://doi.org/10.1016/S0140-7007(97)00004-2).
- [36] K. Stephan, *Heat transfer in condensation and boiling*, Springer, 1992.
- [37] L. Sun, K. Mishima, Evaluation analysis of prediction methods for two-phase flow pressure drop in mini-channels, *Int. J. Multiph. Flow* 35 (2008) 47–54, <https://doi.org/10.1016/j.ijmultiphaseflow.2008.08.003>, [https://catatanstudi.files.wordpress.com/2009/11/2009-evaluation-analysis-of-prediction-methods-for-2-phase-flow-pressure-drop-in-mini-channels\\_sun.pdf](https://catatanstudi.files.wordpress.com/2009/11/2009-evaluation-analysis-of-prediction-methods-for-2-phase-flow-pressure-drop-in-mini-channels_sun.pdf).
- [38] W. Tang, W. Li, A new heat transfer model for flow boiling of refrigerants in microfin tubes, *Int. J. Heat Mass Transf.* 126 (2018) 1067–1078, <https://doi.org/10.1016/j.jheatmasstransfer.2018.06.066>, <https://linkinghub.elsevier.com/retrieve/pii/S0017931018315539>.
- [39] B. Thonon, A review of hydrocarbon two-phase heat transfer in compact heat exchangers and enhanced geometries, *Int. J. Refrig.* 31 (2008) 633–642, <https://www.sciencedirect.com/science/article/pii/S014070070800039X> [https://ac.els-cdn.com/S014070070800039X/1-s2.0-S014070070800039X-main.pdf?\\_tid=7736d389-b443-4b35-8ffb-50ac91ad354f&acdnat=1536823364\\_5438da16af606309302c7cfa3040a78](https://ac.els-cdn.com/S014070070800039X/1-s2.0-S014070070800039X-main.pdf?_tid=7736d389-b443-4b35-8ffb-50ac91ad354f&acdnat=1536823364_5438da16af606309302c7cfa3040a78).
- [40] T.N. Tran, M.W. Wambsgans, D.M. France, Small circular- and rectangular-channel boiling with two refrigerants, *Int. J. Multiph. Flow* 22 (1996) 485–498, [https://doi.org/10.1016/0301-9322\(96\)00002-X](https://doi.org/10.1016/0301-9322(96)00002-X).
- [41] M.-Y. Wen, K.-J. Jang, C.-Y. Ho, The characteristics of boiling heat transfer and pressure drop of R-600a in a circular tube with porous inserts, *Appl. Therm. Eng.* 64 (2014) 348–357, <https://doi.org/10.1016/j.applthermaleng.2013.12.074>, [http://ac.els-cdn.com/S135943111300971X/1-s2.0-S135943111300971X-main.pdf?\\_tid=2640400c-92fe-11e7-a53a-00000aacb360&acdnat=1504700773\\_37ab47261a748685ff5d60c858095227](http://ac.els-cdn.com/S135943111300971X/1-s2.0-S135943111300971X-main.pdf?_tid=2640400c-92fe-11e7-a53a-00000aacb360&acdnat=1504700773_37ab47261a748685ff5d60c858095227).
- [42] Y. Xu, X. Fang, A new correlation of two-phase frictional pressure drop for evaporating flow in pipes, *Int. J. Refrig.* 5 (2012) 2039–2050, <https://doi.org/10.1016/j.jrefrig.2012.06.011>, <https://www.sciencedirect.com/science/article/pii/S0140700712001570>.
- [43] Z. Yang, M. Gong, G. Chen, X. Zou, J. Shen, Two-phase flow patterns, heat transfer and pressure drop characteristics of R600a during flow boiling inside a horizontal tube, *Appl. Therm. Eng.* 120 (2017) 654–671, <https://doi.org/10.1016/j.applthermaleng.2017.03.124>.



## Article III



# Condensation of Hydrocarbons in Compact Smooth and Microfinned Tubes

Ehsan Allymehr <sup>1,\*</sup> , Ángel Álvarez Pardiñas <sup>2</sup> , Trygve Magne Eikevik <sup>1</sup> and Armin Hafner <sup>1</sup>

<sup>1</sup> Department of Energy and Process Engineering, NTNU Norwegian University of Science and Technology, Kolbjørn Hejes vei 1D, 7491 Trondheim, Norway; trygve.m.eikevik@ntnu.no (T.M.E.); armin.hafner@ntnu.no (A.H.)

<sup>2</sup> SINTEF Energy Research, Kolbjørn Hejes vei 1, 7491 Trondheim, Norway; angel.a.pardinas@sintef.no

\* Correspondence: ehsan.allymehr@ntnu.no

**Abstract:** A database for flowing condensation of three hydrocarbons, namely propane (R290), isobutane (R600a), and propylene (R1270), is extended by experimental tests in a smooth tube and two microfinned tubes with an increase of heat exchange area of 1.51 and 2.63, respectively. The outer diameter for all of the test tubes was 5 mm. Heat transfer coefficient and pressure drop are compared between the fluids and tubes. Tests were conducted at saturation temperatures of 35 °C and mass fluxes between 200 to 500 kg m<sup>-2</sup> s<sup>-1</sup>. Results show that isobutane (R600a) has a higher heat transfer coefficient and pressure drop while propylene (R1270) and propane (R290) present very similar characteristics. Both microfinned tubes increase the heat transfer coefficient compared to the smooth tube, but with different magnitude and tendencies and almost independently of the fluid tested. The maximum increase of heat transfer coefficient reached values of up to 1.8 while the maximum increase in pressure drop was by a factor of 1.7. Data have been compared with predictive methods exhibiting accurate correlation for smooth tube, while the accuracy of results for the microfinned are dependent on the type of tube and fluid used.



**Citation:** Allymehr, E.; Pardiñas, Á.Á.; Eikevik, T.M.; Hafner, A. Condensation of Hydrocarbons in Compact Smooth and Microfinned Tubes. *Energies* **2021**, *14*, 2647. <https://doi.org/10.3390/en14092647>

Academic Editor: Andrej Kitanovski

Received: 17 March 2021

Accepted: 29 April 2021

Published: 5 May 2021

**Publisher's Note:** MDPI stays neutral with regard to jurisdictional claims in published maps and institutional affiliations.



**Copyright:** © 2021 by the authors. Licensee MDPI, Basel, Switzerland. This article is an open access article distributed under the terms and conditions of the Creative Commons Attribution (CC BY) license (<https://creativecommons.org/licenses/by/4.0/>).

**Keywords:** hydrocarbon; refrigeration; heat transfer; pressure drop; microfinned

## 1. Introduction

The refrigeration industry has been challenged by its effect on the environment. This problem is exacerbated by the current generation of working fluids that have an exceptionally high Global Warming Potential (GWP). The progress toward a more sustainable and environmentally friendly refrigeration industry requires a broad shift in the utilized working fluids to have a low GWP and zero Ozone Depletion Potential (ODP). Additionally, systems working with novel working fluids need to be more energy-efficient to reduce the indirect impact with lower primary energy usage. Propane (R290), isobutane (R600a), and propylene (R1270) have long been used as working fluids in various applications. For example, isobutane (R600a) is the most used refrigerant in domestic refrigeration and freezer units, especially in Europe [1]. Hydrocarbons offer favorable saturation curves benefiting different use cases while enjoying low GWP and zero ODP. However, the use of hydrocarbons in refrigeration systems has been long limited by flammability concerns. While risk analysis has been performed on these systems showing that with careful installation, reaching the lower flammability limit is improbable [2], concerns remain. Studies have shown that the main amount of charge is stored in heat exchangers [3,4], thus minimizing the heat exchangers' volume seems to be the most effective method of increasing the capacity of these systems with regard to limitations on their charge. This is even more critical in the condenser's case as it could contain 50% of the total charge [4].

Thonon [5] and more recently Moreira et al. [6] have reviewed the literature on two-phase characteristics of flowing hydrocarbons, noting the scarcity of data available from independent laboratories for system design such as HTC and pressure drop. Moreover, the

available data seem to only focus on smooth tubes, and internally enhanced tubes are not studied. Authors are only aware of Nan and Infante Ferreira [7] where evaporation and condensation of propane in a smooth, microfinned, and crosshatched tubes with an outer diameter ( $d_o$ ) of 9.52 mm were studied, showing that HTC increase is more noticeable at higher mass fluxes and experimental data are significantly over-predicted by correlations for internally enhanced tubes.

Macdonald and Garimella [8] studied condensation of propane in two tubes with internal diameter ( $d_i$ ) of 14.45 mm and 7.75 mm in a broad range of saturation temperature, showing that HTC is slightly dependent on diameter while the effect of saturation temperature is much more pronounced on pressure drop. The same authors utilized the obtained data to develop HTC and pressure drop correlations [9]. Lee et al. [10] studied the condensation of three hydrocarbons, namely, R290, R1270, and R600a comparing them to R22 in smooth tubes with  $d_i$  of 12.7 and 9.52 mm. Authors noted that HTC of hydrocarbons was higher by at least 31% compared to R22, while their pressure drop was larger by at least 50%.

Del Col et al. [11] studied the condensation of R290 in a microchannel with an internal bore of 0.96 mm, showing a satisfactory agreement with the predictive methods. Agra and Teke [12] reported experimental results for condensation of R600a in a smooth tube with  $d_i$  of 4 mm, observing that the flow was in annular form. The authors in Qiu et al. [13] simulated the condensation of R290 in minichannels with diameters ranging from 0.5 to 2 mm, visualizing the different flow patterns and the effect of flow on heat transfer and pressure drop characteristics. In another numerical study by Wen et al. [14], authors have compared condensation performance of R1234ze(E), R134a, and R290 in a tube with  $d_i$  of 1.0 mm, reporting that R290 had a lower tendency to be stratified at lower vapor qualities.

Longo et al. [15] studied the condensation of R404A and compared them to suitable hydrocarbon substitutes, namely, R290 and R1270, reporting that the hydrocarbons generally had a higher HTC while the pressure drop was lower compared to R404A, thus proving themselves to be promising candidates as a long term substitute. In a later publication Longo et al. [16], the same authors included data for R600a, noting that, while R600a has a higher HTC, its pressure drop is much higher.

The effect of internally enhanced tubes on the condensation characteristics of various working fluids has been researched in several papers. Colombo et al. [17] reported two phase flow characteristics for R134a in one smooth and two microfinned tubes while Bashar et al. [18] studied condensation of R1234yf inside smooth and microfinned tubes with  $d_o$  of 2.5 mm, showing that the HTC increase in microfinned tube can be up to 3.85 times. Diani et al. [19] compared the condensation of R513A in a smooth tube with  $d_i$  of 3.5 mm to a microfinned tube with  $d_i$  of 3.4 mm, showing that the HTC can be up to 4.5 times higher in the microfinned tube in lower mass fluxes, while, at higher mass fluxes, this increase tends asymptotically towards the increase in the heat transfer area provided by the fins. Condensation of R134a, R22, and R410A in microfinned tubes with  $d_i$  ranging between 8.92 to 4 mm was studied by Han and Lee [20] showing enhancement of HTC and penalization in the pressure drop having the same tendencies with increases in mass flux and vapor quality. The authors proposed a new correlation for the prediction of pressure drop and HTC.

Thus, while there have been several studies on the characteristics of condensation of hydrocarbons in smooth tubes, and others have analyzed the effect of internally enhanced tubes on different fluids, there have not been any studies on hydrocarbons combined with the effect of internal surface enhancement. Moreover, it seems that the comparison between different types of microfinned tubes is not available. Allymehar et al. [21,22] studied the evaporation of hydrocarbons in smooth and two microfinned tubes, demonstrating a high increase in the HTC with minimal increase in the pressure drop. As the amount of charge in the condenser is higher than in the evaporator, any charge reduction in condensers will have a higher impact. Finally, it is crucial to have reliable experimental data to properly design and size heat exchangers, especially in applications where the amount of charge is

limited by regulations. Since no experimental data are available to examine the correlations' accuracy, the predictive method's can be unreliable.

This study expands the database on condensation characteristics of R290, R600a, and R1270 in smooth and internally enhanced tubes by experimental determination of HTC and measurement of pressure drop. Two-phase flow characteristics of two microfinned tubes with different internal geometries were compared to a smooth tube at similar conditions. One of the microfinned tubes represents a more conventional internally enhanced geometry, with an increased surface area of 1.51, while the other tube has a more aggressive increase in internal surface area of 2.63. All three tested tubes have an outer diameter of 5 mm. Mass fluxes ranged from 200 to 500 kg m<sup>-2</sup> s<sup>-1</sup>, and results were compared with relevant correlations to review the prediction methods' accuracy.

## 2. Experimental Setup

The experimental test rig was previously used to measure evaporation characteristics and thus documented in Allymehr et al. [21,22]. As shown in Figure 1, the test rig was modified to allow condensation tests. The setup has two loops, one for the refrigerant and one for the secondary cooling fluid. In the refrigerant circuit, the test fluid is circulated through the system by a gear pump and mass flow is measured downstream of the pump by a Coriolis mass flow meter. The energy required to vaporize the fluid to a desired vapor quality is calculated based on measurement of pressure and temperature upstream and the temperature downstream of the preheater. This energy is provided to the fluid by the preheater by means of electrical heating tape controlled by pulse wave modulation (PWM). There is an adiabatic calming section of 75 mm upstream of the test section. A differential pressure transducer directly measures the pressure drop by pressure taps before and after the test section, located 547 mm away from each other. The average wall temperature is obtained by two pairs of thermocouples brazed to the tube wall, which are located 100 mm from the inlet and outlet of the heated test section. Thermocouples are attached to test tube's outer wall using silver brazing in a way that in each pair one thermocouple is in contact with the top and the other with the bottom part of the tube. Length of the heated section for all the tested tubes is 500 mm. Two absolute pressure sensors connected to the test section using the same pressure taps as for the differential pressure transducer provide the average value of saturation pressure at the test section, which is then used to determine the fluid saturation temperature. As the saturation pressure of R600a at 35 °C is considerably different from R1270 and R290, a different set of pressure sensors was used. Heat is removed from the test section by distilled water flowing through a helical tube wound around the test section. The helical tube geometry for water loop was optimized utilizing Ansys Fluent simulation with the goal of maximizing the temperature difference between the inlet and outlet to lower the measurement uncertainty while providing a uniform heat flux. The condensation was simulated by imposing a heat transfer coefficient and a saturation temperature while the tube diameter and length were varied at different water mass flows. The internal diameter for the cooling water tube was 4.9 mm with a length of 950 mm. The space between the helical tube for secondary fluid and the test tube is filled with melted tin. Silver brazing used for thermocouples ensures contact between the tube and the thermocouples as silver has a higher melting temperature than tin. The water temperature is measured before and after the test section using two RTD elements. Using the temperature difference, the specific heat capacity and water's mass flow, the heat removed from the test section can be calculated. Based on the results from the numerical simulation and uncertainty analysis, the water flow rate was roughly around 1180 mL min<sup>-1</sup>. The heat flow to the test section is controlled by the temperature of water thermostatic bath through a PID controller. The set point for the PID was a heat flow of 155 W, thus giving a temperature change of around 2 °C. A photograph of one of the test sections is shown in Figure 2, while the schematic of the water cooling loop is visualized in Figure 3.

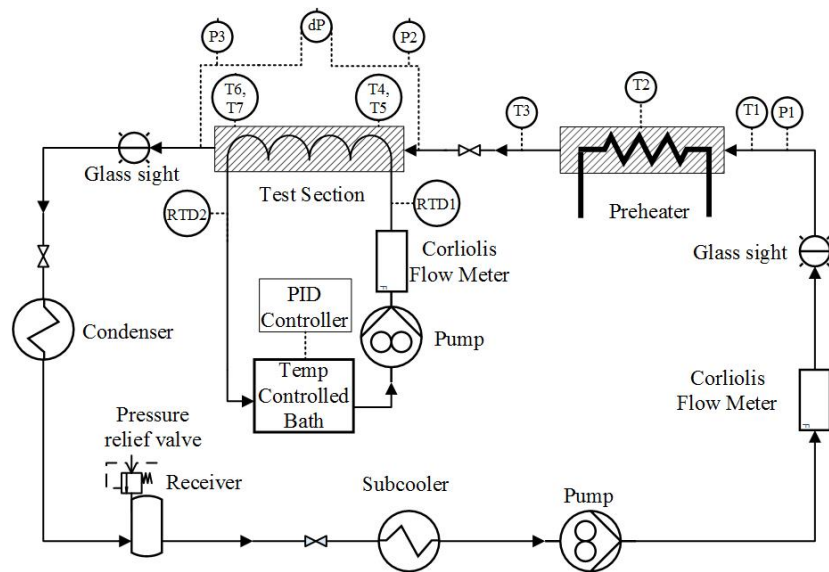


Figure 1. Test rig schematic.

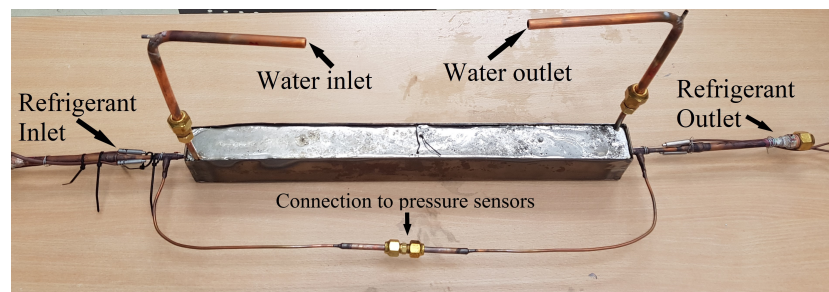


Figure 2. Photograph of one of test sections.

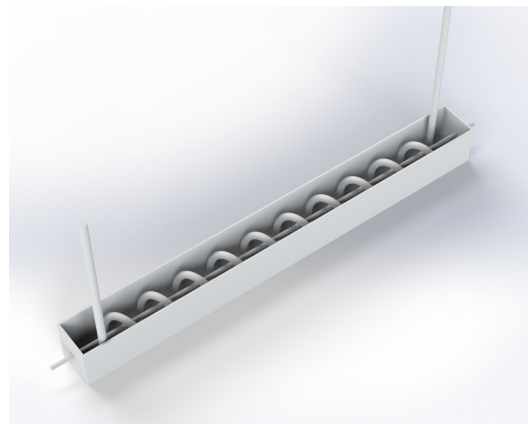


Figure 3. Visualization of test section and the cooling water loop without the filling material.

The sight glasses do not have the same diameter as the tube and therefore cannot be used for reliable detection of flow patterns. The setup is capable of quick test section changes without vacuuming the entire test rig utilizing the valves located upstream and

downstream of the test section. Before introducing new working fluids, the whole test rig is purged with nitrogen and vacuumed. The condenser and the subcooler are both plate heat exchangers. The subcooler and the condenser are connected to two separate chillers, providing a liquid flow to the pump. The condenser is located at the lowest point of the system and has the lowest temperature in the system so that it can control the system's saturation pressure by the thermal bath's temperature connected to the condenser.

### 2.1. Tested Tubes

One smooth tube and two internally enhanced tubes, all with an outer diameter  $d_o$  of 5 mm, were studied. Table 1 reports geometrical parameters for the tubes. Physical representations of geometrical parameters are presented in Figure 4. While the fin dimensions for the two microfinned tubes are approximately the same, MF2 has a higher number of fins and spiral angle, leading to a higher available area for heat transfer. A cross-sectional view of the two tested microfinned tubes is shown in Figure 5.

**Table 1.** Geometrical parameters of the test tubes.

	Unit	Smooth Tube	MF1	MF2
Outer diameter ( $d_o$ )	mm	5	5	5
Internal diameter <sup>a</sup> ( $d_i$ )	mm	4.1	4.32	4.26
Wall thickness <sup>b</sup> ( $t_w$ )	mm	0.45	0.22	0.22
Actual cross sectional area	mm <sup>2</sup>	13.2	15.7	14.8
Effective diameter <sup>c</sup>	mm	-	4.47	4.34
Fin height ( $l_f$ )	mm	-	0.12	0.15
Fin number ( $n$ )	-	-	35	56
Fin angle ( $\gamma$ )	°	-	35	15
Spiral angle ( $\beta$ )	°	-	15	37
Heat exchange area ratio ( $R_x$ )	-	1	1.51	2.63
Heated test section length	mm		500	
Pressure drop measurement length	mm		547	
Test section length	mm		1005	

<sup>a</sup> Internal diameter for smooth tube, fin tip diameter for microfinned tubes. <sup>b</sup> Length between fin root and outer diameter. <sup>c</sup> Equivalent diameter for a smooth tube to have the same actual cross section area.

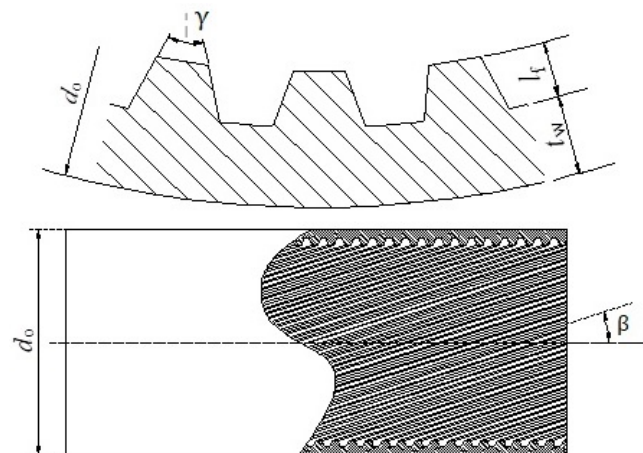


**Figure 4.** Physical presentation of the geometrical parameters.

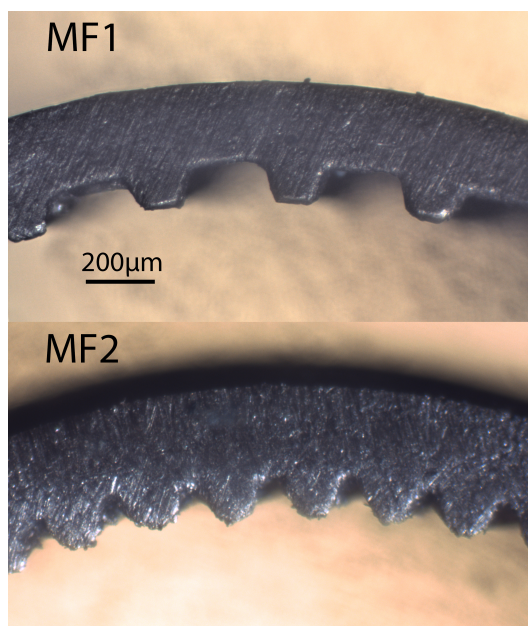


**Figure 5.** Cross sectional view of the microfinned tubes.

## 2.2. Working Conditions

Working conditions are summarized in Table 2. Furthermore, the critical fluid properties that seem to have the greatest effect on the two phase flow characteristics are reported.

**Table 2.** Operating conditions for experimental setup.

	Unit	Range/Value		
		R1270	R600a	R290
<b>Operating conditions</b>				
Saturation Temperature	°C	35	35	35
Heat flow	W	155	155	155
Mass flux [G]	$\text{kg m}^{-2} \text{s}^{-1}$	200–500	200–500	200–500
Vapor quality [x]	-	0.12–0.89	0.13–0.88	0.13–0.84
Quality change [ $\Delta x$ ]	-	0.19–0.07	0.18–0.07	0.18–0.07
<b>Fluid properties at 35 °C, Saturated</b>				
Reduced pressure	-	0.32	0.13	0.28
Liquid Viscosity	$\mu\text{Pa s}$	85.7	136.2	87.3
Surface Tension	$\text{mN m}^{-1}$	5.7	8.9	5.8
Vapor Density	$\text{kg m}^{-3}$	31.5	12.0	26.6

While no visual observation of flow patterns was performed in this paper, the flow pattern map of Dobson and Chato [23] was used to predict flow regimes. This flow pattern map was compared with experimental results for condensation of propane in Milkie et al. [24] showing good agreement. Interestingly, all the data points tested for smooth tube in this study seem to fall in the annular flow. This is not surprising as, with the small diameter of the tube, surface tension's effect becomes more dominant; furthermore because of charge limitations on the test rig, no tests were performed in really low vapor qualities where the stratified flow occurs. Finally, the mass flow was not high enough to reach mist flow in any of the tested cases. There are flow pattern maps available for the MF tubes [25]. These flow patterns show that microfinned tubes initiate the annular

flow sooner by bringing the liquid from the bottom pool with swirl motion to the top of the tube. Thus, there should be no change in the assumption of all tested points being in annular flow.

### 2.3. Uncertainty Analysis and Validation

Uncertainty analysis was performed by the method elaborated in ISO [26], and a confidence level exceeding 95% (coverage factor of 2). Utilized instruments and their respective uncertainty are listed in Table 3. The smaller range of absolute pressure sensors for R600a reduces HTC's uncertainty of measurement. The calibration process and formulation used are provided in Appendix A. The average value for uncertainty of measurement of HTC was 6.4%, and this value remains relatively the same in all test conditions. The average uncertainty of measurement for pressure drop was 14.2% with higher values in lower mass fluxes and smooth tubes. In these cases, the pressure drop is small, while the uncertainty of pressure drop measurement based on the full range of the pressure transducer remains the same.

**Table 3.** List of instruments and their respective uncertainties.

	Type	Range	Uncertainty
<b>Refrigerant Circuit</b>			
Flow meter	Coriolis	0–5 kg min <sup>−1</sup>	±0.1% <sup>a</sup>
Absolute pressure sensor <sup>c</sup>	Strain gauge	0–10 bar	±0.16% <sup>b</sup>
Absolute pressure sensor <sup>d</sup>	Strain gauge	0–20 bar	±0.16% <sup>b</sup>
Differential pressure sensor	Strain gauge	0–0.5 bar	±0.15% <sup>b</sup>
Thermocouples	Type T	-	±0.05 K
Preheater	Electrical	3450 W	±0.44% <sup>a</sup>
<b>Cooling Water Circuit</b>			
Flow meter	Coriolis	0–5 kg min <sup>−1</sup>	±0.1% <sup>a</sup>
RTD	PT 100	-	±0.05 K

<sup>a</sup> Of the reading. <sup>b</sup> Of the set span. <sup>c</sup> Used for R600a. <sup>d</sup> Used for R1270 and R290.

The test rig was validated using a single-phase superheated gas flow of R600a for HTC and R290 for pressure drop in a smooth tube. The Darcy Weisbach formula was used for pressure drop prediction while correlation of Gnielinski V. [27] was used for HTC. The comparison results showed an average absolute deviation of 3.7% and 3.4% for pressure drop and heat transfer coefficient, respectively. To limit the heat leakage to the environment, test sections were insulated using elastomeric foam insulation. Moreover, vacuum heat leakage tests were performed to account for the heat loss to the environment. This was done by flowing water through the helical tube when the test section was under vacuum condition and recording the change in water temperature. This heat loss was taken into account by a linear relationship based on the ambient and test section's surface temperature difference, formulated by Equation (1):

$$Q_{loss} = 0.602 \cdot (T_{element} - T_{amb}) + 0.145 \quad [W] \quad (1)$$

Heat loss was minimal and in most cases less than 1 W; this is mainly because, with the tested saturation temperature (35 °C), cooling water temperature and subsequently the test section surface temperature were very close to ambient temperature. In several cases, the test section's surface temperature was lower than the ambient temperature, and thus there was heat gain instead of heat loss. This was considered in the data reduction process with a negative value for heat loss.

### 2.4. Data Reduction

To characterize steady-state condition, the standard deviation of the last 15 samples was calculated; if this value was lower than 0.1 °C, the system was considered to be in

steady-state. The data from the sensors were recorded for over 120 s to obtain 50 samples, which were then averaged. The average vapor quality value is calculated by Equation (2):

$$x = x_{in} - \frac{\Delta x}{2} = \frac{Q_{pre} - \dot{m} \cdot (i_{sat,l} - i_1)}{\dot{m} \cdot i_{lg}(p_{pre})} - \frac{Q_{test} - Q_{loss}}{2 \cdot \dot{m} \cdot i_{lg}(p_{sat})} \quad (2)$$

$i_1$  is the enthalpy of subcooled fluid before entering the preheater,  $p_{pre}$  is the pressure at the preheater section and  $p_{sat}$  is the arithmetic average of the inlet and outlet pressure in the test section. The heat removed from the test section by the cooling water was calculated with Equation (3):

$$Q_{test} = \dot{m}_{water} \cdot c_{p_{water}} \cdot (RTD_2 - RTD_1) \quad (3)$$

Heat transfer coefficient is calculated using Equation (4):

$$HTC = \frac{Q_{test} - Q_{loss}}{S(\bar{T}_{sat} - \bar{T}_w)} \quad (4)$$

where  $T_{sat}$  is derived from the saturation pressure,  $p_{sat}$ .  $\bar{T}_w$  and  $S$  are defined as:

$$\bar{T}_w = \frac{1}{4} \sum_{i=1}^4 T_{w,i} \quad (5)$$

$$S = \pi d_i L \quad (6)$$

The calculation of parameters such as heat flux and mass flux is dependent on the definition of internal diameter  $d_i$ . While for the smooth tube this definition is unambiguous, for the MF tube different internal diameters can be defined—namely, fin root diameter, fin tip diameter, and effective diameter, where the effective diameter is the equivalent diameter for a smooth tube with the same actual cross-section area. All three internal diameters for MF tubes are reported in Table 1 but only fin tip diameter was considered for the data reduction process. The reason for this was the simplicity of the measurement process in the field, compatibility with predictive methods and its conventional use in literature. This choice is critical and should be kept constant across tests. It should be noted that, because of this definition, the values reported for mass flux and heat flux are not the actual values. Nevertheless, the simplicity of measurement and comparison with other correlations outweigh the slight deviation from actual values. The increase in internal area for MF tubes compared to a smooth tube with the same fin tip diameter is calculated using  $R_x$  value defined as:

$$R_x = \left\{ \frac{2 \cdot l_f \cdot n \cdot [1 - \sin(\gamma/2)]}{\pi \cdot D \cdot \cos(\gamma/2)} + 1 \right\} \cdot \frac{1}{\cos \beta} \quad (7)$$

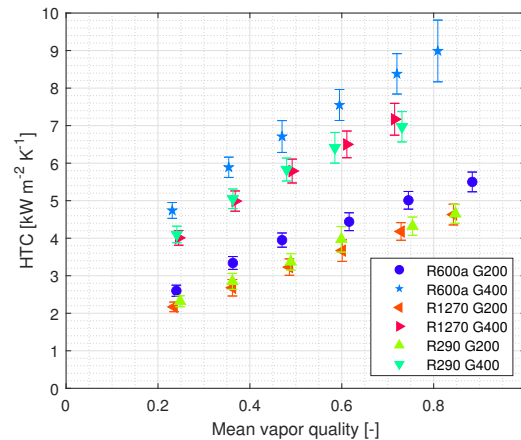
This value is not directly used in the data reduction process and thus values such as heat flux for MF tubes are calculated based on a smooth tube with the internal diameter equivalent to fin tip diameter.

Thermodynamic properties are obtained using REFPROP V10 [28]. The total pressure drop  $\Delta p$  is calculated by the addition of momentum pressure drop  $\Delta p_a$  with frictional pressure drop  $\Delta p_f$ . As momentum pressure drop in condensation is negative, it leads to a pressure gain. The void fraction in the momentum pressure drop calculation was determined using Rouhani and Axelsson [29] correlation. This correlation was initially developed for vertical tubes, but it is used here as it has previously reliably calculated data for horizontal tubes.

### 3. Results and Discussion

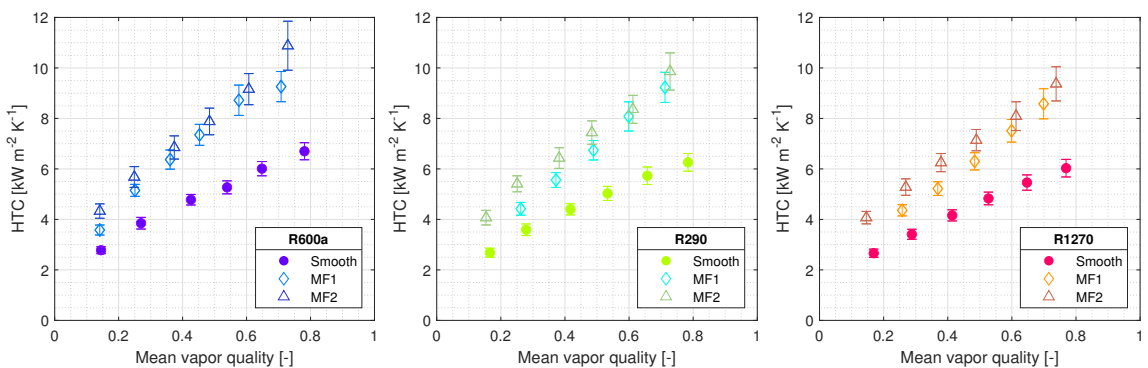
#### 3.1. Experimental Data

Figure 6 displays the HTC in the smooth tube for all the the tested fluids at mass fluxes of 200 and 400  $\text{kg m}^{-2} \text{s}^{-1}$ . The results show that R290 and R1270 have similar behavior in the tested mass fluxes while the HTC of R600a is considerably higher. This can be explained by the thermophysical properties of R600a, specifically, the lower vapor density, which in turn causes a higher superficial velocity of the gas phase, increasing the turbulence at the interface layer between the liquid and gas phase.



**Figure 6.** Condensation HTC for R290, R1270, and R600a in smooth tube mass flux (G) reported in  $\text{kg m}^{-2} \text{s}^{-1}$ .

Figure 7 shows how internally enhanced tubes can affect HTC for each of the tested fluids. There is always an increase in the HTC for microfinned tubes compared to the smooth tube. The difference between MF1 and MF2 in R600a is negligible, while, for R290 and R1270, the MF1 tube has a discernibly lower HTC in lower vapor qualities. Thus, it can be said that the higher turbulence caused by higher gas velocity in R600a and at higher vapor qualities diminish the effect of added number of fins and spiral angle in the MF2 tube.



**Figure 7.** Effect of internal surface enhancement on HTC for R290, R1270, and R600a,  $G = 300 \text{ kg m}^{-2} \text{s}^{-1}$ .

Figure 8 shows the effect of microfinned tubes in different mass fluxes and with the different hydrocarbons. In mass flux of 200  $\text{kg m}^{-2} \text{s}^{-1}$ , the HTC of R600a is distinctly higher than those of R1270 and R290. The differences between HTC of different fluids in

higher mass fluxes are smaller, as the values of MF2 tube with R290 and R1270 reach the values of MF1 with R600a. Interestingly, it seems that, at mass flux of  $200 \text{ kg m}^{-2} \text{ s}^{-1}$ , which is the lowest tested mass flux, the trend of HTC with vapor quality is different compared to higher mass fluxes—while, at higher mass fluxes, the HTC values for MF tubes tend to converge because of the lower effect of turbulence created by the surface enhancements; at the lowest mass flux, this trend is diverging. The authors speculate that this is due to the asymmetrical annular flow pattern where the liquid film thickness is higher at the bottom pool. The asymmetrical annular flow pattern assumption is in agreement with [23] where a transitional Froude number is defined for the development of flow regime from wavy-stratified to symmetrical annular flow. In this transitional flow regime, the internal surface enhancement does not create the turbulence needed at the bottom pool of the fluid to make a tangible increase in HTC. At higher vapor qualities, the swirl motion propels the fluid toward a fully developed annular flow, and the turbulence created by the fins differentiates the tubes from each other.

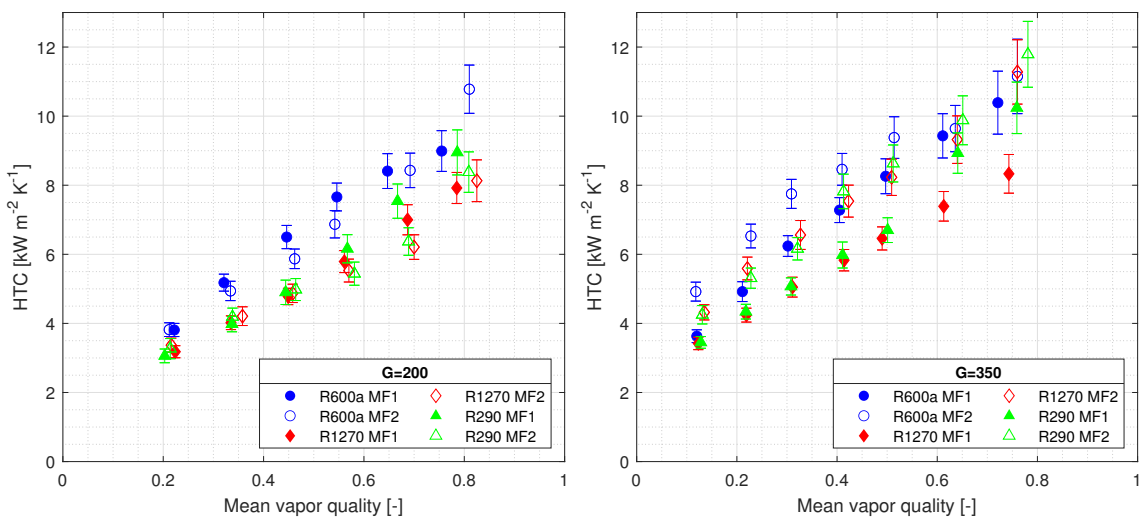


**Figure 8.** Comparison of HTC in microfinned tubes at different mass fluxes, mass flux ( $G$ ) reported in the legend in  $\text{kg m}^{-2} \text{ s}^{-1}$ .

Figure 9 presents the data for the total pressure gradient. Unsurprisingly, the pressure drop is strongly dependent on the mass flux in all tubes and fluids. Comparing the fluids together, it can be seen that R1270 has a slightly lower pressure drop than R290, while R600a has a significantly higher pressure drop than both other hydrocarbons. Reviewing the Table 2 shows that R600a has a significantly higher liquid viscosity than both of the other fluids; the higher liquid viscosity combined with a lower vapor density of R600a leads to higher shear stress and thus a higher pressure drop. A comparison of microfinned tubes with the smooth tube shows a minor increase for the MF1 tube, while MF2 has a more noticeable increase in pressure drop. To compare the heat transfer and pressure drop characteristics of the microfinned tubes to the smooth tube at the different mass fluxes and vapor qualities, three different parameters were defined. These were Enhancement factor  $E$ , Penalization factor  $P$ , and efficiency index,  $I$ , which are formulated as:

$$E = \frac{HTC_{MF}}{HTC_{Smooth}} \quad (8)$$

$$P = \frac{\Delta p_{MF}}{\Delta p_{Smooth}} \quad (9)$$

$$I = \frac{E}{P} \tag{10}$$

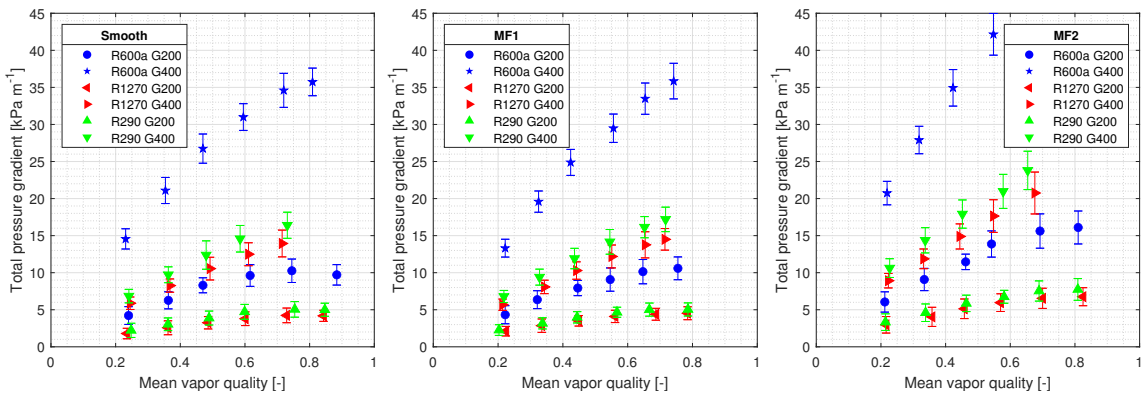


Figure 9. Effect of mass flux on total pressure gradient, mass flux (G) in legend reported in  $\text{kg m}^{-2} \text{s}^{-1}$ .

To distinguish the effect of vapor quality and mass flux, these values were compared at vapor qualities of 0.25 and 0.7 in mass fluxes ranging from 200 to  $500 \text{ kg m}^{-2} \text{s}^{-1}$ . It should be noted that, because of stability issues, not all the data points could be calculated; they mainly lay in the MF2 tube with mass flux of  $400 \text{ kg m}^{-2} \text{s}^{-1}$ . Enhancement factor,  $E$ , for both tubes is presented in Figure 10. The MF1 tube has a decreasing enhancement factor with increasing mass flux. Moreover, the enhancement factor is higher at  $x = 0.7$  than  $x = 0.25$ . Interestingly, while, at lower mass fluxes,  $E$  for both vapor qualities is higher than or close to  $R_x$ , as the mass flux increases  $E$  falls below  $R_x$  meaning that the increase in the internal surface area is not completely utilized. This is more apparent for the MF2 tube where  $E$  is more or less uniform regardless of fluid or vapor quality and much lower than  $R_x$ . These results can be explained by arguing that fins have a twofold effect on flow. First, the fins can agitate the boundary layer at the wall, providing more turbulence and thus removing more heat; this seems to be the dominating contributor at lower mass fluxes. Secondly, the fins provide extra heat transfer area; this is more apparent in higher mass fluxes where the boundary layer is already agitated and the extra turbulence created by fins is not a significant contributing factor.

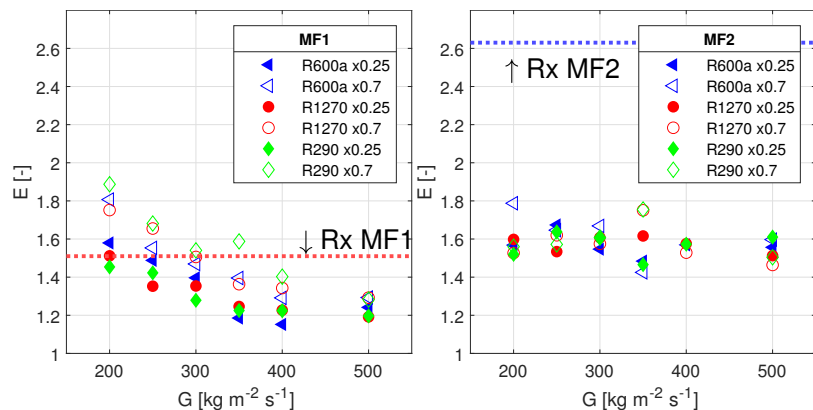
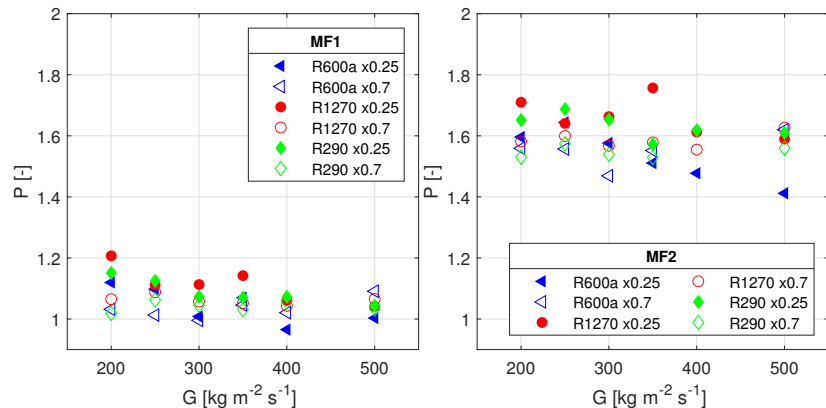


Figure 10. Effect of mass flux on enhancement factor,  $E$ , for MF tubes at  $x = 0.25$  and  $x = 0.7$ , heat exchange area increase shown with  $R_x$ .

Figure 11 displays the penalization factor,  $P$ . Both tubes seem to present more or less stable values for  $P$  regardless of the tested fluid and the vapor quality, although MF2 shows more scatter in the data. Nevertheless, it can be observed that the penalization factor is far higher for MF2 tube than MF1. This was to be expected considering the higher fin number and spiral angle of the MF2 tube. Furthermore,  $P$  does not seem to be a function of mass flux, even if it is the most defining factor for pressure drop.



**Figure 11.** Effect of mass flux on penalization factor,  $P$ , for MF tubes at  $x = 0.25$  and  $x = 0.7$ .

Finally, the efficiency index,  $I$ , is shown in Figure 12. The MF1 tube seems to be more advantageous in higher vapor qualities with values reaching more than 1.8; this was expected since  $E$  is decreasing while  $P$  is stable. R600a seems to enjoy a slightly better  $I$  value at  $x = 0.25$  in low mass fluxes, while, at other conditions, the results are mostly independent of the tested fluid. As for MF2, it can be seen that the results are largely uniform across the fluids, mass fluxes and vapor qualities. More importantly,  $I$  is close to 1 and significantly lower than MF1 for most tested cases. This means that the increase in pressure drop offsets the increase in HTC. If the efficiency index was to be considered a measure of how beneficial an internally enhanced tube is, it could be argued that, with an efficiency index of unity, there is no difference in employing MF2 tube compared to a smooth tube. This is not considering other factors in the design of a heat exchanger such as the extra cost in the production of this tube, header size, or air side resistance. However, if the heat exchanger design goal is to minimize the charge in the system, MF2 provides additional benefits as it provides a higher HTC, especially as this increase is uniform across the vapor qualities. This is important as it seems that the MF1 tube has a lower  $E$  for lower vapor qualities where the majority of charge is located. Hence, heat exchangers can be designed with MF2 tube that have a shorter length for lower vapor qualities, thus reducing the charge significantly.

### 3.2. Correlations

Applicable predictive methods were compared against HTC and pressure drop experimental data in all tested conditions utilizing Mean Relative Deviation (MRD) and Mean Absolute Relative Deviation (MARD), defined as:

$$MRD = \frac{100}{N} \sum_{i=1}^N \frac{Predicted_i - Experimental_i}{Experimental_i} \quad (11)$$

$$MARD = \frac{100}{N} \sum_{i=1}^N \left| \frac{Predicted_i - Experimental_i}{Experimental_i} \right| \quad (12)$$

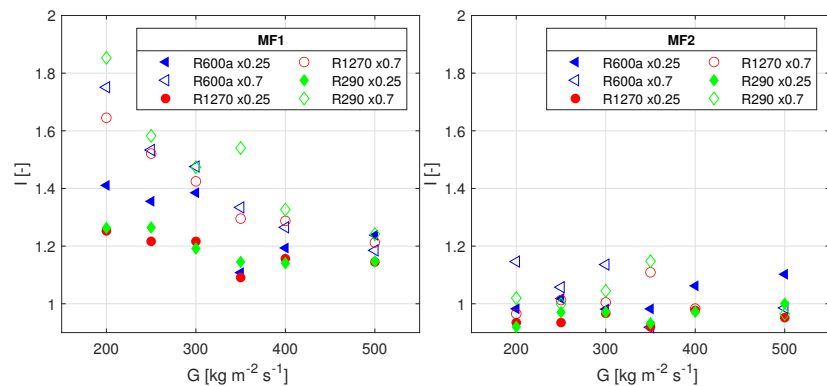


**Figure 12.** Effect of mass flux on efficiency index,  $I$ , for MF tubes at  $x = 0.25$  and  $x = 0.7$ .

Furthermore,  $\delta_{30}$  is defined as the percentage of the predicted values having less than 30% deviation from the experimental data. The correlations were chosen on the basis of the database they were developed with, such as Macdonald and Garimella [9] that considered condensation of hydrocarbons, or Xu and Fang [30] that uses Weber number to take into account surface tension that is important in compact tubes. Table 4 summarizes the results of comparison for both of the fluids in smooth tube.

**Table 4.** Comparison between experimental results and correlations for HTC and pressure drop in smooth tube, with best performing correlations in bold.

	R600a			R1270			R290		
	MRD %	MARD%	$\delta_{30}$	MRD %	MARD%	$\delta_{30}$	MRD %	MARD%	$\delta_{30}$
<b>Pressure Drop Correlations</b>									
Müller-Steinhagen and Heck [31]	−18.4	19.0	97.4	−14.1	14.9	100	−16.2	16.7	100
Cavallini et al. [32]	2.0	11.6	94.7	−14.5	17.6	100	−13.0	16.1	97.3
Macdonald and Garimella [9]	10.9	14.0	97.4	<b>−6.1</b>	<b>6.4</b>	<b>100</b>	<b>−7.8</b>	<b>7.9</b>	<b>100</b>
Xu and Fang [30]	<b>−6.5</b>	<b>11.0</b>	<b>100</b>	−3.2	9.4	100	−4.6	10.1	100
Friedel [33]	−18.3	19.0	100	−5.5	9.3	100	−9.3	11.7	100
<b>HTC Correlations</b>									
Macdonald and Garimella [9]	−21.9	21.9	89.5	−23.5	23.5	81.1	−25.3	25.3	67.6
Shah [34]	18.6	18.6	97.4	24.3	33.4	24.3	28.4	28.4	62.2
Dorao and Fernandino [35]	<b>−5.0</b>	<b>5.8</b>	<b>100</b>	<b>11.0</b>	<b>11.0</b>	<b>100</b>	<b>4.9</b>	<b>4.9</b>	<b>100</b>

All of the correlations chosen for prediction of pressure drop performed reasonably well, with correlations of Macdonald and Garimella [9] and Xu and Fang [30] providing slightly more accurate results. Thus, any of these correlations could be used for reliable prediction of the pressure of hydrocarbons in smooth tubes. As for HTC correlations, it seems that, while Macdonald and Garimella [9] and Shah [34] can be reasonably accurate for R600a, their error increases for other tested hydrocarbons. The most accurate correlation was Dorao and Fernandino [35] in which authors have proposed a correlation where the two-phase HTC is substituted with an analogous single phase flow HTC. This correlation was able to predict all HTC data points for all fluids with less than 30% error; this is shown as a parity plot in Figure 13. In addition to being accurate, this correlation is much simpler to implement than other correlations where parameters such as liquid film thickness must be calculated.

It should be noted that, for microfinned tubes, the formulation and parameter definition in each paper was used, i.e., the formulation and parameters in this study were adapted accordingly to match the correlation's definition.

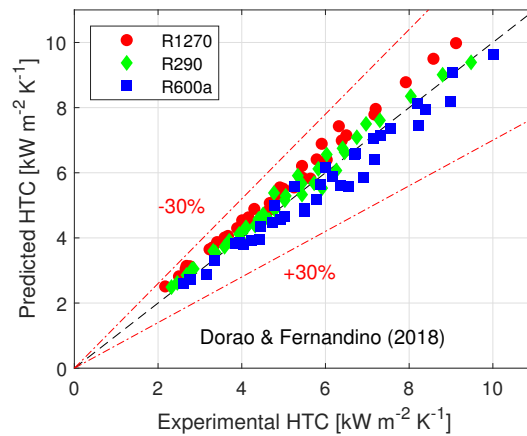


**Figure 13.** Comparison between experimental data and correlations of Dorao and Fernandino [35] for prediction of HTC in smooth tubes.

Table 5 compares the prediction methods for pressure drop with experimental data in microfinned tubes. As the tube’s geometry has a notable effect on pressure drop characteristics, the data for each tube are reported separately. In the MF1 tube, correlation of Diani et al. [36] reliably predicts pressure drop for all fluids, the same correlation can predict pressure drop values in MF2 tube as well, albeit with a relatively higher error. Correlation of Choi et al. [37] underpredicts the MF1 pressure drop values but has the lowest MARD for R290 and R1270 in MF2. In general, the Diani et al. [36] correlation provides a reliable and safe method to predict pressure drop with an acceptable level of error in evaporation flow as well as condensation flow Allymehr et al. [21,22].

**Table 5.** Comparison between experimental data and correlations for prediction of pressure drop in microfinned tubes, with best performing correlations highlighted in bold.

	R600a			R1270			R290		
	MRD %	MARD%	$\delta_{30}$	MRD %	MARD%	$\delta_{30}$	MRD %	MARD%	$\delta_{30}$
<b>MF1 tube</b>									
Rollmann and Spindler [38]	14.6	14.6	97.4	12.2	14.0	91.9	12.1	13.5	94.6
Choi et al. [37]	−29.5	29.5	52.6	−32.0	32.0	45.9	−32.1	32.1	43.2
Diani et al. [36]	<b>12.8</b>	<b>12.8</b>	<b>94.7</b>	<b>5.7</b>	<b>8.1</b>	<b>97.3</b>	<b>−7.3</b>	<b>5.4</b>	<b>97.3</b>
<b>MF2 tube</b>									
Rollmann and Spindler [38]	−26.1	26.1	75.0	−28.5	28.5	59.5	−28.7	28.7	59.5
Choi et al. [37]	14.1	17.0	88.9	<b>8.1</b>	<b>11.7</b>	<b>100</b>	<b>8.0</b>	<b>11.8</b>	<b>100</b>
Diani et al. [36]	<b>−16.7</b>	<b>16.7</b>	<b>100</b>	−22.2	22.2	94.6	−22.1	22.1	100

Comparison of the experimental data with HTC correlations of microfinned tubes is reported in Table 6. Cavallini et al. [39] accurately predicts the data for all fluids in the MF1 tube. The results for MF2 tube are mixed, and, in general, correlations cannot predict the results as accurately as with MF1. This is expected as the MF2 tube has a novel geometry with a higher number of fins and spiral angle, and this geometry has not been widely studied for two-phase flow characteristics and thus incorporated in the correlations database. Cavallini et al. [39] seems to underestimate HTC considerably. A closer look at the correlation reveals that authors have considered a term to lower the effect of microfinned in the forced convective condensation term if the number of fins is deemed higher than an optimum level. This condition applies to the MF2 tube and, based on the results in this paper, is a reasonable assumption to make. A simple change

in the values proposed for the equation of reducing term enables the correlation to fit the experimental results. As the MF2 tube was the only tube that needed the reduction term to be calculated, the authors cannot advise this method as a revised formulation of Cavallini et al. [39] correlation.

**Table 6.** Comparison between experimental data and correlations for prediction of HTC in microfinned tubes, with best correlations highlighted in bold.

	R600a			R1270			R290		
	MRD %	MARD%	$\delta_{30}$	MRD %	MARD%	$\delta_{30}$	MRD %	MARD%	$\delta_{30}$
<b>MF1 tube</b>									
Cavallini et al. [39]	<b>5.5</b>	<b>7.8</b>	<b>100</b>	<b>12.3</b>	<b>13.6</b>	<b>100</b>	<b>5.2</b>	<b>7.9</b>	<b>100</b>
Yu and Koyama [40]	52.6	52.6	18.4	46.2	46.2	13.5	40.5	40.5	32.4
Kedzierski and Goncalves [41]	−25.7	25.7	89.5	−18.2	18.2	97.3	−24.5	24.5	89.2
<b>MF2 tube</b>									
Cavallini et al. [39]	−41.5	41.5	0	−39.1	39.1	13.5	−42.0	42.0	5.4
Yu and Koyama [40]	33.8	33.8	50.0	<b>25.6</b>	<b>25.6</b>	<b>67.6</b>	<b>23.0</b>	<b>23.0</b>	<b>78.4</b>
Kedzierski and Goncalves [41]	−32.2	<b>32.2</b>	<b>44.4</b>	−26.6	26.6	54.1	−31.1	31.1	37.8

This study's goal was not to develop a new correlation and the data in this paper clearly indicate that the extra heat exchange area is not the only parameter affecting the heat transfer characteristics. However, for a back-of-the-envelope calculation for HTC, the authors suggest using correlations developed for smooth tubes and multiplying them by the increased area with a reducing term for highly finned tubes. A quick calculation showed that, considering this method with Dorao and Fernandino [35] for MF1, most data points can be calculated with less than 30% error while grossly over-predicting HTC in MF2 tube. An analysis of the effect of various internal surface enhancements on HTC can help develop a better reduction term and simplify the prediction of HTC in microfinned tubes.

The accuracy of Kedzierski and Goncalves [41] and Cavallini et al. [39] for both MF tubes is visualized in Figure 14. Cavallini et al. [39] can follow MF1 data accurately while MF2 data are underpredicted, and this error is slightly higher for R290. On the other hand, while the correlation of Kedzierski and Goncalves [41] underpredicts HTC values for both MF1 and MF2, this under prediction is rather constant at around 30% suggesting an offset problem.

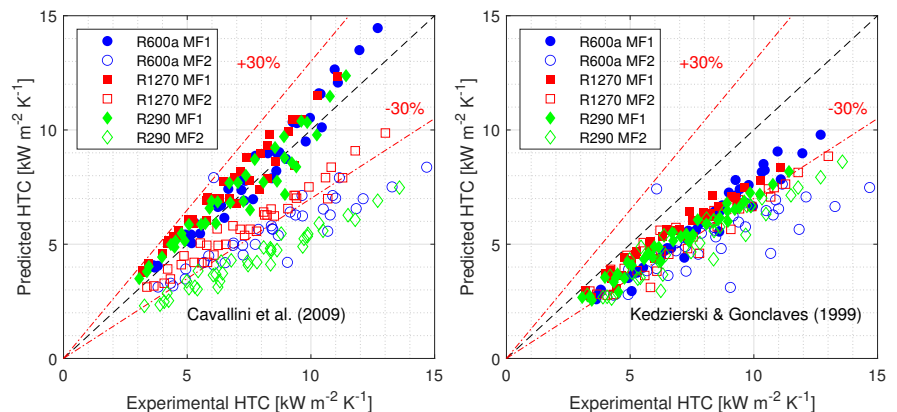


**Figure 14.** Prediction of HTC in two microfinned tubes by correlations of Cavallini et al. [39] and Kedzierski and Goncalves [41] compared to experimental data.

#### 4. Conclusions

Internally enhanced tubes offer the possibility of a more efficient and smaller heat exchanger, providing a higher capacity with a reduced charge. The lack of data for elements such as heat transfer coefficient and pressure drop makes the design process of these heat exchangers challenging, especially for hydrocarbons where the amount of charge is critical. This paper tries to address this problem by reporting experimental results on the condensation flow characteristics of three hydrocarbons, namely, propane (R290), isobutane (R600a), and propylene (R1270). Three tubes with an outer diameter of 5 mm were tested, one smooth tube and two microfinned tubes with an increased heat exchange area of 1.51 and 2.63 for MF1 and MF2, respectively. Experimental tests were performed at saturation temperatures 35 °C and mass fluxes from 200 to 500 kg m<sup>-2</sup> s<sup>-1</sup>.

The results are critically compared, noting the effect of surface enhancements and different fluids. Data obtained show that mass flux strongly affects HTC and pressure drop. R600a has a higher HTC and pressure drop mainly because of its lower vapor density, while the characteristics of R1270 and R290 seem to be very close.

The microfinned tubes behave differently; MF1 tube increases the HTC coefficient more in lower mass fluxes and higher vapor qualities, while the MF2 tube has a relatively constant increase in the HTC in all vapor qualities and mass fluxes. The increase of HTC for both tubes seems to be independent of fluid tested. The maximum increase of HTC for MF1 tube reached up to 1.8 while the increase of HTC for MF2 mainly is around 1.6. It can be deduced that the increase in the number of fins and heat exchange area have a diminishing return on the HTC capabilities of an internally enhanced tube. The increase of pressure drop between smooth and internally enhanced tubes was relatively constant for all the fluids, mass fluxes, and vapor qualities, being around 1.2 for MF1 and significantly higher, at around 1.7, for MF2 tube. All in all, for the MF1 tube with an increase in mass flux, the pressure drop increases stay the same, while the increase in HTC decreases, discouraging its use in higher mass fluxes. The MF2 tube seems to have the same effectiveness at all mass fluxes but at a lower level than MF1. A more detailed evaluation of some of these results and trends, including potential instabilities, dryout and flow patterns, is not possible with the current design of the test section and sight glass available. The unit is being upgraded with a fitting sight glass and high-speed camera to allow the next step in this research line by flow visualization of two-phase hydrocarbon flow in compact, smooth, and microfinned tubes. The comparison of experimental data with predictive methods shows that the HTC and pressure drop in the smooth tube are reliably predicted by Dorao and Fernandino [35] and Macdonald and Garimella [9], respectively. For microfinned tubes, Diani et al. [36] predicted pressure drop data for both MF1 and MF2 tube. As for HTC in microfinned tubes, the accuracy of the prediction methods varied based on the tested tube, with the data of MF1 being accurately predicted by Cavallini et al. [42] for all fluids. No reliable equations were found for HTC prediction in the MF2 tube.

**Author Contributions:** Conceptualization, E.A., A.H., T.M.E., and Á.Á.P.; methodology, E.A and Á.Á.P.; software, E.A.; validation, E.A.; formal analysis, E.A. and Á.Á.P.; investigation, E.A. and Á.Á.P.; resources, A.H. and T.M.E.; data curation, E.A. and Á.Á.P.; writing—original draft preparation, E.A. and Á.Á.P.; writing—review and editing, E.A. and Á.Á.P.; visualization, E.A.; supervision, A.H. and T.M.E.; project administration, A.H. and T.M.E.; funding acquisition, A.H., T.M.E. All authors have read and agreed to the published version of the manuscript.

**Funding:** This publication has been funded by HighEFF—Centre for an Energy Efficient and Competitive Industry for the Future, an 8-year Research Centre under the FME-scheme (Centre for Environment-friendly Energy Research, 257632). The authors gratefully acknowledge the financial support from the Research Council of Norway and user partners of HighEFF.

**Institutional Review Board Statement:** Not applicable.

**Informed Consent Statement:** Not applicable.

**Conflicts of Interest:** The authors declare no conflict of interest.

## Abbreviations

### Greek

$\beta$	Spiral angle
$\delta_{30}$	Percentage of predicted values with less than 30% error
$\gamma$	Fin angle

### Roman

$c_{p_{water}}$	Specific heat of water [ $J g^{-1} K^{-1}$ ]
$d_i$	Fin tip diameter for MF tubes, internal diameter for smooth tube [mm]
$d_o$	Outer diameter [mm]
$E$	Enhancement Factor [-]
$G$	Mass flux [ $kg m^{-2} s^{-1}$ ]
$HTC$	Heat Transfer Coefficient [ $kW m^{-2} K^{-1}$ ]
$I$	Efficiency index [-]
$i_{lg}$	Enthalpy of vaporization [ $kJ kg^{-1}$ ]
$l_f$	Fin height [mm]
$m$	Mass flow [ $kg s^{-1}$ ]
$MARD$	Mean Absolute Relative Deviation [-]
$MRD$	Mean Relative Deviation [-]
$N$	Dataset size [-]
$n$	Number of fins [-]
$P$	Penalization Factor [-]
$p$	Pressure [Pa]
$P_r$	Reduced pressure [-]
$Q$	Heat input [W]
$q$	Heat flux [ $kW m^{-2}$ ]
$R_x$	Heat exchange area ratio to a smooth tube [-]
$RTD$	Resistance thermometers [-]
$S$	Heat exchange area [ $m^2$ ]
$T$	Temperature [ $^{\circ}C$ ]
$t_w$	Wall thickness [mm]
$x$	Vapor quality [-]

### Subscripts

$a$	Advectional
$amb$	Ambient condition
$element$	Heating Element
$f$	Frictional
$in$	Inlet conditions
$l$	Liquid phase
$lg$	Liquid to gas phase change
$loss$	Heat loss to environment
$pre$	Preheater section
$sat$	Saturated condition
$test$	Test section
$w$	Wall

## Appendix A. Calibration Process and Uncertainty Propagation

In order to calibrate the thermocouples, AMETEK JOFRA RTC 157 Reference Temperature Calibrator with the procedure advised by the manufacturer has been used. This unit has an accuracy of  $\pm 0.04$   $^{\circ}C$  and stability of  $\pm 0.005$   $^{\circ}C$ . The thermocouples were connected in the same manner as the testing condition (same cables, connections, DAQ) and the values were read each five degrees in the desired temperature range ( $-10$   $^{\circ}C$  to  $30$   $^{\circ}C$ ). The same procedure was used to calibrate the RTD elements in a temperature range of  $-20$  to  $70$   $^{\circ}C$ . The obtained data from the calibration process were used to create a calibration file in LabVIEW.

Below, the formulation used for propagating of uncertainty is summarized. Uncertainty for wall temperature:

$$u(T_w) = \sqrt{(1/4)^2 \cdot \sum_{i=4}^7 u(T_i)} \quad (\text{A1})$$

Uncertainty for Saturation temperature:

$$u(T_{sat}) = \sqrt{\left(\frac{\partial T_{sat}}{\partial P_{sat}}\right)^2 \cdot u(p_{sat})^2} \quad (\text{A2})$$

From the Antoine equation, the relationship between saturation temperature and saturation pressure can be found; by derivation, it can be written:

$$\left(\frac{\partial T_{sat}}{\partial P_{sat}}\right) = \frac{803.99}{P_{sat} \cdot (3.9228 - \log_{10}(P_{sat}))} \quad (\text{A3})$$

Uncertainty for heat transfer coefficient:

$$u(h) = \sqrt{\left(\frac{u(Q_{test})}{T_w - T_{sat}}\right)^2 + \left(\frac{Q_{test} \cdot u(T_w)}{(T_w - T_{sat})^2}\right)^2 + \left(\frac{Q_{test} \cdot u(T_{sat})}{(T_w - T_{sat})^2}\right)^2} \quad (\text{A4})$$

where the uncertainty of the heat input is calculated as:

$$u(Q_{test}) = \frac{1}{\sqrt{(u(\dot{m}_{water}) \cdot c_{p_{water}} \cdot (RTD_2 - RTD_1))^2 + (\dot{m}_{water} \cdot c_{p_{water}})^2 \cdot (u(RTD_1)^2 + u(RTD_2)^2)}} \quad (\text{A5})$$

Uncertainty for inlet vapor quality:

$$u(x_{in}) = \sqrt{\left(\frac{u(Q_{pre})}{\dot{m} \cdot i_{lg}(P_1)}\right)^2 + \left(\frac{Q_{pre} \cdot u(\dot{m})}{i_{lg}(P_1) \cdot \dot{m}^2}\right)^2} \quad (\text{A6})$$

Uncertainty for the change in vapor quality:

$$u(\Delta x) = \sqrt{\left(\frac{u(Q_{test})}{\dot{m} \cdot i_{lg}(P_{sat})}\right)^2 + \left(\frac{Q_{test} \cdot \ln(\dot{m}) \cdot u(\dot{m})}{i_{lg}(P_{sat})}\right)^2} \quad (\text{A7})$$

Uncertainty for the average vapor quality:

$$u(x) = \sqrt{u(x_{in}) + 1/4 \cdot u(\Delta x)^2} \quad (\text{A8})$$

## References

1. Straub, M. Alternative Refrigerants For Household Refrigerators. In *International Refrigeration and Air Conditioning*; Purdue University: West Lafayette, IN, USA, 2018; Volume 2002, pp. 1–10.
2. Tang, W.; He, G.; Zhou, S.; Sun, W.; Cai, D.; Mei, K. The performance and risk assessment of R290 in a 13 kW air source heat pump. *Appl. Therm. Eng.* **2018**, *144*, 392–402. [[CrossRef](#)]
3. Palm, B. Hydrocarbons as refrigerants in small heat pump and refrigeration systems—A review. *Int. J. Refrig.* **2008**, *31*, 552–563. [[CrossRef](#)]
4. Li, T.; Lu, J.; Chen, L.; He, D.; Qiu, X.; Li, H.; Liu, Z. Measurement of refrigerant mass distribution within a R290 split air conditioner. *Int. J. Refrig.* **2015**, *57*, 163–172. [[CrossRef](#)]
5. Thonon, B. A review of hydrocarbon two-phase heat transfer in compact heat exchangers and enhanced geometries. *Int. J. Refrig.* **2008**, *31*, 633–642. [[CrossRef](#)]

6. Moreira, T.A.; Furlan, G.; e Oliveira, G.H.D.S.; Ribatski, G. Flow boiling and convective condensation of hydrocarbons: A state-of-the-art literature review. *Appl. Therm. Eng.* **2021**, *182*, 116129. [[CrossRef](#)]
7. Nan, X.H.; Infante Ferreira, C. In tube evaporation and condensation of natural refrigerant R290 (Propane). In Proceedings of the Gustav Lorentz Conference, Purdue, IN, USA, 25–28 July 2000; Volume 290, p. 3.
8. Macdonald, M.; Garimella, S. Hydrocarbon condensation in horizontal smooth tubes: Part I—Measurements. *Int. J. Heat Mass Transf.* **2016**, *93*, 75–85. [[CrossRef](#)]
9. Macdonald, M.; Garimella, S. Hydrocarbon condensation in horizontal smooth tubes: Part II—Heat transfer coefficient and pressure drop modeling. *Int. J. Heat Mass Transf.* **2016**, *93*, 1248–1261. [[CrossRef](#)]
10. Lee, H.S.; Yoon, J.I.; Kim, J.D.; Bansal, P. Condensing heat transfer and pressure drop characteristics of hydrocarbon refrigerants. *Int. J. Heat Mass Transf.* **2006**, *49*, 1922–1927. [[CrossRef](#)]
11. Del Col, D.; Stefano, B.; Matteo, B.; Luisa, R. Condensation Heat Transfer and Pressure Drop with Propane in a Minichannel. In Proceedings of the International Refrigeration and Air Conditioning Conference, West Lafayette, IN, USA, 16–19 July 2012.
12. Agra, Ö.; Teke, İ. Experimental investigation of condensation of hydrocarbon refrigerants (R600a) in a horizontal smooth tube. *Int. Commun. Heat Mass Transf.* **2008**, *35*, 1165–1171. [[CrossRef](#)]
13. Qiu, G.; Li, M.; Cai, W. The condensation heat transfer, frictional pressure drop and refrigerant charge characteristics of R290 in minichannels with different diameters. *Int. J. Heat Mass Transf.* **2020**, *158*, 119966. [[CrossRef](#)]
14. Wen, J.; Gu, X.; Wang, S.; Li, Y.; Tu, J. The comparison of condensation heat transfer and frictional pressure drop of R1234ze(E), propane and R134a in a horizontal mini-channel. *Int. J. Refrig.* **2018**, *92*, 208–224. [[CrossRef](#)]
15. Longo, G.A.; Mancin, S.; Righetti, G.; Zilio, C. Saturated vapour condensation of HFC404A inside a 4 mm ID horizontal smooth tube: Comparison with the long-term low GWP substitutes HC290 (Propane) and HC1270 (Propylene). *Int. J. Heat Mass Transf.* **2017**, *108*, 2088–2099. [[CrossRef](#)]
16. Longo, G.A.; Mancin, S.; Righetti, G.; Zilio, C. Saturated vapor condensation of hydrocarbons inside A 4 mm ID horizontal smooth tube. *Refrig. Sci. Technol.* **2018**, *2018*, 620–627. [[CrossRef](#)]
17. Colombo, L.; Lucchini, A.; Muzzio, A. Flow patterns, heat transfer and pressure drop for evaporation and condensation of R134A in microfin tubes. *Int. J. Refrig.* **2012**, *35*, 2150–2165. [[CrossRef](#)]
18. Bashar, M.K.; Nakamura, K.; Kariya, K.; Miyara, A. Condensation heat transfer of R1234yf in a small diameter smooth and microfin tube and development of correlation. *Int. J. Refrig.* **2020**, *120*, 331–339. [[CrossRef](#)]
19. Diani, A.; Brunello, P.; Rossetto, L. R513A condensation heat transfer inside tubes: Microfin tube vs. smooth tube. *Int. J. Heat Mass Transf.* **2020**, *152*, 119472. [[CrossRef](#)]
20. Han, D.; Lee, K.J. Experimental study on condensation heat transfer enhancement and pressure drop penalty factors in four microfin tubes. *Int. J. Heat Mass Transf.* **2005**, *48*, 3804–3816. [[CrossRef](#)]
21. Allymehr, E.; Pardiñas, Á.Á.; Eikevik, T.M.T.; Hafner, A. Comparative analysis of evaporation of Isobutane (R600a) and Propylene (R1270) in compact smooth and microfinned tubes. *Appl. Therm. Eng.* **2021**, *188*, 116606. [[CrossRef](#)]
22. Allymehr, E.; Pardiñas, Á.Á.; Eikevik, T.M.; Hafner, A. Characteristics of evaporation of propane (R290) in compact smooth and microfinned tubes. *Appl. Therm. Eng.* **2020**, *181*, 115880. [[CrossRef](#)]
23. Dobson, M.K.; Chato, J.C. Condensation in smooth horizontal tubes. *J. Heat Transf.* **1998**, *120*, 193–213. [[CrossRef](#)]
24. Milkie, J.A.; Garimella, S.; Macdonald, M.P. Flow regimes and void fractions during condensation of hydrocarbons in horizontal smooth tubes. *Int. J. Heat Mass Transf.* **2016**, *92*, 252–267. [[CrossRef](#)]
25. Rollmann, P.; Spindler, K. A new flow pattern map for flow boiling in microfin tubes. *Int. J. Multiph. Flow* **2015**, *72*, 181–187. [[CrossRef](#)]
26. ISO. Guide to Expression of Uncertainty in Measurement. 1993. Available online: [https://www.bipm.org/documents/20126/2071204/JCGM\\_100\\_2008\\_E.pdf/cb0ef43f-baa5-11cf-3f85-4dcd86f77bd6](https://www.bipm.org/documents/20126/2071204/JCGM_100_2008_E.pdf/cb0ef43f-baa5-11cf-3f85-4dcd86f77bd6) (accessed on 5 May 2021).
27. Gnielinski, V. New equations for heat and mass transfer in the turbulent flow in pipes and channels. *Forsch. Ingenieurwesen* **1975**, *41*, 8–16. [[CrossRef](#)]
28. Lemmon, E.W.; Bell, I.H.; Huber, M.L.; McLinden, M.O. NIST Standard Reference Database 23: Reference Fluid Thermodynamic and Transport Properties-REFPROP. Version 10.0. National Institute of Standards and Technology. Available online: [https://tsapps.nist.gov/publication/get\\_pdf.cfm?pub\\_id=912382](https://tsapps.nist.gov/publication/get_pdf.cfm?pub_id=912382) (accessed on 5 May 2021).
29. Rouhani, S.Z.; Axelsson, E. Calculation of void volume fraction in the subcooled and quality boiling regions. *Int. J. Heat Mass Transf.* **1970**, *13*, 383–393. [[CrossRef](#)]
30. Xu, Y.; Fang, X. A new correlation of two-phase frictional pressure drop for condensing flow in pipes. *Nucl. Eng. Des.* **2013**, *263*, 87–96. [[CrossRef](#)]
31. Müller-Steinhagen, H.; Heck, K. A simple friction pressure drop correlation for two-phase flow in pipes. *Chem. Eng. Process. Process. Intensif.* **1986**, *20*, 297–308. [[CrossRef](#)]
32. Cavallini, A.; Censi, G.; Col, D.D.; Doretti, L.; Longo, G.; Rossetto, L. Condensation of Halogenated Refrigerants Inside Smooth Tubes. *HVAC&R Res.* **2002**, *8*, 429–451. [[CrossRef](#)]
33. Friedel, L. Improved friction pressure drop correlation for horizontal and vertical two-phase pipe flow. In Proceedings of the European Two-Phase Flow Group Meeting, Ispra, VA, Italy, 5–7 June 1979; pp. 485–492.
34. Shah, M.M. An Improved and Extended General Correlation for Heat Transfer during Condensation in Plain Tubes. *HVAC&R Res.* **2009**, *15*, 889–913. [[CrossRef](#)]

35. Doraó, C.A.; Fernandino, M. Simple and general correlation for heat transfer during flow condensation inside plain pipes. *Int. J. Heat Mass Transf.* **2018**, *122*, 290–305. [[CrossRef](#)]
36. Diani, A.; Mancin, S.; Rossetto, L. R1234ze(E) flow boiling inside a 3.4 mm ID microfin tube. *Int. J. Refrig.* **2014**, *47*, 105–119. [[CrossRef](#)]
37. Choi, J.Y.; Kedzierski, M.A.; Domanski, P.A. Generalized Pressure Drop Correlation for Evaporation and Condensation in Smooth and Micro-Fin Tubes. In Proceedings of the IIF-IIR-Commission B1, Paderborn, Germany, 2–5 October 2001.
38. Rollmann, P.; Spindler, K. New models for heat transfer and pressure drop during flow boiling of R407C and R410A in a horizontal microfin tube. *Int. J. Therm. Sci.* **2016**, *103*, 57–66. [[CrossRef](#)]
39. Cavallini, A.; Del Col, D.; Mancin, S.; Rossetto, L. Condensation of pure and near-azeotropic refrigerants in microfin tubes: A new computational procedure. *Int. J. Refrig.* **2009**, *32*, 162–174. [[CrossRef](#)]
40. Yu, J.; Koyama, S. Condensation heat transfer of pure refrigerants in microfin tubes. In Proceedings of the International Refrigeration and Air Conditioning Conference, West Lafayette, IN, USA, 14–17 July 1998.
41. Kedzierski, M.A.; Goncalves, J.M. Horizontal Convective Condensation of Alternative Refrigerants Within a Micro-Fin Tube. *J. Enhanc. Heat Transf.* **1999**, *6*, 161–178. [[CrossRef](#)]
42. Cavallini, A.; Del Col, D.; Matkovic, M.; Rossetto, L. Pressure drop during two-phase flow of R134a and R32 in a single Minichannel. *J. Heat Transf.* **2009**, *131*, 1–8. [[CrossRef](#)]

## Article IV



Article

# Numerical Study of Hydrocarbon Charge Reduction Methods in HVAC Heat Exchangers

Ehsan Allymehr <sup>1,\*</sup> , Geir Skaugen <sup>2</sup>, Torsten Will <sup>3</sup>, Ángel Álvarez Pardiñas <sup>2</sup>, Trygve Magne Eikevik <sup>1</sup>, Armin Hafner <sup>1</sup> and Lena Schnabel <sup>3</sup>

<sup>1</sup> Department of Energy and Process Engineering, NTNU Norwegian University of Science and Technology, Kolbjørn Hejes vei 1D, 7491 Trondheim, Norway; trygve.m.eikevik@ntnu.no (T.M.E.); armin.hafner@ntnu.no (A.H.)

<sup>2</sup> SINTEF Energy Research, Kolbjørn Hejes vei 1, 7491 Trondheim, Norway; Geir.Skaugen@sintef.no (G.S.); angel.a.pardinas@sintef.no (Á.Á.P.)

<sup>3</sup> Fraunhofer Institute for Solar Energy Systems ISE, Heidenhofstr. 2, 79110 Freiburg, Germany; torsten.will@ise.fraunhofer.de (T.W.); lena.schnabel@ise.fraunhofer.de (L.S.)

\* Correspondence: ehsan.allymehr@ntnu.no

**Abstract:** Required refrigerant charge in heat pump systems with propane is analyzed. Two systems are compared: the first a direct heat pump, with fin-and-tube heat exchangers, and the second an indirect system, with plate heat exchangers with an additional brine-to-air heat exchanger. Each system was considered to be able to work reversibly, with 5 kW design cooling capacity in summer and 8 kW design heating capacity in winter. Two separately developed simulation codes were used to calculate the required refrigerant charge and the efficiency of each of the systems. The charge was reduced by the use of microfinned tubes up to 22% in direct system reduced using microfinned tubes compared to the smooth tube. For the indirect system using specially designed plate heat exchangers with the minimum internal volume, their charge was reduced by up to 66% compared to normal plate heat exchangers.



**Citation:** Allymehr, E.; Skaugen, G.; Will, T.; Pardiñas, Á.Á.; Eikevik, T.M.; Hafner, A.; Schnabel, L. Numerical Study of Hydrocarbon Charge Reduction Methods in HVAC Heat Exchangers. *Energies* **2021**, *14*, 4480. <https://doi.org/10.3390/en14154480>

Academic Editor: Moonis Raza Ally

Received: 21 June 2021

Accepted: 19 July 2021

Published: 24 July 2021

**Publisher's Note:** MDPI stays neutral with regard to jurisdictional claims in published maps and institutional affiliations.



**Copyright:** © 2021 by the authors. Licensee MDPI, Basel, Switzerland. This article is an open access article distributed under the terms and conditions of the Creative Commons Attribution (CC BY) license (<https://creativecommons.org/licenses/by/4.0/>).

**Keywords:** hydrocarbon; heat exchanger; system charge; optimization

## 1. Introduction

The impact of refrigeration, air conditioning and heat pump (RACHP) systems on the environment has led to efforts to limit the use of different working fluids with initiatives and regulations such as the European F-gas regulation [1]. The current generation of working fluids has an exceptionally high global warming potential (GWP) and the progress toward a more sustainable and environmentally friendly RACHP industry requires a broad shift to working fluids with low GWP and zero ozone depletion potential (ODP). Additionally, systems working with more environmentally friendly refrigerants need to be more energy-efficient to reduce the indirect impact with lower primary energy usage. Hydrocarbons, such as Propane (R290), isobutane (R600a), and propylene (R1270) have long been used as working fluids in various applications. For example, isobutane (R600a) is the most used refrigerant in domestic refrigeration and freezer units, especially in Europe [2]. Hydrocarbons offer favorable saturation curves befitting different use cases while enjoying low GWP and zero ODP; thus, they are considered to replace several groups of working fluids by 2030 [3]. However, the use of hydrocarbons in refrigeration systems has been long limited by flammability concerns. While risk analysis has been performed on these systems showing that with careful installation, reaching the lower flammability limit is improbable [4], concerns remain. Studies have shown that the majority of charge is stored in heat exchangers [5,6], thus minimizing the heat exchangers' volume seems to be the most effective method of increasing the capacity of these systems with regards to limitations on their charge. This is even more critical in the condenser's case as it could contain 50% of

the total charge [6]. In an air sourced heat pump, the majority of the charge is stored in the condenser; nevertheless, the evaporator charge is still considerable, especially in lower temperatures where it can be more than 20% of the total charge [6].

Different studies have shown the possibility to run specially designed low charge heat pumps with capacities up to 8 kW with a maximum charge of 150 g to fulfill regulations and provide maximum safety by minimizing inner volume, especially for components containing liquid refrigerant [7–9]. Studies have shown that hydrocarbons' heat transfer coefficient can be increased substantially by using microfinned tubes with minimum penalization in pressure drop [10–12], which could be utilized to reduce refrigerant charge of heat pumps. Moreover, brazed plate heat exchangers (BPHE) are favorable for condensation and evaporation due to their low inner volume at high thermal capacity. However, heat transfer in the secondary side of hydrocarbon heat exchangers, being that a liquid (water or brine) or air, may limit the potential of heat exchanger and refrigerant charge reduction.

Thus, while some research has studied the two-phase characteristics of hydrocarbons in different geometries, the resulting effect on the design of heat exchangers is not investigated. Furthermore, the benefits and drawbacks of direct and indirect systems in relation to charge and capacities are not fully understood. This article analyzes the refrigerant charge and efficiency of two R290 reversible heat pumps, one with indirect heat transfer using BPHE and intermediate circuits with an brine-to-air outdoor heat exchanger and an indoor panel heating and cooling system with water as heat transfer fluid, and another with direct air-to-air system, using fin-and-tube heat exchangers. The design heating (winter) and cooling (summer) capacities are 8 kW and 5 kW, respectively. Two independent models, one per heat pump system, were utilized to design the corresponding heat exchangers (condenser and evaporator). These utilized models were based on correlations developed by experimental data on two-phase flow of propane.

## 2. Tested Systems

### 2.1. Heat Pump Architectures

Two R290 reversible heat pump systems are defined and compared in this work: a direct air to air unit and an indirect brine to water system, using air as heat source and sink. For each system, only the evaporator and condenser have been analyzed, and elements such as compressor, tubes and other installations are not evaluated. The different systems and testing conditions are shown in Figure 1. The direct system (System A) uses a fin-and-tube heat exchanger configuration where one smooth (SM) and two microfinned tubes (MF1 and MF2) are considered for the indoor and outdoor heat exchangers. The indirect system (System B) is a more compact solution comprising of two brazed plate heat exchangers, with an intermediate brine loop to the outdoor heat exchanger, and water loop to the indoor unit, which is defined as a panel heating/cooling configuration. Both systems have been analyzed for summer and winter conditions, with equal design capacities of 5 kW cooling in summer and 8 kW heating in winter. The standards DIN EN 14511 and DIN EN 14825 [13,14] define temperatures for air to air and air to water heat pumps and air conditioners. The nominal values for average climate were used for the basis of the calculations. The defined input parameters are declared in Table 1 and in context with the different systems in Figure 1.

Both systems were considered with a superheating degree of 5 K at the compressor suction port and a subcooling of 3 K at the condenser's outlet. For System B, an isentropic efficiency for the compressor has been set at 0.85. For System A, the isentropic efficiency was not a free parameter in the used simulation tool HXSim. The inlet temperature to the condenser, i.e., compressor discharge temperature, must be balanced with the condenser subcooling degree, which was given a higher priority as it strongly affects the charge. Nevertheless, after several iterations it was possible to reach an acceptably close value of 0.86–0.82 for isentropic efficiency in the different tested cases.

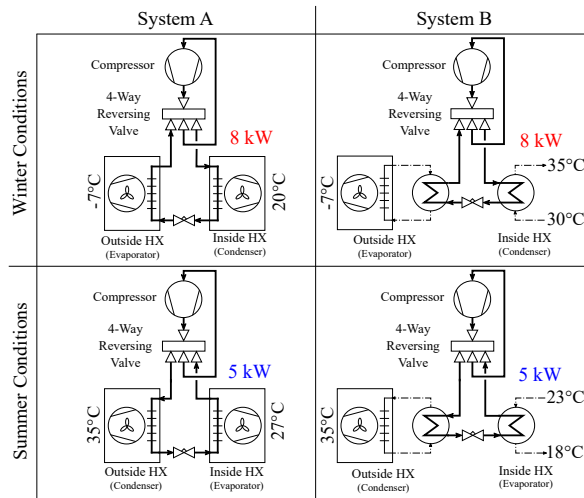


**Figure 1.** Overview of the tested systems. System A: direct system with fin-and-tube heat exchangers, System B: indirect system with plate heat exchangers and intermediate brine and water loops.

**Table 1.** Parameters set based on standard DIN EN 14511 and DIN EN 14825 for summer and winter conditions.

	Thermal Capacity [kW]	Ambient Dry-Bulb Temperature (Wet-Bulb Temperature) [°C]	Inside Dry-Bulb Temperature (Wet-Bulb Temperature) (System A) [°C]	Water Temperature (System B) [°C]
Summer	5	35 (24)	27 (19)	23/18
Winter	8	−7 (−8)	20 (max. 15)	30/35

2.2. System A—Fin-and-Tube Heat Exchanger

For the fin-and-tube heat exchangers, three tubes were considered with different internal geometries, as represented in Figures 2 and 3 and with detailed information in Table 2. The two microfinned tubes (MF1 and MF2) differ in the number of fins and the spiral angle, being both parameters higher in the MF2 tube and resulting in a higher area available for heat exchange, this increase in relative heat exchange area of a microfinned tube compared to a smooth tube with the same fin tip diameter can be calculated as  $R_x$  which is calculated as:

$$R_x = \left\{ \frac{2 \cdot l_f \cdot n \cdot [1 - \sin(\gamma/2)]}{\pi \cdot D \cdot \cos(\gamma/2)} + 1 \right\} \cdot \frac{1}{\cos \beta} \tag{1}$$

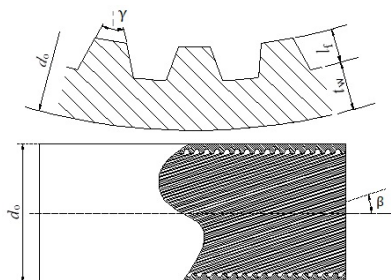


**Figure 2.** Physical presentation of the geometrical parameters.

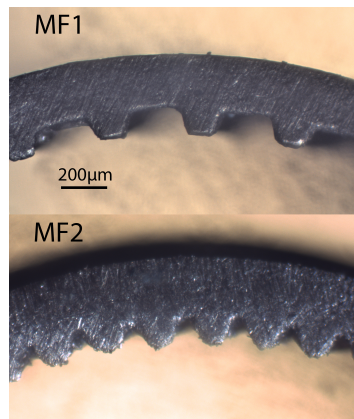


**Figure 3.** Cross sectional view of the microfinned tubes.

**Table 2.** Geometrical parameters of the tubes considered.

	Unit	Smooth Tube	MF1	MF2
Outer diameter ( $d_o$ )	mm	5	5	5
Internal diameter <sup>a</sup> ( $d_i$ )	mm	4.1	4.32	4.26
Wall thickness <sup>b</sup> ( $t_w$ )	mm	0.45	0.22	0.22
Actual cross sectional area	mm <sup>2</sup>	13.2	15.7	14.8
Effective diameter <sup>c</sup>	mm	-	4.47	4.34
Fin height ( $l_f$ )	mm	-	0.12	0.15
Fin number ( $n$ )	[-]	-	35	56
Fin angle ( $\gamma$ )	°	-	35	15
Spiral angle ( $\beta$ )	°	-	15	37
Heat exchange area ratio ( $R_x$ )	[-]	1	1.51	2.63

<sup>a</sup> Internal diameter for smooth tube, fin tip diameter for microfinned tubes. <sup>b</sup> Length between fin root and outer diameter. <sup>c</sup> Equivalent internal diameter for a smooth tube to have same actual cross section area.

In addition to the parameters mentioned in Table 1, some other parameters are set for the fin side as reported in Table 3. The airside fin pitch is higher for the outside unit to prevent frost blockage while the air face velocity is lower in the inside unit to have an acceptable level of fan noise. Most values are based on Thulukkanam [15]. The fin pattern is plain in all the designed heat exchangers and the tubes are arranged in a staggered design.

**Table 3.** Set parameters for the fin-and-tube heat exchangers.

	Air Side Fin Pitch [mm]	Vertical Tube Pitch [mm]	Fin Thickness [mm]	Air Face Velocity [ $\text{m s}^{-1}$ ]
Inside Unit	2	50	0.075	2
Outside Unit	3.2	50	0.09	5

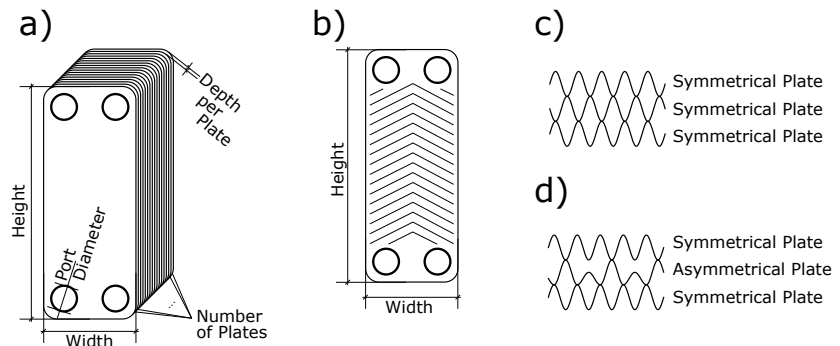
### 2.3. System B—Braze Plate Heat Exchangers

Plate heat exchangers provide compact, highly efficient and adaptable designs with high heat transfer area to inner volume ratio. Different designs and plate patterns such as sinusoidal, fishbone, dimple structure, or specially designed insert plates exist to optimize heat transfer and pressure drop mechanisms [16,17]. One of the last developments in this field has been asymmetrical patterns that reduce the inner volume only of the refrigerant channels with a low influence on heat transfer coefficients and pressure drop for both fluids aiming to reduce refrigerant charge. However, for this study three different brazed plate heat exchangers with symmetrical patterns were selected due to limitations in the modelling tool utilized for this selection. BPHE1 is a brazed plate heat exchanger with no optimization

in terms of inner volume, both BPHE2 and BPHE3 have reduced pattern depths to minimize the inner volume. Geometrical values for the brazed plate heat exchangers are reported in Table 4, the given geometry parameters of the BPHE are shown in Figure 4. Three configurations were simulated each with the same type of plate heat exchanger as condenser and evaporator.

**Table 4.** Geometry of the selected brazed plate heat exchangers.

	Unit	BPHE1	BPHE2	BPHE3
Number of Plates	-	40	36	40
Height	mm	471	324	328
Width	mm	81	94	90
Depth per plate	mm	2.3	1.46	0.95
Inner volume (Refrigerant)	L	1.0	0.53	0.33
Inner Volume (Secondary Fluid)	L	1.1	0.54	0.34
Heat transfer area	m <sup>2</sup>	1.50	0.95	0.78
Port Diameter	mm	20	27	25



**Figure 4.** Brazed plate heat exchanger Geometry: (a) General parameters (b) Plate design of a sinodial herringbone-type plate (c) Side view of a symmetrical pattern (d) Side view of an asymmetrical pattern.

As intermediate brine circuit, a fin-and-tube outdoor unit was assumed with a heat transfer area of 25 m<sup>2</sup> and a heat transfer coefficient of 40 W m<sup>-2</sup> K<sup>-1</sup> at the airside and a heat transfer area of 1.5 m<sup>2</sup> and a heat transfer coefficient of 3 kW m<sup>-2</sup> K<sup>-1</sup> for the brine side. The temperatures of the brine circuit have been estimated using an  $\epsilon$ -NTU method [18]. In order to prevent the brine from freezing, an ethylene glycol-water mixture with a mass fraction of 50% glycol and a freezing temperature of  $-36$  °C was used. The water temperatures for the panel heating and cooling system are fixed and given in Table 1.

### 3. Simulation Method

#### 3.1. HXSim

The results for fin-and-tube heat exchangers are obtained using an in-house code, HXSim, developed by SINTEF Energy Research. This code has been detailed and validated against experimental data in Skaugen [19]. This is a rating program that estimates the heat exchanger performance for a fully described geometry and operating conditions. It has been used extensively to design compact CO<sub>2</sub> heat exchangers [20]. The code was updated to include the latest heat transfer coefficient (HTC) and pressure drop prediction correlations on the refrigerant side, both for smooth and microfinned tubes. The correlations for microfinned tubes are specially developed to consider specific geometrical characteristics of the tubes that can significantly affect HTC and pressure drop values. The prediction methods considered in the current study are based on the best performing correlations

shown in [10–12], they are summarized in Table 5 where  $\delta 30\%$  presents the number of experimental data points that the correlation can predict with less than 30% error.

**Table 5.** Correlations used for prediction of two phase flow characteristics, values in parenthesis present the  $\delta 30\%$  for both tubes.

		Evaporation ( $\delta 30\%$ )	Condensation ( $\delta 30\%$ )
HTC	Smooth MF	Liu and Winterton [21] (100)	Dorao and Fernandino [22] (100)
		Rollmann and Spindler [23] (MF1 = 100, MF2 = 66.7)	Cavallini et al. [24] (MF1 = 100, MF2 = 5.4)
$\Delta P$	Smooth MF	Xu and Fang [25] (100)	Xu and Fang [25] (100)
		Diani et al. [26] (100)	Diani et al. [26] (MF1 = 98, MF2 = 100)

The correlation from Granryd [27] was used for the airside heat transfer and pressure drop. This model is also described by Verma et al. [28] and validated against experiments and CFD by Lindqvist et al. [29]. The evaporator is calculated as a dry expansion type where the evaporation temperature and degree of superheat are defined at the outlet, specified by the pressure and temperature upstream of the expansion valve. The heat exchanger duty is found by iteration on the refrigerant flow rate. The refrigerant side's capacity and pressure loss are integrated from the outlet towards the inlet with an estimated air temperature relative humidity profile. After one integration, the refrigerant duty, wall and fin root temperatures are found, and the airside profile can be updated. The solution has converged when the correct inlet refrigerant enthalpy corresponds with the expansion enthalpy and the refrigerant and airside duties are equal. The two main differential equations for integrating the capacity (enthalpy) and pressure in a direction  $z$  are:

$$\dot{m} \cdot dh = q \cdot P_r \cdot dz \quad (2)$$

$$dp = - \left( \frac{\partial P}{\partial z} \right) dz \quad (3)$$

where  $P_r$  is the refrigerant side surface perimeter and  $q$ , refrigerant side heat flux is calculated by:

$$q = U_r \Delta T_{LMTD} \quad (4)$$

where  $\Delta T_{LMTD}$  is the logarithmic temperature difference between the air and the refrigerant and  $U_r$  is the overall heat transfer coefficient referred to the refrigerant side based on the local refrigerant side heat transfer coefficient, tube wall resistance and the apparent local airside heat transfer coefficient.

Most correlation used for prediction of HTC do not have into account the heat transfer mechanism after dryout is initiated. Thus, in simulations, HTC would increase up to  $x = 1$  and suddenly drop to single phase HTC values, usually an order of magnitude smaller. This huge drop at a single point of calculation would destabilize the iterative process and stop the simulation. To ensure a good convergence behavior on the refrigerant side, HTC needed to be smoothed between the two-phase and single-phase regions. An asymptotic interpolation via weighed tanh-function was used between HTC at vapor fraction 0.8 and superheated vapor at 20 K superheat. Figure 5 illustrates this principle where the blue markers show the calculated HTC directly from the correlation (depending on temperature, pressure, vapor quality and heat flux) and the orange line show the smoothing function between vapor fraction 0.8 with superheating values of 0.0 and 20.0 K. The justification of smoothing against a non-equilibrium vapor fraction bigger than one is based on [30]. It is noteworthy that while the smoothing of HTC between the phases might seem aggressive and show a considerable difference, the longitudinal heat conduction along the length of copper tubes walls would have a similar effect where the dryout will not be localized to a single point and thus smoothed. The dry-out point can also be calculated from a correlation, and the asymptotic interpolation regarded as a post-dryout heat transfer.

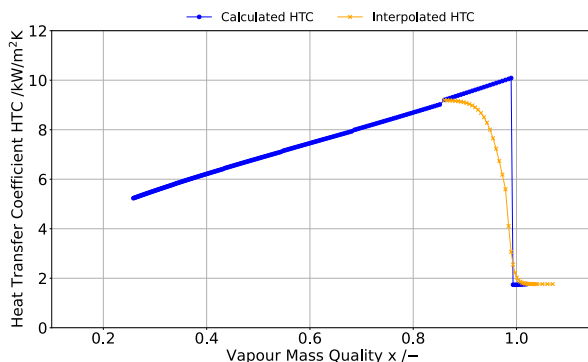


**Figure 5.** Heat transfer coefficients based on correlation of two-phase flow ( $x < 1$ ) and single phase vapour flow ( $x > 1$ ) (blue) and smoothing function at dry-out region ( $0.8 < x < 1.1$ ) for HXSim program.

### 3.2. IMST-ART

The plate heat exchangers were simulated with the simulation software IMST-ART Version 3.9.0 developed by the Universidad Politecnica de Valencia (UPV) which is a commercial tool for the design and optimization of refrigeration cycles [31]. On the refrigerant side, the used heat transfer and pressure drop correlations for two-phase flow in plate heat exchangers utilize correlations for tubular geometries with measurements done at the UPV. For single-phase flow, the correlation of [32] is used. The void fraction and refrigerant mass are calculated with the correlation of [33]. Only symmetrical plate heat exchangers can be modeled since there is no difference in the two fluids’ geometry. The software requires the dimensional data of the plate heat exchanger and enhancement factors for the heat transfer and pressure drop for both fluids, plus the conditions of both fluids at the inlet and the mass flow rate or outlet conditions. The enhancement factors were adapted in order to achieve same overall heat transfer coefficients and pressure drop which the distributors suggested. The software only calculates the masses and volumes in the core and neglects the ports, these were added manually with a homogeneous void fraction model.

## 4. Results and Discussion

### 4.1. Fin-and-Tube Heat Exchanger Designs

Fin-and-tube heat exchangers need to be designed based on the requirements of the tested case. The goal of the design was to limit the available volume in the heat exchanger. The most important design parameters are reported in Table 6. The higher HTC for MF allowed for shorter lengths of passes but led to a slightly higher number of passes to attain higher capacities. The inlet and outlet header for all heat exchangers had an internal diameter of 12 mm.

**Table 6.** Geometrical design parameters of Fin-and-tube heat exchanger units.

Tube Type	Unit Location	Parallel Circuits (Rows)	Passes in Each Circuit	Total Heat Exchanger Tube Length [m]
Smooth (SM)	Inside unit	8	4	33.6
	Outside Unit	18	4	46.8
MF	Inside unit	9	2	17.1
	Outside Unit	19	2	22.8

While two internally enhanced tubes were used to design fin-and-tube heat exchangers, the authors were unable to find a satisfactory simulation of the MF2 tube. The significant challenge was the evaporator in summer condition (inside unit), where no converging solution was found. On the other hand, the condensation unit at winter condition (inside

unit) seemed to have higher than anticipated HTC. These problems are explained by the inability of the correlations to predict HTC of microfinned tubes with a high number of fins. This was expected and it is well documented in Allymehr et al. [10,11]. It can be seen in Table 5 where the  $\delta 30\%$  value for MF2 tube is significantly lower than MF1 tube. In addition to higher  $\delta 30\%$  values, the results for MF2 have a high level of scattering, which the authors believe to be the underlying reason for simulation convergence problems. Additionally, the performance of the internal units in both summer and winter conditions are related to the outer unit, so the results from these units are also not dependable; therefore, MF2 results were not included in this study. However, the details of the MF2 tube are kept to show the limitations of this numerical simulation and the need for the experimental test in certain scenarios.

#### 4.2. System Comparison

The capacities, saturation pressures and saturation temperatures for both system are shown in Figures 6–8. For System A, HXSim calculates each heat exchanger separately and needs to manually balance parameters such as mass flow between the indoor and outdoor units. This limits the control over the design parameters such that reaching identical conditions between the MF tube and smooth tube design was not possible. The differences in these parameters were not significant, nevertheless Figure 6 shows the deviation from the design parameter for capacity while Figures 7 and 8 visualize the disparity of saturation temperature in the two tested systems. System A was designed with the goal of charge reduction in heat exchangers, thus the saturation temperatures were chosen to give the maximum reasonable temperature difference between the fluid and the air, additionally this provides a chance to compare the charges in systems on a more equitable basis in relation to efficiency of the system. For System B all calculated capacities match the design capacity, the deviation in the saturation pressure and saturation temperatures are very small and result from a changed thermal transmittance, which is best in BPHE2. Qualitatively, the results for summer and winter conditions are identical.

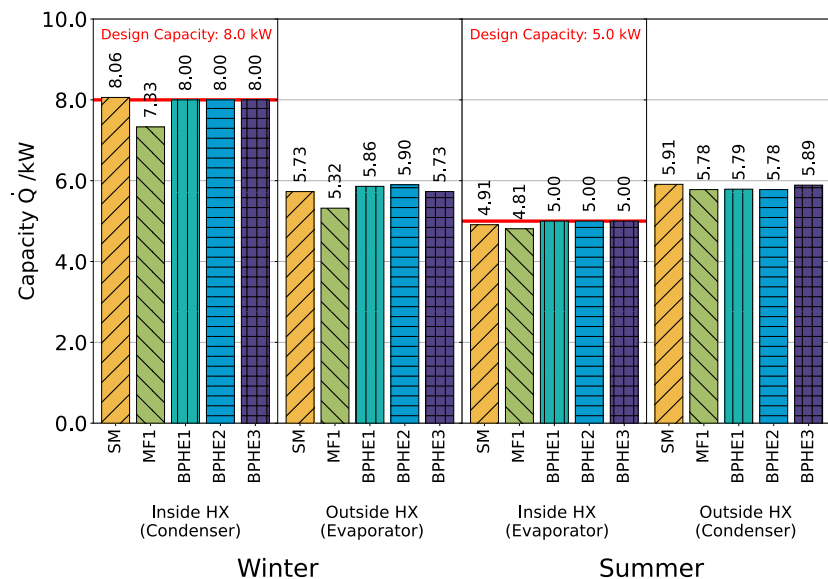


Figure 6. Designed capacity and the actual capacity of the systems simulated.

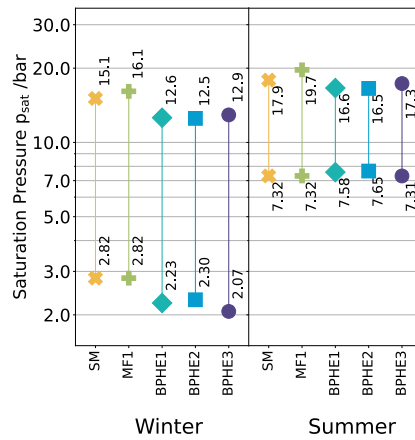


Figure 7. Saturation pressure of the designed systems.

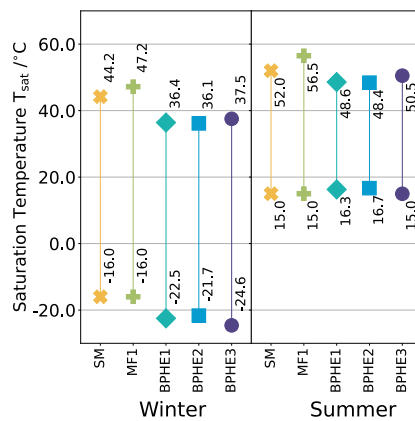
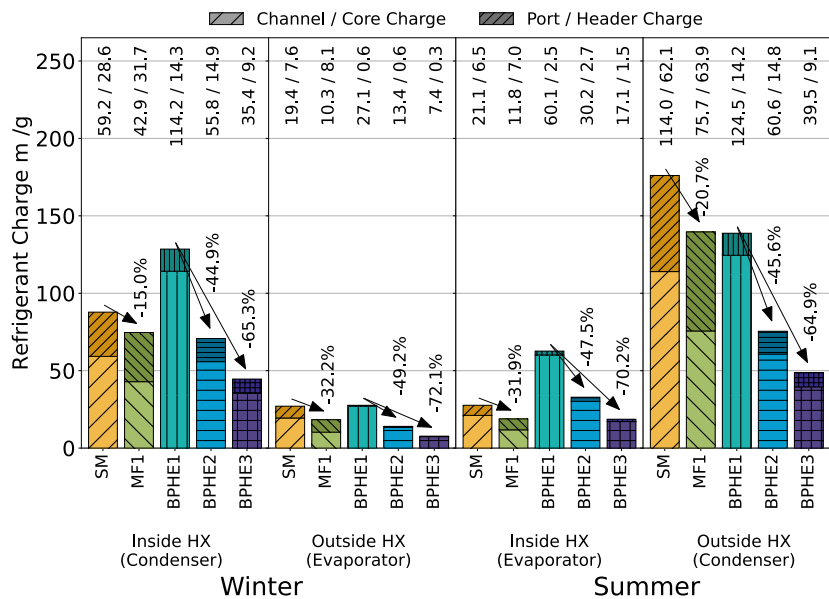


Figure 8. Saturation temperature of the designed systems.

#### 4.3. Charge

Figure 9 shows the charge distribution in the heat exchangers in winter conditions (Heating mode) and summer conditions (air conditioning mode) for both fin-and-tube heat exchangers (System A) and the plate heat exchangers (System B). The charge required for other components and dissolved in the oil was not the focus of this study and thus has not been discussed. The simulation results show that the configuration with BPHE1 requires the largest amount of refrigerant followed by the configuration with a fin-and-tube heat exchanger with smooth tubes (SM). The fin-and-tube heat exchanger with microfinned tubes (MF1) and BPHE2 need a comparable amount of refrigerant while MF1 requires less charge inside the core but more in the header, only for the summer condition the outside unit requires a much higher amount of refrigerant. BPHE3 required the lowest charge for all conditions. All condensers show a considerably higher charge for the header and core than the evaporators resulting from the presence of completely liquefied refrigerant. The summer condition requires a higher charge for all compared systems than winter condition because of higher saturation pressures in both evaporator and condenser leading to a higher vapour density, a lower inlet quality and a lower density ratio of the gaseous and liquid refrigerant. For System A the different heat exchanger designs of the inside and outside unit affects the charge additionally. For System A, in summer conditions, microfinned tube (MF1) yield a higher HTC; thus, the circuit length is substantially reduced compared to smooth tubes (SM). However, in order to compensate for the resistance on the

airside, more parallel circuits are required. The longer header section required for the larger number of parallel circuits holds a high amount of charge. This is because in the evaporator, the inlet header has the lowest vapor quality and thus the lowest void fraction. Since most of the charge is in the liquid phase, the evaporator's inlet header can contain a considerable amount of charge, leading to a diminishing effect of charge reduction of microfinned tubes. Correspondingly for the condenser, the outlet header is a subcooled fluid with the highest density and, therefore, the mass. The charge distribution for System A in winter conditions follows the same pattern as summer conditions. The lower condenser charge in winter condition compared to summer condition seems to result from the higher number of fins on the airside for the inside unit and the resulting heat flux increase. Thus, the air can remove more heat from the same length of the tube. For System B the required charge for the configurations with BPHE2 and BPHE3 compared to BPHE1 are reduced by 45% to 49% and 65% to 72%, respectively. These values are similar to the reduction of the inner volume (Figure 10). The logarithmic mean temperature difference (LMTD) for BPHE2 compared to BPHE1 is approximately the same as the heat transfer coefficient rises on both sides and the heat transfer area reduces. For BPHE3 both heat transfer area and heat transfer coefficient are reduced compared to BPHE2 leading in a 60–70% higher LMTD. For all configurations the pressure drop on the refrigerant side is negligible but for the secondary fluids' side the pressures drop in BPHE2 and BPHE3 can be up to 50 kPa which can be considered excessive. This is the problem of the symmetrical plate pattern and is already solved by using asymmetrical plate patterns which provide an increased cross sectional area for the secondary fluid and thus reduced velocities and pressure drops.



**Figure 9.** Charge distribution for all tested heat exchangers, numbers on top of figure show the charge for channel/core and port/header.

The inner volume and total charge of the different configurations for both systems are shown in Figures 10 and 11. For System A, microfinned tubes reduced the charge by 19% for winter and 22% for summer conditions. While the reduction in charge is notable, the increase of the charge in the header (up to 11% for winter inside HX) and a slight reduction in capacity in some cases reduce the benefit of utilizing microfinned tubes. The reduction of volume for plate heat exchanger seems to translate to the same level of reduction in charge. BPHE2 configuration has a reduced volume of 48% and the configuration with BPHE3 has a reduced volume of 68% compared to a configuration

utilizing BPHE1 as condenser and evaporator. While different parameters such as high inlet mass fraction, higher mass flux, increased density ratio between gaseous and liquid phase and reduced pressure lead to a charge reduction but the defining parameter for charge reduction seems to be the reduction of the inner volume. Similar to System A, the required charge for all configurations in the summer condition in System B exceeds the winter condition charge. The main increase charge seems to be in the evaporator were a lower inlet quality and a higher pressure, lead to increased vapor phase density.

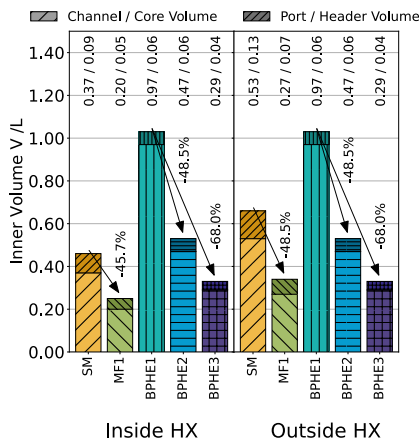


Figure 10. Total inner volume of the heat exchangers, numbers on top of figure show the volume for channel/core and port/header.

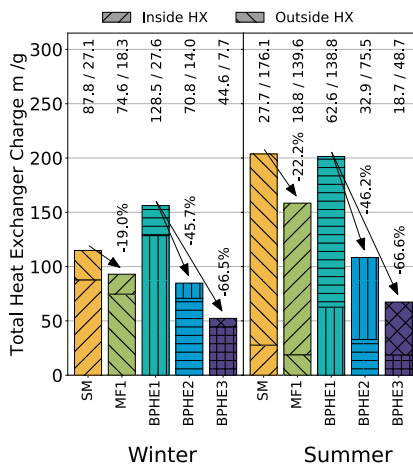


Figure 11. Total charge of the heat exchangers, numbers on top of figure shows the charge for inside/outside heat exchangers.

#### 4.4. System Effectiveness

The performance indicators coefficient of performance (COP for winter) and energy efficiency ratio (EER for summer) of all systems was calculated in summer and winter conditions considering isentropic efficiency of 0.82 to 0.86 for System A and 0.85 for System B. For System A, no heat loss in compressor was assumed. Additionally the ventilator energy consumption was not included in the calculations. For system B, the pumps (assumed efficiency: 70%) with additional pressure losses in the brine circuit and water circuit of 30 kPa and 20 kPa, respectively, inverter and motor losses (assumed efficiency:

90%) and energy consumption of the ventilator of the brine-to-air heat exchanger of 100 W have been taken into account for the performance calculation. Defrost cycles have been neglected. The performance indicators for each condition can be formulated as:

$$COP = \frac{Q_{Heating}}{W_{Comp} \cdot 1/\eta_{Comp} + W_{Pumps} \cdot 1/\eta_{Pumps}} \quad (5)$$

$$EER = \frac{Q_{Cooling}}{W_{Comp} \cdot 1/\eta_{Comp} + W_{Pumps} \cdot 1/\eta_{Pumps}} \quad (6)$$

The performance indicators of the different systems are visualized in Figure 12. Because of the slightly higher pressure ratio between condensation and evaporation. Nevertheless, as the saturation temperatures chosen for the System A are close to saturation temperatures of the System B, performance of both systems are similar. System B using plate heat exchangers manages to achieve a slightly higher performance than System A using fin-and-tube heat exchangers. In fin-and-tube heat exchangers, the smooth tube has a slightly higher performance, especially in summer because of the lower condensation saturation temperature. As for the plate heat exchangers, BPHE3 performs slightly worse than the other plate heat exchangers which is again caused by the slight variation in saturation temperatures.

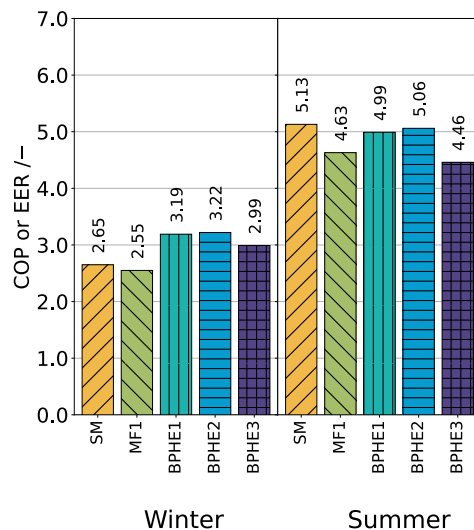


**Figure 12.** Coefficient of performance (COP for winter) and energy efficiency ratio (EER for summer) in different configurations.

## 5. Conclusions

This article numerically studies two different charge reduction methods for a reversible air conditioning/ heat pump system using propane (R290) as working fluid. Heating and cooling capacities were 8 kW and 5 kW, respectively. A direct system with fin-and-tube heat exchanger, System A, is compared with an indirect system using brazed plate heat exchangers, System B. System A is designed with tubes with smooth internal surface and with microfinned tubes. System B was simulated with three brazed plate heat exchangers with different internal volumes. System A was simulated with HXSim, an in-house built code, while simulation of System B was performed with IMST-ART. The refrigerant charge is primarily influenced by the inner volume. Microfinned tubes in System A (Fin-and-tube) compared to the smooth tube resulted in a maximum charge reduction and volume reduction of 22% of 48%, respectively. For System B, using specially designed BPHE with the minimum internal volume, these values were 66% and 68%, respectively. In general,

the charge can be reduced more aggressively using BPHE with a smaller internal volume. Other parameters such as higher mass flux seem to reduce the charge, albeit to a lesser extent. The charge reduction by using microfinned tubes in System A (Fin-and-tube) heat exchangers is negated by the increase in the volume and, consequently, the header's charge (up to 11%). System B achieve a higher COP than System A in winter conditions (System A 2.6, System B 3.1) and similar values in summer conditions (System A 4.9, System B 4.9). COP is reduced by microfinned tubes in System A (up to 9%) and specially designed BPHE in System B (up to 10.8%). This is most notable in summer conditions. Both systems provide a possibility of charge reduction or capacity increase in RACHP equipment. Effects such as maldistribution and other components of a functional system such as liquid line have not been considered in this study which could have a considerable effect on the charge of the system. Simulation of these parameters was not possible with the used simulation tools and requires further studies. Moreover, cost analysis between two systems can be suggested for further research.

**Author Contributions:** Conceptualization, E.A., T.W., A.H., T.M.E. and Á.Á.P.; methodology, E.A., T.W. and Á.Á.P.; software, G.S., E.A., T.W.; validation, E.A., T.W.; formal analysis, E.A., T.W. and Á.Á.P.; investigation, E.A., T.W. and Á.Á.P.; resources, G.S., A.H., T.M.E.; data curation, G.S., E.A., T.W. and Á.Á.P.; writing—original draft preparation, E.A., T.W. and Á.Á.P.; writing—review and editing, E.A. and Á.Á.P.; visualization, E.A.; supervision, A.H., L.S., T.M.E.; project administration, A.H., T.M.E.; funding acquisition, A.H., T.M.E. All authors have read and agreed to the published version of the manuscript.

**Funding:** This publication has been funded by HighEFF—Centre for an Energy Efficient and Competitive Industry for the Future, an 8-years' Research Centre under the FME-scheme (Centre for Environment-friendly Energy Research, 257632). The authors gratefully acknowledge the financial support from the Research Council of Norway and user partners of HighEFF.

**Institutional Review Board Statement:** Not applicable.

**Informed Consent Statement:** Not applicable.

**Data Availability Statement:** Not applicable.

**Conflicts of Interest:** The authors declare no conflict of interest.

## Nomenclature

### Greek

$\beta$	Spiral angle
$\delta_{30}$	Percentage of predicted values with less than 30% error
$\eta$	Efficiency
$\gamma$	Fin angle

### Roman

<i>BPHE</i>	Brazed plate heat exchangers [-]
<i>COP</i>	Coefficient of Performance [-]
$d_i$	Fin tip diameter for MF tubes, internal diameter for smooth tube [mm]
$d_o$	Outer diameter [mm]
<i>EER</i>	Energy Efficiency Ratio [-]
$h$	Enthalpy [ $\text{kJ kg}^{-1}$ ]
<i>HTC</i>	Heat Transfer Coefficient [ $\text{kWm}^{-2} \text{K}^{-1}$ ]
$l_f$	Fin height [mm]
$m$	Refrigerant mass [g]
$n$	Number of fins [-]
$p$	Pressure [Pa]
$P_r$	Refrigerants side heat exchange perimeter [m]
$Q$	Capacity [kW]
$q$	Heat flux [ $\text{kWm}^{-2}$ ]

$R_x$	Heat exchange area ratio of a MF tube to a smooth tube [-]
$SM$	Smooth tube [-]
$T$	Temperature [°C]
$t_w$	Wall thickness [mm]
$U_r$	Refrigerants overall heat transfer coefficient [ $\text{kWm}^{-2} \text{K}^{-1}$ ]
$W$	Power [W]
$x$	Vapor quality [-]
$z$	Length of tube simulated [m]
<b>Subscripts</b>	
$sat$	Saturated condition

## References

- Schulz, M.; Kourkoulas, D. Regulation (EU) No 517/2014 of The European Parliament and of the council of 16 April 2014 on fluorinated greenhouse gases and repealing Regulation (EC) No 842/2006. *Off. J. Eur. Union* **2014**, *2014*, L150.
- Straub, M. Alternative Refrigerants For Household Refrigerators Alternative Refrigerants For Household Refrigerators. *Int. Refrig. Air Cond.* **2018**, *2002*, 1–10.
- Mota-Babiloni, A.; Makhnatch, P. Predictions of European refrigerants place on the market following F-gas regulation restrictions. *Int. J. Refrig.* **2021**, *127*, 101–110. [[CrossRef](#)]
- Tang, W.; He, G.; Zhou, S.; Sun, W.; Cai, D.; Mei, K. The performance and risk assessment of R290 in a 13 kW air source heat pump. *Appl. Therm. Eng.* **2018**, *144*, 392–402. [[CrossRef](#)]
- Palm, B. Hydrocarbons as refrigerants in small heat pump and refrigeration systems—A review. *Int. J. Refrig.* **2008**, *31*, 552–563. [[CrossRef](#)]
- Li, T.; Lu, J.; Chen, L.; He, D.; Qiu, X.; Li, H.; Liu, Z. Measurement of refrigerant mass distribution within a R290 split air conditioner. *Int. J. Refrig.* **2015**, *57*, 163–172. [[CrossRef](#)]
- Andersson, K.; Granryd, E.; Palm B. Water to water heat pump minimum charge of propane. In Proceedings of the 13th IIR Gustav Lorentzen Conference on Natural Refrigerants (GL2018), Valencia, Spain, 18–20 June 2018. [[CrossRef](#)]
- Dankwerth, C.; Methler, T.; Oltersdorf, T.; Peter, S.; Marek, M.; Schnabel, L. Entwicklung einer Propan-Wärmepumpe mit einer Kältemittelfüllmenge von 150 Gramm. *DKV-Tagungsband 2019*, **2019**, 60–61.
- Dankwerth, C.; Methler, T.; Oltersdorf, T.; Schossig, P.; Schnabel, L. Kältemittelreduktion in Propan-Wärmepumpen—Aktuelle Arbeiten. *DKV-Tagungsband 2020*, **2020**, 70.
- Allymehr, E.; Pardiñas, Á.Á.; Eikevik, T.M.; Hafner, A. Characteristics of evaporation of propane (R290) in compact smooth and microfinned tubes. *Appl. Therm. Eng.* **2020**, *181*, 115880. [[CrossRef](#)]
- Allymehr, E.; Pardiñas, Á.Á.; Eikevik, T.M.; Hafner, A. Condensation of Hydrocarbons in Compact Smooth and Microfinned Tubes. *Energies* **2021**, *14*, 2647. [[CrossRef](#)]
- Allymehr, E.; Pardiñas, Á.Á.; Eikevik, T.M.T.; Hafner, A. Comparative analysis of evaporation of Isobutane (R600a) and Propylene (R1270) in compact smooth and microfinned tubes. *Appl. Therm. Eng.* **2021**, *188*, 116606. [[CrossRef](#)]
- CEN. *Air Conditioners, Liquid Chilling Packages and Heat Pumps for Space Heating and Cooling and Process Chillers Using Electrically Driven Compressors—Part 1: Terms and Definitions*; DIN EN 14511-1:2015-12; DIN Standards Committee Refrigeration Technology: Berlin, Germany, 2015.
- CEN. *Air Conditioners, Liquid Chilling Packages and Heat Pumps, with Electrically Driven Compressors, for Space Heating and Cooling—Testing and Rating at Part Load Conditions and Calculation of Seasonal Performance*; DIN EN 14825:2016-10; DIN Standards Committee Refrigeration Technology: Berlin, Germany, 2016.
- Thulukkanam, K. *Heat Exchanger Design Handbook*; CRC Press: Boca Raton, FL, USA, 2013.
- Dovič, D.; Palm, B.; Švaić, S. Generalized correlations for predicting heat transfer and pressure drop in plate heat exchanger channels of arbitrary geometry. *Int. J. Heat Mass Transf.* **2009**, *52*, 4553–4563. [[CrossRef](#)]
- Piper, M.; Olenberg, A.; Tran, J.M.; Kenig, E.Y. Determination of the geometric design parameters of pillow-plate heat exchangers. *Appl. Therm. Eng.* **2015**, *91*, 1168–1175. [[CrossRef](#)]
- VDI Verein Deutscher Ingenieure e.V. *VDI-Wärmeatlas*; Springer GmbH: Berlin/Heidelberg, Germany, 2013.
- Skaugen, G. Simulation of extended surface heat exchangers using CO<sub>2</sub> as refrigerant. In Proceedings of the 4th IIR-Gustav Lorentzen Conference on Natural Working Fluids, West Lafayette, IN, USA, 25–28 July 2000; pp. 306–314.
- Petterson, J.; Hafner, A.; Skaugen, G.; Rektad, H. Development of compact heat exchangers for CO<sub>2</sub> air-conditioning systems. *Int. J. Refrig.* **1998**, *21*, 180–193. [[CrossRef](#)]
- Liu, Z.; Winterton, R.H. A general correlation for saturated and subcooled flow boiling in tubes and annuli, based on a nucleate pool boiling equation. *Int. J. Heat Mass Transf.* **1991**, *34*, 2759–2766. [[CrossRef](#)]
- Dorao, C.A.; Fernandino, M. Simple and general correlation for heat transfer during flow condensation inside plain pipes. *Int. J. Heat Mass Transf.* **2018**, *122*, 290–305. [[CrossRef](#)]

23. Rollmann, P.; Spindler, K. A new flow pattern map for flow boiling in microfin tubes. *Int. J. Multiph. Flow* **2015**, *72*, 181–187. [[CrossRef](#)]
24. Cavallini, A.; Del Col, D.; Mancin, S.; Rossetto, L. Condensation of pure and near-azeotropic refrigerants in microfin tubes: A new computational procedure. *Int. J. Refrig.* **2009**, *32*, 162–174. [[CrossRef](#)]
25. Xu, Y.; Fang, X. A new correlation of two-phase frictional pressure drop for evaporating flow in pipes. *Int. J. Refrig.* **2012**, *5*, 2039–2050. [[CrossRef](#)]
26. Diani, A.; Mancin, S.; Rossetto, L. R1234ze(E) flow boiling inside a 3.4 mm ID microfin tube. *Int. J. Refrig.* **2014**, *47*, 105–119. [[CrossRef](#)]
27. Granryd, E. Forced Convection Heat Transfer and Pressure Drop in Tube-in-Fin Heat Exchangers. Licentiate Thesis, Kungliga Tekniska Högskolan, Stockholm, Sweden, 1964.
28. Verma, P.; Bullard, C.W.; Hrnjak, P.S. *Design Tool for Display Case Heat Exchanger Frosting and Defrosting*; Technical Report TR-201; Air Conditioning and Refrigeration Center, College of Engineering, University of Illinois at Urbana-Champaign: Urbana, IL, USA, 2002.
29. Lindqvist, K.; Skaugen, G.; Meyer, O.H.H. Plate fin-and-tube heat exchanger computational fluid dynamics model. *Appl. Therm. Eng.* **2021**, *189*, 116669. [[CrossRef](#)]
30. Shah, M.M.; Siddiqui, M.A. A General Correlation for Heat Transfer During Dispersed-Flow Film Boiling in Tubes. *Heat Transf. Eng.* **2000**, *21*, 18–32. [[CrossRef](#)]
31. IMST-ART. *Simulation Tool to Assist the Selection, Design and Optimization Of Refrigerator Equipment and Components*; Institute for Energy Engineering, Universitat Politècnica de València: Valencia, Spain, 2010.
32. Cooper, A.; Dennis Usher, J. 3.7 Plate Heat Exchangers: 3.7.5 Heat Transfer Correlations. In *Heat Exchanger Design Handbook*; VDI Verein Deutscher Ingenieure e.V., Ed.; Hemisphere Publishing Corporation: London, UK, 1983.
33. Crisholm, D. A theoretical basis for the Lockhart-Martinelli correlation for two-phase flow. *Int. J. Heat Mass Transf.* **1972**, *10*, 1767–1778. [[CrossRef](#)]